

PZero - Electric Paramotor

A high performance, low-cost, electrically powered paramotor capable of crossing the Netherlands

A.D.J. Beets

4031385

A.J. de Leeuw

4096096

J.L. Dorscheidt

4091981

R.C. Nijman

1356941

M.P.J. Eversdijk

4142705

B.W. Ossenkoppele

4077067

S.J. Folmer

4047214

J.K. Sothmann

4164644

M.N. Hirsch

4161424

Final Report
Design Synthesis Exercise

Preface

At the faculty of Aerospace Engineering at the TU Delft, every student has to complete the Design Synthesis Exercise (DSE) as the final bachelor thesis project. For this purpose Bart Remes came up with a hands on project: The group of nine students has to design a performance and cost efficient electrically powered paramotor, which can cross the Netherlands within one day.

The final report provides an extensive elaboration on the final design, as well as the layout and characteristics of each subcomponent. Moreover, all design supporting elements will be shown together with the possible Post-DSE activities that can be performed to accomplish the mission and product market sales. The feedback on the midterm review was an appreciated input, that was then incorporated in the final design. Comments, regarding the process and design during the project were given by the tutor of the project, Bart Remes, as well as by the two assisting coaches, Jan Schneiders and Salvatore Vitale. For all the support, advice and guidance throughout the whole project, we, DSE Group 06, would like to express our deepest gratitude to you.

Furthermore we would also like to thank all other people contributing to our work. Special thanks goes to Frank Moorman, who answered all our questions concerning the paramotor market in the Netherlands and also spread our questionnaire over the whole KNVvL network, which resulted in a high number of responses and very good feedback for our market analysis. Hence we also want to thank all those diligent men and women, who completed our questionnaire. Especially Arthur Glaser and Gerard Visser supported us a lot with their professional feedback on our concept ideas during the midterm presentation.

Finally we would like to thank all other people who weren't personally mentioned but should not be forgotten for sharing their knowledge with us or supporting us personally.

For this report it is assumed that the reader has a technical background with knowledge of aerospace engineering and some basic understanding of electrical engineering.

Delft, Tuesday 27th January, 2015

Table of Contents

Preface	ii
Nomenclature	v
List of Figures	vii
List of Tables	x
1 Introduction	2
2 Mission Plan	3
2.1 Mission Description	3
2.2 Flight Strategy	4
2.3 Operations & Logistics Concept Description	9
2.4 Conclusion Mission Plan	12
3 System Analysis	13
3.1 Chosen Concept	13
3.2 Reference Frames	14
3.3 Energy Storage & Generation	14
3.4 Motor & Controls	24
3.5 Propeller	38
3.6 Chassis	48
3.7 Aerodynamic Fairing	56
3.8 Layout and Characteristics of the Overall System	66
4 Verification & Validation	68
4.1 Verification & Validation of the Flight Simulation MATLAB Script	68
4.2 Verification & Validation of Motor and Controls	69
4.3 Verification & Validation of the Propeller	70
4.4 Verification & Validation of the Batteries	72
4.5 Verification & Validation of Chassis	73
4.6 Verification & Validation of the Fairing	74
4.7 Verification & Validation Conclusion	75
5 System Design Support	76
5.1 Risk Analysis Assessment	76
5.2 RAMS	79
5.3 Communication Flow Diagram	80
5.4 Sensitivity Analysis Mission	80
5.5 Sustainability Development Strategy	83
5.6 Conclusion of System Design Support	87
6 Production Plan	88
6.1 Manufacturing	88
6.2 Name and Type of Purchased Parts	88
6.3 Assembly	89
7 Business & Marketing	90
7.1 Market Analysis & Planning	90
7.2 Return on Investment & Operational Profit	97

7.3	Project Design & Development Logic	99
7.4	Conclusion Business & Marketing	99
8	Conclusion	101
8.1	Recommendations	102
	Bibliography	103
A	Requirements	104
B	Resource Allocation	112
C	Functional Breakdown Structure	114
D	Functional Flow Diagram	116
E	Battery Terms	119
F	Battery Standards	122
G	Power Distribution during Powered Flight	123
H	Battery Wiring	124
I	Motor Selection	125
J	Particle Swarm Optimization for Airfoil Selection	126
K	Drive Shaft Analysis Method	129
L	Mail Exchange with Russel Ogden	131
M	Prototype Cost Breakdown	132
N	SWOT Analysis Detailed Design	133

Nomenclature

A	Surface area	A	Cross-sectional area
A	Vibration mode factor	$A_{air\,foil}$	Airfoil area
A_{min}	Minimum area	B_g	Air gap flux density
C	Capacitance	C_d	Drag coefficient
	Drag coefficient		Drag coefficient
$C_{d_{head}}$	pilot's head		of interference drag
	Drag coefficient	$C_{d_{arms,interference}}$	of the arms
	induced by free		
$C_{d_{arms,freeflow}}$	flow around the arms	C_l	Lift coefficient
C_P	Power coefficient	C_T	Thrust coefficient
D	Drag	E	Young's modulus
EA	Extensional stiffness	E_{IXX}	In-plane stiffness
$EIYY$	Out-of plane stiffness	EK	Extensional/torsional stiffness
F	Load	F_d	Aerodynamic drag force
F_h	Loads on hang point	F_m	Peak Force
GJ	Torsional stiffness	GR	Gear ratio
I	Moment of inertia	I	Current
I_s	Slot current	K	Column effective length factor
L	Length	L	Active motor length
L	Conductor length	L	Lift
M	Mass density/length	M_e	Mass
M_s	Suspended mass	M_y	Maximum moment
MXX	Pitch axis inertia/length		
N_m	Number of magnet poles	P	Power
P_{req}	Power required	R	Resistance
R	Radius	R_{inner}	Inner radius
R_{outer}	Outer radius	Re	Reynolds number
RST	Structural radius	S	Surface area
	Surface area of		Surface area of
	the arms outside	$S_{arms,interference}$	the arms in the
$S_{arms,freeflow}$	the interference area		interference area
T	Thrust	T	Torque
T_{motor}	Motor torque	$T_{propeller}$	Propeller torque
V	Velocity	V_t	Tangential Velocity
V_∞	Free stream velocity	V_{local}	Local air velocity
V	Voltage	V_s	Supply voltage
V_e	Induced voltage	W	Weight
$XOCG$	$\frac{x}{c}$ of section CG	$XOSG$	$\frac{x}{c}$ of section shear center
	a	Acceleration	
b	Fin span	b	Short side length
c	Fin chord	d	Diameter
k_e	Motor back-EMF constant	k_t	Motor torque constant
k_v	Motor speed constant	l	Length
m	Mass	$m_{battery}$	Battery mass
m_{unit}	Mass per unit length	g	Gravitational acceleration

q	Distributed load	r	Radius
r_{blade}	Blade radius	$r_{max,body}$	Maximum radius fairing
t	Thickness	u_0	Free stream velocity
w	Width	x	Distance to centre of gravity
α	Panel dimensions ratio quantity	β	Panel dimensions ratio quantity
λ	Advance ratio	μ_{prop}	Propulsive efficiency
ρ	Density	ρ	Resistivity
ρ_e	Energy density	μ	Kinematic viscosity
μ	Propeller efficiency	μ_{prop}	Propulsive efficiency
σ	Stress	σ_y	Tensile yield strength
σ_c	Compressive stress	τ	Shear stress
ω	Revolutional speed	ω_{nf}	Eigenfrequency

List of Abbreviations

AC	Alternating Current	AF	Alkaline
AL	Aluminum	Ast	All stakeholders
BL	Boundary Layer	BLDC	Brushless direct current
BLDCPM	Brushless direct current permanent magnet	BLIP	Boundary Layer Information Prediction
BMS	Battery Management System	CAD	Computer Aided Design Computer Aided Three
CAN	Controller Area Network	CATIA	Dimensional Interactive Application
CBP	Chassis Back Plate	CE	Conformit Europeenne
CFD	Computational Fluid Dynamics	CH	Chassis Harness
CHP	Chassis Hang Point	CNC	Computer Numerical Control
COG	Centre Of Gravity	CRPC	Chassis Reserve Parachute Container
CSS	Chassis Safety System	CTR	Control Zone
DC	Direct Current	DGR	Dangerous Goods Regulations
DIY	Do It Yourself	DOT	Design Option Tree
DOT UN	Department of Transport United Nations	DSE	Design Synthesis Exercise
DT	Drive Train	DULV	Deutscher Ultraleichtflugverband
DUT	Delft University of Technology	EASA	European Aviation Safety
ECO	Ecological	EG	Energy Generation
EMF	Electromotive Force	EP	Electric Paramotor
ES	Energy Storage	ESC	Electronic Speed Controller
FAI	Federation Aeronautique Internationale	FBS	Functional Breakdown Structure
FEM	Finite Element Method	FFD	Functional Flow Diagram
FET	Field-effect Transistor	FS	Flight Strategy
FOD	Field Oriented Control	GPS	Global Positioning System
HTD	High-Torque Drive	IATA	International Air Transport Association
IC	Input Controller	ICI	Input Controller Interface
IFR	Instrumental Flight Rules Koninklijke Nederlandse	IPPI	International Pilot Proficiency Information
KNVvL	Vereniging voor Luchtvaart	KNMI	Royal Netherlands Meteorological Institute
L	Inductor	LCA	Life Cycle Analysis
LHR	Luchthavenregelin	LiPo	Lithium Polymer
LiThio	Lithium-Thionyl	LMW	Main Lift Device
LR	Reserve Lift Device	LSG	Suspension Line Geometry
LSL	Suspension Lines	LWC	Main Wing Control
MATLAB	Matrix Laboratory	MCFC	Molten Carbonate
MCU	Micro Controller Unit	MDF	Medium-density fibreboard

TABLE OF CONTENTS

MLA	Micro Light Airplanes National Advisory Committee for Aeronautics	MR	Mission Risk
NACA		NOTAM	Notice to airmen
OPC	Open Circuit Voltage	PAFC	Phosphoric Acid
PCB	Printed Circuit Board	PCM	Protection Circuit Module
PDD	Project Design Development Polymer electrolyte membrane fuel cell	PEM	Polymer electrolyte membrane
PEMFC		PH	Pays-Bas/Holland registration number
PM	Permanent Magnet	PMA	Paramotoring Manufacturing Association
PPD	Propulsion Device	PPM	Pulse Position Modulation
PR	Project Risk	PSO	Particle Swarm Optimization Reliability, Availability, Maintainability and Safety
PWM	Pulse Width Modulation Regional Atmospheric Soaring Prediction	RAMS	
RASP		RC	Remote Control
RDT	Requirement Discovery Tree	RoI	Return on Investment
RPM	Revolutions Per Minutes	R	Resistance
RT	Radio License Regelingsveilig gebruik luchthavens en andere terreinen	SF	Safety Factor Strengths, Weaknesses, Opportunities and Threats
RVGLT		SWOT	
SOFC	Solid Oxide	TR	Team Risk
Sys	System	TBA	Total Beauty Analysis
V&V	Verification and Validation	UL	Underwriters Laboratories
UAV	Unmanned aerial vehicle	VSV	Vliegtuigbouwkundige Studievereniging
VFR	Visual Flight Rules	WFD	Work Flow Diagram
WBS	Work Break-down Structure	WRF	Weather Research & Forecasting
WLW	Wet Luchtvaart		

List of Figures

2.1	Mission constraints	4
2.2	RASP BLIP maps showing wind velocity and direction changing during the day at an altitude of 10 meter on Jan 8 th 2015.	5
2.3	Red line showing the mission's planned flight route	6
2.4	MATLAB flight simulation explanation	7
2.5	Fragment of a RASP BLIP map which shows the possibilities for soaring and the required wind direction and speed to do so. The compass shows the wind direction reference frame.	7
2.6	Resulting charts from MATLAB simulation	9
2.7	Operational Flow Diagram giving a quick mission overview	9
3.1	Body fixed reference frame for a paramotor	14
3.2	Different types of battery configurations ¹	19
3.3	Battery pack design	23
3.4	Final battery layout	23
3.5	Electric block diagram of the entire BMS including all communications between the batteries and the microprocessor as well as the software and hardware connections	24
3.6	To supply the torque the motor draws a certain current. A certain amount of the supply voltage is dropped over the resistance. The back-EMF increases proportionally with speed. Thus to increase the speed while the torque load stays the same a larger voltage needs to be applied to the motor.	26
3.7	The idealized speed-torque curve, power curve, efficiency curve and torque-current curve for a BLDC motor are all shown in this figure. It can also be seen that the motor cannot be operated at the stall-torque but only at considerably lower torque values. This is indicated by the continuous, short and very short operating regions.	27
3.8	Exact mapping of motor efficiency for the 3kW continuous power motor from Sonceboz. Torque is here displayed on the vertical axis. Such an indication of the efficiency for the different operating points is unfortunately not available for the motors that were considered.	28
3.9	In these figures the difference between the propeller connection options for two different motors that were considered can be seen	29
3.10	A CAD generated design of the drivetrain layout. The large gear ratio is clearly visible. The part of the drivetrain shown here will be located inside the fairing.	30
3.11	With this graph the belt type for the gearing can be selected.	31
3.12	Toothed gear such as will be used in our design next to a gear that is used in a commercially available paramotor.	31
3.13	MGM Compro HBC 18063-3 motor controller	34
3.14	Electrical block diagram of BLDC motor, ESC and input controller	34
3.15	Design of the input controller and interface. (The various switches that will be on the grip are not visible in this figure).	36
3.16	Electrical block diagram of the hand control and its connection to the BMS and ESC.	37
3.17	Plot of the ideal disk efficiency showing the constant efficiency lines versus thrust and speed at 12m/s cruise speed. It is obvious that having a large disk area and a low thrust setting is beneficial for the flight range, hence the large radius of the propeller.	40
3.18	Thrust and airspeed distribution of powered flight	40

¹<http://www.epectec.com/batteries/battery-configuration.html> Visited on Jan 6th of 2015

3.19	Aerodynamic comparison of existing airfoil (Clark-Y) and final generated airfoil using particle swarm optimization. Efficiency curves are calculated using XFOIL. It is clear that it is beneficial to generate airfoils for this specific case instead of using existing airfoils from internet databases.	41
3.20	Airfoil selection after iteration 1	42
3.21	General process for designing the propeller	43
3.22	Structural properties as a function of radial station of the blade, given in SI units	45
3.23	Visualisation of propeller noise at different distances	46
3.24	Final propeller layout	47
3.25	Strains on the final design of the propeller. All SI units	47
3.27	Free body diagram of the paramotor frame side view with forces due to the mass of the batteries (Fb), drivetrain (Fd), propeller (Fp) and complete paramotor system (Ft)	50
3.26	Sketch to visualize COG locations of the different parts	50
3.28	Results of F.E.M. analysis on paramotor frame. Cutout shows location of max. Von Mises stress location and value	52
3.29	Visualisation of driveshaft lay-out and free body diagram	53
3.30	Plot showing the relation between change in driveshaft mass per meter due to changes in R_{outer} , AL6061-T6 coincides with AL6161-T913 and AL2024-T6 coincides with AL2024-T86	54
3.31	Plot showing the relation between Von Mises stress and outer R_{outer} . Data point indicates design point with safety factor of 2 for AL7075-T6.	55
3.32	Neo String harness	55
3.33	The relation between friction and separation drag.	56
3.34	Lightweight axisymmetric low-drag fairing. Not in widespread use due to practical difficulties. ²	57
3.35	Streamlined bodies optimized for different criteria, in different ways.	58
3.36	Drag coefficients on frontal area of streamline bodies as a function of their fineness ratio ($\frac{length}{diameter}$). (<i>Hoerner</i> , 1965, section 6-18)	59
3.37	Streamlined bodies optimized for different criteria, in different ways.	60
3.38	XFlow results on cutting plane in 3D simulation for four different 2.2m 25% thickness axisymmetrical bodies at $11\frac{m}{s}$ and sea-level atmospheric conditions. The body with airfoil shape NACA66025 has the lowest drag.	60
3.39	XFlow results on fairing. Length of body 2.2m, velocity $V_{\infty} = 11\frac{m}{s}$	61
3.40	Drag coefficient on frontal surface of small plates or disks attached at 50% of chord, as a function of main-body thickness ratio, used to model interference drag of pilot's head. (<i>Hoerner</i> , 1965)	62
3.41	Drag coefficient on frontal surface of cylinder plotted against Reynolds number, used to model arm drag. (<i>Hoerner</i> , 1965)	62
3.42	Drag estimates of entire system for $V_{local} = 12\frac{m}{s}$ (local airspeed at head and arms is higher due to the air accelerating around the streamlined body) and $\rho = 1.2\frac{kg}{m^3}$	63
3.43	Statistical evaluation of the effectiveness of fins attached to the end of streamline bodies. (<i>Hoerner</i> , 1967)	64
3.44	Flow around airship with stern-mounted propeller, the same configuration as the proposed fairing with pusher prop (<i>Th. Lutz</i> , 1996).	65
3.45	CATIA render of fairing, showing dynamic pressure port on its nose, holes for head and arms, and fins.	66
3.46	CAD visualisation of final system design	67
3.47	Exploded view of final system	67
4.2	the convergence of the particles on the rastrigin function to the global optimum of (0,0)	71
4.1	The heavily multi-modal rastrigin function, used to test the effectiveness of particle swarm optimization on multi-modal problems	71
4.3	Discharge rate characteristics graph from the manufacturers data sheet	73
4.4	Discharge rate characteristics graph from the hobbyists data sheet	73

²<http://www.paraglidingforum.com/viewtopic.php?t=9081>, visited on December 19th, 2014

4.5	Device that can be connected between riser and carabiner, to measure in-flight loads.	75
5.1	Communication flow diagram of the electric paramotor with secondary batteries. . .	81
7.2	Reasons for paragliders not to paramotor, and reasons to be convinced for starting with paramotoring	92
7.3	Bar chart showing what respondent would like to use a paramotor for and what current paramotor gliders use their paramotor for	93
7.4	Gantt Chart representing Post-DSE Activities, needed to be performed for mission and sales	100
8.1	Visual representation of the PZero electric paramotor design	102
A.1	Requirement Discovery Tree	105
C.1	Functional Break-down Structure	115
D.1	Functional Flow Diagram Part 1	117
D.2	Functional Flow Diagram Part 2	118
J.1	General algorithm for particle swarm optimization. ω , ϕ_g and ϕ_f are optimization parameters.	126
L.1	Extract from the mail conversation with Russel Ogden, a professional paragliding test pilot, where he confirms that the 2-liner wing is safe to fly the paramotor with. . . .	131
N.1	Confrontation matrix SWOT analysis	136

List of Tables

3.1	Battery specifications by battery characteristics	16
3.2	Primary battery chemistry, characteristics and comments explaining the advantages and disadvantages of every specific type of battery cell ³	17
3.3	Rechargeable battery chemistry, characteristics and comments explaining the advantages and disadvantages of every specific type of battery cell ⁴	17
3.4	Composite characteristics, total surface needed for the casings and final total weight and cost ⁵	20
3.5	Wiring overview	22
3.6	Performance table primary battery (ER17505M)	22
3.7	Characteristics of the motor	29
3.8	Gearing characteristics	32
3.9	Different ESCs characteristics such as cost, weight, communication options and voltage sensing needed to make a good choice	33
3.10	Components required for the hand controller and costs	37
3.11	Example airfoil characteristics used as input for XROTOR	42
3.12	Input for calculating deflections in XROTOR, "i" being the blade section	44
3.13	Global and performance parameters of the propeller	46
3.14	Off-design performance data	46
3.15	Optimal Placement of System Components and Pilot	49
3.16	Assumed weights of subsystems for frame design and geometry of frame	51
3.17	Forces, compression or tension, in each beam with minimal beam cross-sectional area or moment of inertia and corresponding cross-section geometry designed for extreme loading case (7g+2 S.F.).	52
3.18	Material selection driveshaft design	54
3.19	Optimal driveshaft design results for different materials with a safety factor of 2 on the Von Mises stress	55
3.20	Pilot surface area estimates of exposed limbs.	63
3.21	Drag estimate of head and arms, with interference effects on main body taken into account.	63
5.1	Summary and nomenclature of team and project risks determined in the first phase of the project.	76
5.2	Commands CFD in figure 5.1	82
5.3	Change in battery percentage used caused by change in system parameters	83
5.4	LiPo cell total beauty analysis showing the environmental impact throughout the life cycle of the cell.	85
5.5	Results Sustainability analysis LiThio Cell	86
6.1	Used material and manufacturing process for all manufactured parts	88
6.2	Purchased Parts	89
6.3	Assembly Process	89
7.1	Paramotor design program characteristics	95
A.1	General Stakeholder Requirements	106
A.2	Requirement List Flight Strategy	106
A.3	Requirement List Energy	107

³<http://www.epectec.com/batteries> Visited on Dec 18th of 2014

⁴<http://www.epectec.com/batteries> Visited on Dec 18th of 2014

⁵<http://www.carbonwinkel.nl/> Visited on Jan 14th of 2015

A.4	Requirement List Drivetrain and Controller	108
A.5	Requirement List Propulsion Device	109
A.6	Requirement List Chassis	110
A.7	Requirement List Lift Device	111
B.1	First Budget Breakdown	112
B.2	Latest Budget Breakdown	113
E.1	Battery Terms 1 ⁶	119
E.2	Battery Terms 2 ⁷	120
E.3	Battery Terms 3 ⁸	121
F.1	General battery standards ⁹	122
F.2	Lithium battery standards ¹⁰	122
H.1	Wiring Type 1	124
H.2	Wiring Type 2	124
H.3	Wiring Resistances	124
I.1	Different Motors and their characteristics	125
M.1	Cost Breakdown for the whole paramotor	132

⁶<http://www.epectec.com/batteries/glossary-of-battery-terms.html#UN-Tests>, visited on Dec 19th, 2014

⁷<http://www.epectec.com/batteries/glossary-of-battery-terms.html#UN-Tests>, visited on Dec 19th, 2014

⁸<http://www.epectec.com/batteries/glossary-of-battery-terms.html#UN-Tests>, visited on Dec 19th, 2014

⁹<http://www.epectec.com/batteries> Visited on Dec 18th of 2014

¹⁰<http://www.epectec.com/batteries> Visited on Dec 19th of 2014

1 Introduction

"Paragliding is one of the purest ways of enjoying flight"

This is something that many people want to, and actually do experience each year as they go into the mountains to paraglide. Unfortunately, in the flatlands of the Netherlands there are no mountains to take off from. The only option is to soar along the dunes given the right wind conditions or to use a stationary winch on a long field. Some Dutch paraglider pilots also take up the motorised version, a paramotor, offering more flexibility. The big disadvantage of paramotors is that only combustion motors can guarantee long and far flights. These however are often perceived as noisy, smelly, and induce strong vibrations, taking away the experience of pure flying. One option to overcome this is to use an electrical motor instead. Since the advent of high-efficiency electric motors and batteries of high specific energy, this has actually become a feasible option. Unfortunately, the currently acquirable electrical paramotors are quite expensive and only offer a limited flight time of about 15-30 minutes, not comparable to the more than two hour flight time achievable using combustion-powered paramotors.

Therefore Bart Remes came up with the idea of designing an electrically powered paramotor, which is powerful and reliable enough to be able to cross the Netherlands from South to North within a day, covering a distance of 314 km with a minimum amount of landings.

This final report presents the work performed during the project and the resulting final design. It depicts the layout and characteristics of the whole system as well as the system design support and future plannings, such as prototyping, mission planning and market opportunities.

The report starts by clearly stating the mission plan, which describes the set goals, the operations and logistics needed to accomplish the mission and the strategy chosen to achieve the goals. After the mission plan, a thorough analysis of all subsystems is executed, including a recapitulation of the overall chosen system. The system analysis of the subsystems comprises their performance, material, aerodynamic and structural characteristics, as well as their function and incorporation in the total system. As soon as the system is analysed, it can be verified and validated. The procedures applied to do so are concisely described in the subsequent chapter. The final segment of the report covers the processes needed to support the desired final design. These supporting processes include a risk analysis, an analysis of the communications within the system, a thorough sensitivity analysis and a sustainability development strategy. Following these processes, the future of this project is reflected upon. As the intention is to actually execute this mission, a production plan for a prototype has been written, which can be found in the equally named chapter. Likewise, the market has been analysed, accompanying a business plan and the development logistics, which can be found in the last chapter. Finally, the report will be completed by a concise conclusion and recommendations.

2 Mission Plan

The mission plan is defined by the requirements set in the first phase of the project, which are repeated in table A.2. The mission goals follow from these requirements. However, the weather conditions and the air space regulations have a big influence on the mission plan as both of them set constraints on the route or strategy possibilities. They can nonetheless also be used in an advantageous manner.

The mission and its goals and challenges are firstly described in section 2.1. The chosen flight strategy and what it consists of is then described in section 2.2. Finally, some practical matters about the mission itself such as where to land and what the pilot should take with him are described in section 2.3. Section 2.2 and section 2.3 are then combined to conclude with the actual mission plan.

2.1 Mission Description

The mission plan is driven by the requirements as mentioned in table A.2 of Appendix A. The first requirement, EP-AST-FS-01, defines the mission; the Netherlands must be crossed by paramotor. It also defines the distance that needs to be flown in one day. The distance from the most southern point of the Netherlands in Limburg right up to the most northern point on Rottumerplaat is approximately 300 km. This will therefore roughly be the distance that needs to be covered in the final mission.

From the remaining requirements, the ones that have a major influence on the mission planning are EP-Ast-FS-02, EP-Ast-FS-05 and EP-Ast-FS-06, which comprise of the requirements that a minimal amount of stops should be used, regulations should be obeyed and hazardous weather has to be avoided. When looking at these requirements, one can immediately see that there should be a focus on reducing the number of stop as set in EP-Ast-FS-02, as regenerating a battery costs a lot of time and otherwise requirement EP-AST-FS-01 comes into danger.

The next one to be omitted, is the simplified route. When obeying the airspace regulations as has been set in requirement EP-Ast-FS-05, one will be obliged to avoid certain areas of the airspace. Hence, flying in a straight line is not possible.

2.1.1 Flight Route Constraints

The first aspect that has a major influence on the mission plan is the potential flight route. The flight route is dependent on the mapping of the airspace and the boundaries that come with it. As a paramotor pilot flies only considering Visual Flight Rules (VFR), he is not allowed to enter the regions of the airspace where flying Instrumental Flight Rules (IFR) is required. Paramotoring is allowed in the class E and G areas, and sometimes class C by exception. The biggest share of the lower part of the Dutch airspace is registered as class G. CTR's (control zones around airfields, figure 2.1a) are usually class C, thus need clearance from air traffic control, and it is not allowed to cross them without transponder. Also, cities and other built-up areas must be avoided, as they are devoid of emergency landing spots.

Next to the different classes, one has to take into account cities and other built-up areas. It is not allowed to fly over such areas as there is no possibility to land in case of an emergency. Another group of areas that needs to be avoided, are the CTR's. These so called control zones extend from the surface to a specified upper limit. They can be seen in figure 2.1a. They are usually situated around an airport, where air traffic control guides all air traffic operating to and from that airport. Hence, flying in the CTR is only allowed when having clearance from air traffic control, thus one

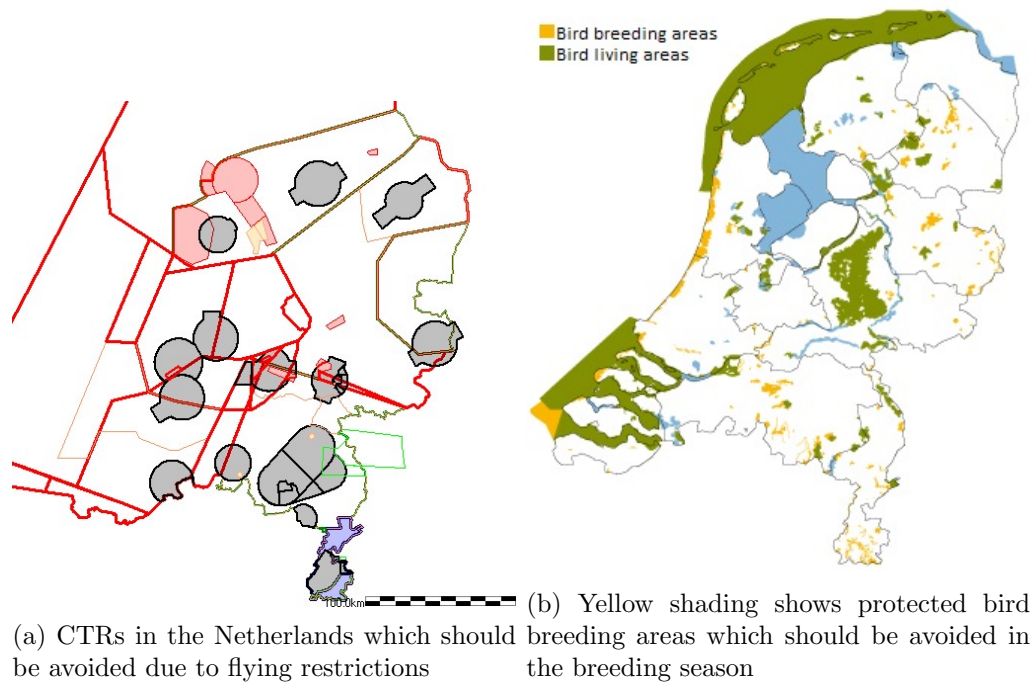


Figure 2.1: Mission constraints

needs a transponder to fly there. As a consequence CTR's are prohibited areas for paramotors and flying around them is what this missions' strategy will depict.

2.2 Flight Strategy

In a very preliminary calculation, using a speed of $10 \frac{m}{s}$, 200N drag and a 50% efficiency of the total system, it was estimated that approximately seventeen landings would be needed for recharging the electric paramotor. This assumes a 2kWh battery is used as an energy source. Current recharging techniques do not allow for recharging the battery seventeen times in a day, due to the time constraint set in the mission requirements. Alternatives for flying the mission in a less energy consuming way will therefore have to be investigated.

2.2.1 Flight Route

Due to the previously stated complication, the desired flight strategy will be obtaining a route that is as efficient as possible. One way to do so would be by using thermals to gain height, and fly from thermal to thermal. However, getting to a proper height using a thermal several times will take too long to be able to complete the mission in one day.

Another way to use less energy during the mission is by using a West to North-West wind together with the elevated dune landscape to perform soaring along the coast of the Netherlands. The motor can then be shut off during these periods. Soaring might also be a possibility over the elevated landscape in southern Limburg and the "Utrechtse Heuvelrug", which is a set of hills that is stretched north to south-east in the province of Utrecht. However, the CTR's as shown in figure 2.1a and the bird breeding areas as shown in figure 2.1b along both routes should be taken into account. The yellow shaded areas indicate bird breeding spots, and therefore landing during the breeding season should be avoided. However, flying over those areas is allowed¹. The third possibility would be to fly at high(er) altitude(s) where, especially at the coast, the wind is stronger and the less turbulent wind flows can be used to gain distance.

¹<http://www.compendiumvoordeleefomgeving.nl/indicatoren/nl1308-Vogel--en-Habitatrichtlijngebieden-in-Nederland.html?i=19-75>, visited on the 13th of January 2015

2.2.2 Mission Simulation Program

A MATLAB script was written in order to determine the amount of stops needed to complete the mission. In the following the functioning of this script is explained.

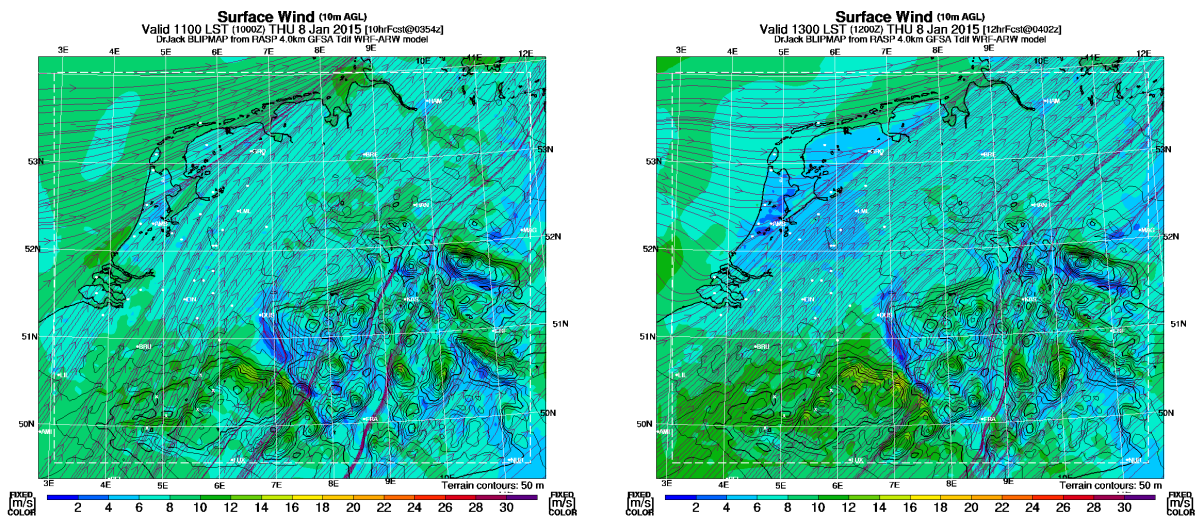
Loading the Wind Data

The written script retrieves its wind data from the ground wind Regional Atmospheric Soaring Prediction (RASP) Boundary Layer Information Prediction (BLIP) maps. Data is accumulated by assigning each pixel of this picture to a certain wind speed using the different colours of the map. Furthermore the wind vectors are used to determine the wind direction. The RASP BLIP maps are generated every half an hour from 08:30 to 19:00 and display the wind speed and its direction at ten meters above the ground, as shown in figure 2.2 ². The maps themselves are based on data processed by the Weather Research & Forecasting (WRF) model ³.

The MATLAB script determines the number of stops needed based on the final paramotor performance parameters such as:

- Overall efficiency
- System mass
- Drag Polar
- Pilot mass
- Battery mass
- Energy density

Furthermore the wind data are taken into account. The route to be flown is determined by 108 stations along the route. Although this seems like a fixed route, this can easily be altered. Regulations and constraints should be considered when designing a new route. The flight route that will be taken during the mission is shown in figure 2.3.



(a) Wind properties at 11 o'clock AM

(b) Wind properties at 1 o'clock PM

Figure 2.2: RASP BLIP maps showing wind velocity and direction changing during the day at an altitude of 10 meter on Jan 8th 2015.

²<http://rasp.kzc.nl/>, visited everyday from 1st to 13th of January 2015

³<http://www.wrf-model.org/index.php>, visited on the 9th of January 2015

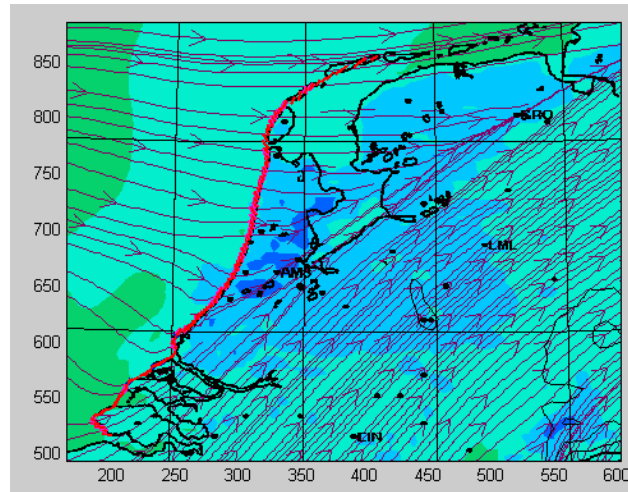


Figure 2.3: Red line showing the mission's planned flight route

Determining the Flight Path

At each station the local wind speed is determined and knowing the wind direction, it can be computed which flight path should be flown, in order to minimize the energy usage for the mission. Figure 2.4a clarifies the functioning of the MATLAB code. If the paramotor would simply fly in a straight line in between two stations it would never reach its destination, since the wind is pushing the paramotor away from its flight path. Therefore the wind speed as well as the wind direction need to be incorporated in the selection of the flight path. The program compares all possible paths to complete the mission, but for simplicity only three are shown in figure 2.4a.

Path A would require a high paramotor velocity, in order for the wind to have little effect on the flight route. In this case the drag caused by the wind is low, but the drag caused by the paramotor velocity is extremely high. The complete opposite occurs on route B, where the paramotor is facing more wind, but travels at a lower velocity. However the drag due to the wind speed is very high. The best compromise lies in between those two lines, indicated by line C, where the overall drag value for this section is minimum. All parameters of the flight between station 1 and station 2 are summarized in figure 2.4b. It should be added, that the program uses the standard mathematical angle definition, starting at 0 degrees on the positive x-axis.

This process is repeated for all stations, which results in the final flight path. The operating velocity for the paramotor is constrained by the wing's operating range, which is between $8.3 \frac{m}{s}$ and $19.4 \frac{m}{s}$. The airspeed has to stay within this range in order to create enough lift for the system. So even in tail wind conditions the propeller needs to create enough thrust to maintain a relative airspeed of at least $8.3 \frac{m}{s}$.

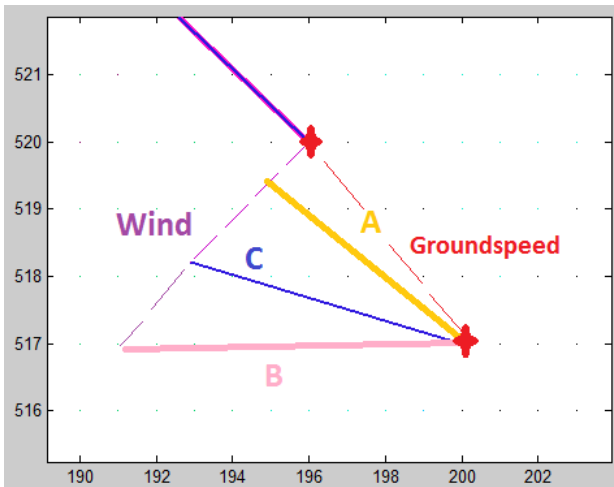
Including Soaring

Using wind data, a height map of the Netherlands and the expertise from paragliding pilots, it was determined at which locations on the route soaring is possible. As can be seen in figure 2.5, there are only soaring possibilities along the coast route. The "Utrechtse Heuvelrug" was evaluated not to be steep enough for soaring possibilities.

As can be seen in the previous image certain sections allow for soaring. The script uses the specific wind conditions between two stations to determine if soaring is possible. During the mission, 57% of the complete distance can be covered using soaring, which reduces the energy consumption tremendously.

Determining the Mission Day

Obviously, perfect and very beneficial wind directions could be considered to fly the mission. This would however mean, that the mission could only be performed when such a perfect day occurs. Up until now, only very recent RASP BLIPMAP data has been retrieved as there is no archive available. So far, the wind directions on the 8th of January 2015 were close to perfect. In approximately 92% of the places where soaring is possible, the wind directions are such that soaring can be performed. Only the wind speed is a little high on this particular day. Therefore, for illustrative purpose, the



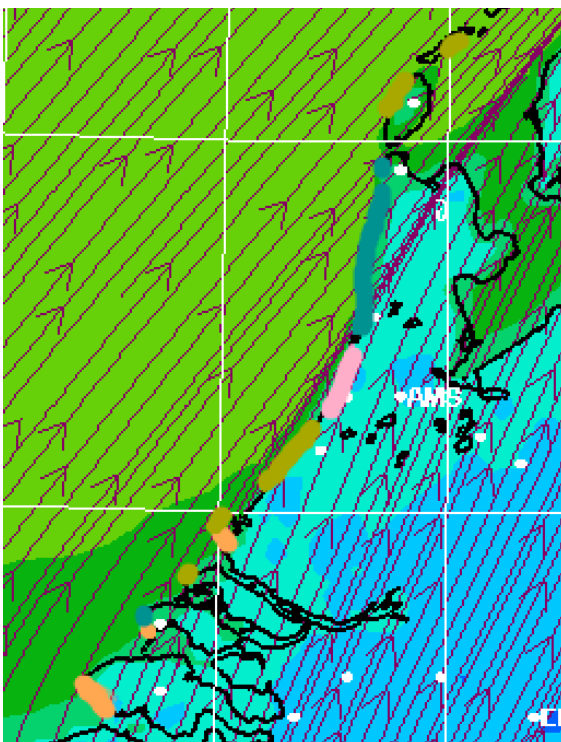
(a) Possible flight routes in section 1. Flight path C resulting in the least energy consumption.

```

Section 1
-----Flight path-----
Direction to next destination: 143.1301°
Flight direction: 170.3448°
Flight distance: 4743.2002m
Flight time: 0h 6min 44seconds
Thrust: 120.632N
-----Wind-----
Wind direction in which wind is blowing: 30°
Wind Velocity facing Paramotor: 4.4911m/s
-----Vector Triangle-----
Airspeed (8.33 m/s-19.44 m/s): 16.221m/s
Wind speed: 5.8333m/s
Ground speed: 8.14m/s
-----Soaring-----
-----no soaring-----
-----Energy-----
Velocity Paramotor: 11.73m/s
Energy used: 264.899Wh
Power needed: 2.3583kW
Energy left: 8605.726Wh
Energy left: 97.0138 %
-----Mission-----
# of Recharges : 0
Mission completed: 1.1201%
    
```

(b) Output section 1

Figure 2.4: MATLAB flight simulation explanation



	$\alpha_{wind,min}$ [°]	$\alpha_{wind,max}$ [°]	$V_{wind,min}$ [m/s]	$V_{wind,max}$ [m/s]
Orange	225	260	4	7
Pink	270	330	5	8
Yellow	290	345	5	8
Teal	235	310	5	8

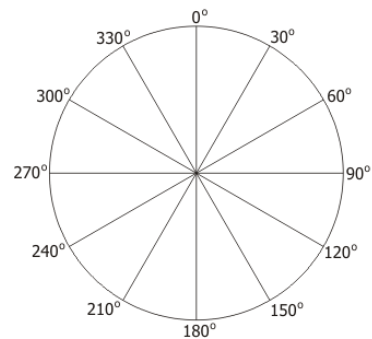


Figure 2.5: Fragment of a RASP BLIP map which shows the possibilities for soaring and the required wind direction and speed to do so. The compass shows the wind direction reference frame.

wind direction has been taken as on the 8th of January, but the wind speed has been reduced by $2m/s$ everywhere. However a logical wind pattern is still maintained, as it could occur on another day in the year.

In general it can be said that the slower the wind speed, the less energy is required, however the wind speed should be above $5\frac{m}{s}$ in order to allow for soaring.

Another great advantage of the wind on this particular day was that it turned during the day as shown in figure 2.2. When the mission was started, the wind conditions for the end of the mission were not perfect for soaring. However during the day, the wind conditions changed and at the moment at the end of the day, when the paramotor reached this section of the route, the wind would have turned in such a way, that it would allow for soaring.

Climb Rate Assumption

Another point that should be taken into account is the approach to be used for climbing. In certain areas where water needs to be crossed a minimum height of $50m$ is desirable. It was decided to have a small climb rate, since the minimum height during those parts of the mission could be easily reached with a low climb rate, when climbing is initiated early enough. However, the final system can achieve a maximum climb rate of $0.7\frac{m}{s}$ in emergency situations. Considering the flight simulation, climbing from ground to $50m$ height only uses 0.3% of the total energy consumed during this mission. Therefore climbing was considered not affecting the outcome of the mission and thus left out of the simulation.

Furthermore additional assumptions used in the simulation are:

1. Constant efficiency regardless airspeed
2. Constant vertical wind profile
3. Constant wind within a section
4. No thermals were included
5. Paramotor speed during soaring is the same as it would be during powered flight under the section's windconditions. Only required power was set to $0N$.

The first assumption would be easy to incorporate, but since the propeller design is based on the average airspeed and average thrust required during the mission, the efficiency value is also already averaged. Thus a more accurate model would not lead to much more precise results.

For assumptions 2,3 and 4 including a proper model of the wind profile would not require much work, but due to the small impact on the results and the time constrain for this project, it was not implemented.

Since the actual groundspeed of the paramotor during soaring is dependant on many factors that can not be read from the available data, assumption 5 was used.

Final Outcome

Finally, when using $22.5kg$ of primary batteries, with an energy density of $415\frac{Wh}{kg}$ the simulation results in:

- Total flight time: 7h 4min
- Distance covered: $294km$
- Total energy consumed: $5.65kWh$
- Maximum power: $2.67kW$
- Stops needed: 0

The required power over the course of the mission is presented in graph 2.6a. Furthermore the power distribution can be obtained in figure 2.6b. Here the soaring parts are clearly visible, as the required power during the soaring periods is $0kW$.

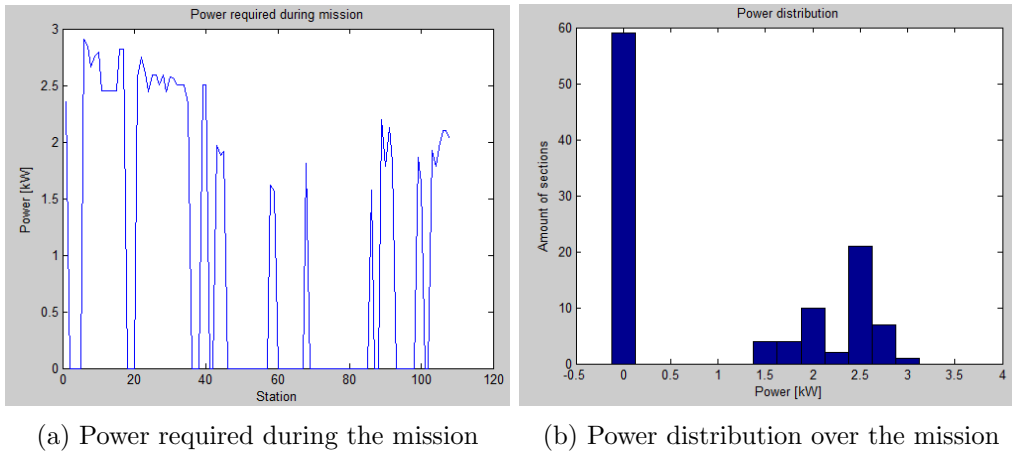


Figure 2.6: Resulting charts from MATLAB simulation

Based on these data, decisions on the design of the battery configuration and motor size could be made. In addition, a design point for the propeller could also be determined.

2.3 Operations & Logistics Concept Description

The mission will be flown in one go, how this is done energy-wise is discussed in chapter 3.3. Relevant for the mission plan with respect to this fact is that no in-between landings are needed and the regeneration logistics are not applicable either. An updated version of the operational flow diagram is given in figure 2.7. An extensive functional flow diagram of the mission is also shown in Appendix D, which is based on the Functional Breakdown Structure, shown in Appendix C. If the paramotor is adjusted and to be used in a broader sense than for the mission only, regeneration should be an option as discussed in section 7.1.

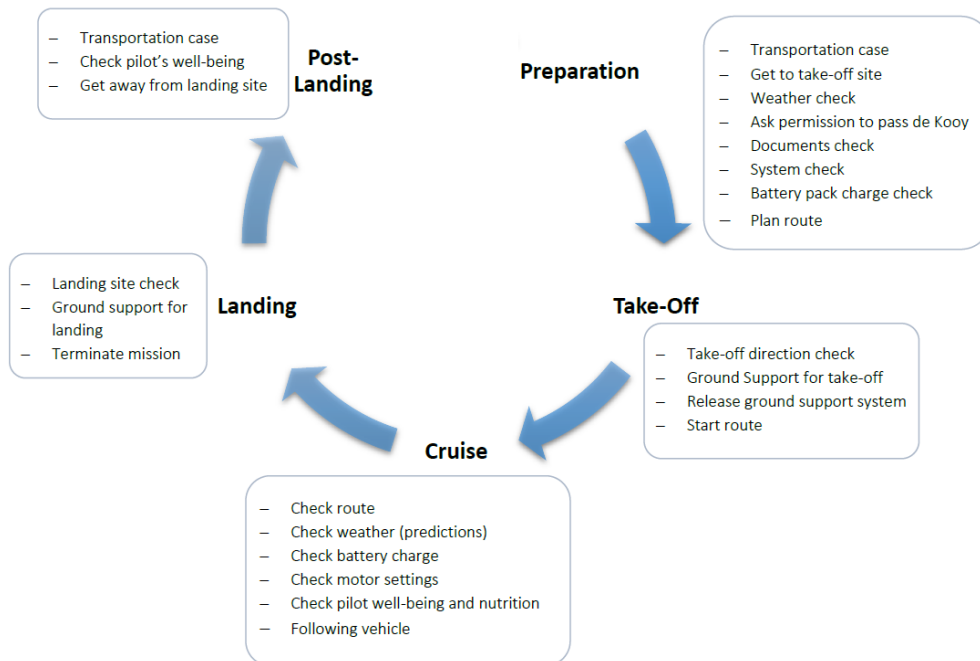


Figure 2.7: Operational Flow Diagram giving a quick mission overview

2.3.1 Mission Date

A possible date for the mission should also be investigated. Obviously, a possible window should be chosen, as the weather and wind conditions can only be investigated a couple of days beforehand or on the day itself. Besides that the mission should be carried out in one day, and it should be kept in mind that the paramotor is only allowed to fly from 15 minutes before sunrise until 15 minutes after sunset. The day picked should thus be long enough, but as the mission takes approximately 7 hours this is not a driving requirement.

When one chooses to fly outside the bird breeding season (15th of march and the 15th of august), this means that the mission cannot be flown in the summer and weather conditions should be watched carefully as rain or too cold weather cannot be used either. Due to the rain drops the airflow over the wing changes and the cloth of the wing gets too heavy, the wing will become uncontrollable and dangerous to fly. When it is too cold the pilot may get cold and not perform adequate anymore. In addition, the battery performance goes down (slightly) when it is colder.

Another point to be taken into account for preparation is asking for permission to fly past military airport de Kooy at den Helder. This can only be done on the day itself. However, a schedule for planned activities is available online, so getting permission should be possible.

2.3.2 Insurance and Documents Pilot

Insurance also needs to be taken care of before the mission. In order to be allowed to fly with a paramotor, the complete set (paramotor+wing) needs to be registered, and the bottom side of the wings needs to show its PH-registration number.

In order to get a newly designed paramotor registered and insured it firstly needs to be certified by the DULV (Deutschen Ultraleichtflugverbandes). This certification includes a noise check (max 50 dB when flying at 50 m height) and a test-pilot who flies it and sees how it handles.⁴

When a pilot is flying he should always have a set of documents with him. These documents include:

- A medical statement
- Personal identification
- Personal KNVvL certificate
- A logbook

In addition, the pilot needs to have a reserve parachute for safety. He is also obliged to carry an altimeter and wear a helmet.⁵

2.3.3 Maintenance

The paramotor has to undergo a list of pre-flight checks before starting the take-off procedure. This part of the mission plan has been determined in an earlier phase of the project. During these checks it can be determined if the harness, chassis, propeller and wing are still intact and suited for the mission. These parts will need to be repaired when damages are noticed, and if the damages are crucial, the mission will have to be rescheduled. As the mission should be carried out at once, there is no scheduled maintenance for these parts. Scheduled maintenance activities in the preparation of the mission and while building the paramotor do include the checking of bearings and if the belt gear is still under the right belt tension. Furthermore, the bearings are lubricated frequently, the brushless DC motor requires no maintenance, and the safety chute should be refolded twice a year. The battery pack is designed in such a way that the batteries don't leak or short circuit.

⁴<http://www.dulv.de/Motorschirm/Musterpruefung/Antrieb/K183.htm>, visited on the 10th of December 2014

⁵<http://www.knvv.nl/afdelingen/schermvliegen/regelgeving/>, visited on December 8th 2014

2.3.4 Take-off

Requirement EP-Ast-FS-03 describes a maximum take-off distance of twenty meters. As the wind conditions are beneficial on the day the mission is flown, a zero meter take-off should be possible, in particular with assistance from people on the ground, by using a leash to pull the paramotor into the air like a kite. A release system is attached to the hangpoints of the paramotor for easy detachment as soon as the paramotor is up to speed.

The benefit of having a zero meter take-off is that the movement of the legs during take-off can be limited which is beneficial for the cocoon design. Furthermore the propeller size can be increased, since no thrust is needed during the take-off phase. This change leads to an increase in efficiency of the propulsion device.

2.3.5 Following Vehicles

A following vehicle is required for safety reasons. As the mission is flown over land as well as over water both a car and a boat are needed. In Den Helder the car crew will transfer to a boat and the rest of the route is carried out over water, avoiding the sandbanks of the Wad.

The ground crew will consist of three people, including a chauffeur. The other two will both have a laptop with an internet connection. One of them will keep an eye on the expected weather and wind on the planned route while the other one checks if the pilot is still flying in the planned direction. This person will also keep in contact with the pilot to check his well-being. Together with the pilot the ground crew can decide on changing the planned route or, if conditions change drastically, aborting the mission.

2.3.6 Pilot Well-being

As the mission will take approximately seven hours, the pilot will need hydration and nutrition. Dehydration could threaten the mission as it will affect the pilots ability to make correct judgments and decisions as stated by the Iowa State University website: "Even a small drop in body fluids (1% of body weight, or 1.5 pounds in a 150 pound person) can impair performance"⁶. Furthermore it is advised that "During practice/competition 4 to 8 ounces of fluid should be consumed approximately every 15 minutes."⁷. This comes down to drinking 0.5 to 1L an hour depending on temperature and the intensity of the exercise. It is advisable to provide the pilot with the amount of fluid needed, based on estimated flight duration. Furthermore, caffeine and carbohydrates could be added to help the pilot stay focused and prevent hunger. Adding the carbohydrates could also decrease the amount of solid food that the pilot will need to consume in flight.

Approximately 3 litres of water and 0.4kg of energy bars/gels will be taken along on the mission. The water is put in a camel bag put on the pilot's belly.

Another point of well-being/safety for the pilot is communication with the ground crew. Every 15 minutes the pilot will contact the ground crew and give some general parameters from his flight just to see how he is doing. A slightly adapted smartphone with a headset built into the pilot's helmet will be taken along for this purpose. This smartphone will also have a GPS function to be able to follow the paraglider and have this data sent directly to the ground crew. The motor controller is also equipped with a GPS sensor which can be followed by the groundcrew, for redundancy.

Communication with the ground crew can also include tasks for the pilot to do some leg exercises. As the flight time for the mission is considerable, one could get trouble with the circulation of blood in ones legs. Hence, the pilot should be able to move his legs from time to time to avoid problems with his leg movement during landing. This point is also taken into account when designing the cocoon.

⁶<http://www.extension.iastate.edu/humansciences/fluids>, visited on December 16th 2014

⁷<http://www.extension.iastate.edu/humansciences/fluids>, visited on December 16th 2014

2.3.7 Motor Settings in Flight

To ensure maximum efficiency during flight, the pilot has to ensure that the motor is set at the right RPM suited for that specific speed. This should also be checked by the ground crew. The propeller has been analysed for off-design points, and the best RPM at the encountered speeds during the mission are given in table 3.14.

2.3.8 Landing

When the mission has been accomplished (or needs to be aborted due to unforeseen circumstances) a landing needs to be planned. As stated in article 8.1a WLW, aerial vehicles are only allowed to take-off and land from/on airports. However, article 8a.51 WLW is exemption to this. This article states that for certain categories, as set by the Ministry, temporary airports may be assigned. This then leads to the article 20 RvGL, which states the rules for airports in general, and article 26 RvGL, which specifically state the demands for the surroundings when taking off with a paraglider. In addition to article 20 RvGL, there is obviously still the prohibition of getting people or goods into danger, according to general Dutch law, so the landing site should be sought out carefully.

Since the first of August 2012, the whole of the Dutch coast has been assigned as an airport, with the exemption of having to follow all rules described in article 20 RvGL. This was done to take paragliding and deltaflyers who use the wind on the beach to take-off out of illegality. Before this date, soaring through the dunes was officially illegal as soon as a paraglider took off.

One may not just land anywhere; the exact legislation for where to land was discussed in the Mid Term Report. However, according to article 26 RvGL, in extraordinary cases, when one for example runs out of fuel, one may also land in protected nature areas. The pilot might also need some help when landing as he might be cold, tired and have poor blood flow in his legs, which may cause him to collapse upon landing. The ground crew should therefore be at the landing area beforehand.

In case the pilot has to make an emergency landing on the water, he has a hook knife with him to cut the paragliding system loose, as described in section 5.2.4. The ground crew will be in a boat close to the pilot to get him out of the water.

2.4 Conclusion Mission Plan

The mission will be flown from the south to the north of the Netherlands over a distance of approximately 300km. There should be a focus on designing the paramotor in such a way that it consumes the least energy as possible, in order to guarantee the least landings possible. This way, the mission can be fulfilled according to the requirements set in Appendix A.2.

The wind conditions play a huge role in whether the mission can be carried out and when and how this will happen. A MATLAB program was written to simulate the energy consumption of a certain route, taking wind conditions of a specific day into account. This way, decisions on the design of the battery configuration and motor size could be made. In addition, a design point for the propeller could be determined.

3 System Analysis

This chapter will show the detailed characteristic analysis of all system components. First an overview of the design is given in 3.1, followed by a more detailed description of all subparts in sections 3.3 up to 3.7.

3.1 Chosen Concept

The final concept was chosen by going through three main phases. First every possible design option for each part was determined and visualized in Design Option Trees (DOT). Many of those options were not feasible for the final product and therefore eliminated, whereas all feasible design possibilities were traded off against each other based on the requirements they need to fulfill and assigned weight factors. This process in the majority of the cases resulted into two to four concepts, which were combined into three overall design concepts. The final step was then to perform basic characteristic analysis on the chosen concept options and compare the range gain to make a final concept decision.

The final design, which was selected by the method as described above, can be briefly summarized as the following:

- **Energy Storage & Generation (section 3.3)**

It was determined that primary batteries will be used to perform the mission. To perform the mission without any stops, the overall weight will be extended by about 10 kg for more battery weight and therefore power output. For market sales the product will be equipped with rechargeable batteries to reduce the price and weight and increase sustainability. The rechargeable batteries will then be able to be charged via regular sockets.

- **Motor (section 3.4)**

A geared outrunner motor (Hacker A-80-10 & self-designed gear), delivering about 3 kW continuous power with a ratio of 1:5.5 will be used for the final design. This combination was chosen to match the power output of the batteries as well as the lower required torque of the propeller.

- **Motor Control (section 3.4)**

The speed controller will be bought off the shelf. The input controller and controller interface will be integrated in to one handheld grip.

- **Single Propeller (section 3.5)**

One wooden 2-blade propeller will be placed behind the pilot and connected to the motor via a driveshaft and the gearing. The propeller radius is selected to be 1 m, wherefore the propeller will be locked in horizontal position during take-off and landing to prevent ground strike.

- **Chassis Structure (section 3.6)**

The frame of the paramotor is attached to the wing, instead of to the pilot, in order to keep the propeller in a horizontal position at all times during the mission. Furthermore it supports the battery pack in front of the pilot and the drivetrain behind the pilot.

- **Aerodynamic Chassis Structure (section 3.7)**

A choice was made to not include a safety structure, in terms of a cage, but place the propeller at a safe distance to the pilot. To reduce drag, an airfoil shaped fairing will be used, covering the pilot and all system parts, which will be inflatable by pressure difference, inserting a small hole in the stagnation point. During the detailed design the exact layout will be determined.

- **High Efficiency Paragliding Canopy**

The wing chosen for the mission will be a competition wing as the Ozone Mantra R11, a two-liner with a shark nose wing profile. Such a wing will have a maximum glide ratio of 11.

3.2 Reference Frames

The used reference frame concerning the paramotor is shown in figure 3.1 below. The reference frame is body fixed.

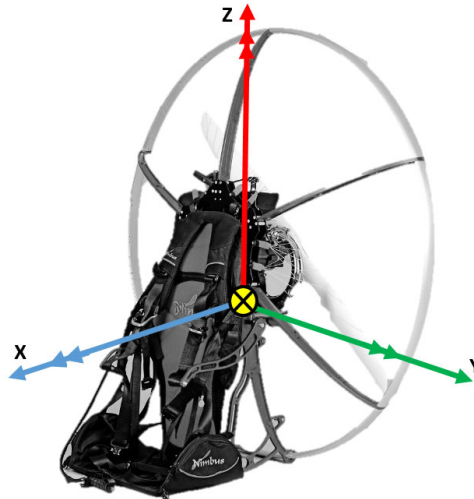


Figure 3.1: Body fixed reference frame for a paramotor

3.3 Energy Storage & Generation

This section covers the final design of the entire battery pack. First, a synopsis of the design choices made since the midterm is given, followed by the actual detailed design. The detailed design contains all the details on the battery choice, the development and assembly of the battery pack and the possible configurations of the batteries. After having discussed the batteries, the structural design, such as the casing and the wiring, is elaborated on. Last but not least, the performance of the system is analysed, followed by the final subsection which comprises the lay-out of the Battery Management System (BMS). A lot of new terms will be used in this section and therefore a list of battery terms is presented in Appendix E.

3.3.1 Design Choices Synopsis

In the Mid-term report for this project several different energy storage systems were analysed. The trade off method mentioned in the the system analysis section (section 3)

The following energy storage types were discarded on basis of the fact that they were found to be unfeasible.

- Static electricity
- Electromagnetic
- Kinetic energy

The energy storage type that was found to be feasible was the electrochemical energy.

Electrochemical Energy

- **Fuel cells** did not come out as the most suitable energy storage system. The biggest reason for this is the fact that fuel cells are too heavy to be used in the paramotor.
- **Flow batteries** were also found to be unsuitable for the paramotor design. Just like the fuel cells, organic cells are also too heavy for the design. Apart from this, it is a very new technology, and therefore these cells are unavailable at the moment which makes them impossible to be used in the design.
- **Rechargeable batteries** Were found to be the most suitable energy storage system for the paramotor design.

All data found for the midterm report (*DSEgroup6, 2014b*) was presented to the customer and project advisers before commencing with the detailed design. During this discussion the customer requested an analysis of primary batteries. Due to this request this section will include an extra analysis in which primary cells will be discussed and compared to secondary batteries. Since secondary batteries were found to be the best energy storage solution from the mid-term analysis, a direct comparison between primary and secondary batteries is sufficient to conclude what is the most suitable energy storage solution.

More details about the different energy storage systems can be found in the midterm report (*DSEgroup6, 2014b*)

3.3.2 Battery Pack Development

The design of the battery is fully dependant on two different features, firstly the characteristics of the batteries that will be used, and secondly the characteristics of the subsystems that the energy source needs to power. In this project that second part is the motor.

The characteristics of the energy source are defined by the manufacturer of the cell. This is therefore very clear once the final decision is made of what cell to use. From the scope of this project one of the most important characteristics of the cell will be the energy density and the maximum power that the cell can deliver.

The characteristics of the motor that influence the battery design are the input voltage and current that it needs. The motor that was chosen for the paramotor is the Hacker A80-10 This motor needs 36 volts and is further elaborated on in section 3.4.1.

The motor has been selected on basis of how much power is needed at different parts of the mission. The calculations for this are presented in the mission plan (flight strategy, section 2.2). For the battery design it is important to know the the maximum power that needs to be delivered. From the analysis in the flight strategy section this was found to be 2.6725kW.

Battery Characteristics

This subsection mentions the general battery characteristics. These characteristics determine the Battery choice and further battery pack development decisions.

Specifications by Battery Characteristics

As mentioned in the design synopsis of the energy storage, a comparison between primary and secondary batteries will be presented to decide what cell type will be used for the paramotor design.

Table 3.1: Battery specifications by battery characteristics

Specifications	Lead Acid	NiCd	NiMH	Li-ion		
				Cobalt	Manganese	Phosphate
Specific Energy Density (Wh/kg)	30-50	45-80	60-120	150-190	100-135	90-120
Internal Resistance (m)	< 100 (12V pack)	100-200 (6V pack)	200-300 (6V pack)	150-300 (7.2V pack)	25-75 per cell	25-50 per cell
Life Cycle (80% discharge)	200-300	1000	300-500	500-1,000	500-1,000	1,000-2,000
Fast-Charge Time	8-16h	1h typical	2-4h	2-4h	1h or less	1h or less
Overcharge Tolerance	High	Moderate	Low	Low. Cannot tolerate trickle charge		
Self-Discharge per month (room temp)	5%	20%	30%	<10%		
Cell Voltage (nominal)	2V	1.2V	1.2V	3.6V	3.8V	3.3V
Charge Cutoff Voltage (V/cell)	2.40 (float 2.25)	Full charge detection by voltage signature		4.20		3.6
Discharge Cutoff Voltage (V/cell, 1C)	1.75	1.00		2.50-3.00		2.80
Peak Load Current [best result]	5C -0.2C	20C -1C	5C -0.5C	> 3C - < 1C	> 30C - < 10C	> 30C - < 10C
Charge Temperature	-20 to 50C	0 to 45C		0 to 45C		
Discharge Temperature	-20 to 50C	-20 to 65C		-20 to 60C		
Maintenance Requirement	3-6 Months - (topping charge)	30-60 days - (discharge)	60-90 days - (discharge)	Not required		
Safety Requirements	Thermally stable	Thermally stable, fuse protection common		Protection circuit mandatory		
In Use Since	Late 1800s	1950	1990	1991	1996	1999
Toxicity	Very High	Very High	Low	Low		

From table 3.1 it is clear that the most suitable secondary battery type is the Li-ion, since they have the highest specific energy density.

Battery Chemistry

When comparing tables 3.2 and 3.3 it is clear that the primary batteries have a higher energy density than the secondary batteries. Therefore these cells would be more suitable for the mission. The only problem with the primary batteries is that they have a very low discharge rate and therefore a lot of them would have to be combined to achieve the demanded power.

Table 3.2: Primary battery chemistry, characteristics and comments explaining the advantages and disadvantages of every specific type of battery cell ^a

Primary battery chemistry			
Chemistry	Cell Voltage	Energy Density (MJ/kg)	Elaboration
Zincarbon	1.5	0.13	Inexpensive
Zinc chloride	1.5		Also known as "heavy duty", inexpensive
alkaline	1.5	0.4-0.59	Moderate energy density
(zincmanganese dioxide)			Good for high and low drain uses
oxy nickel hydroxide	1.7		Moderate energy density
(zinc-manganese dioxide/oxy nickel hydroxide)			Good for high drain uses
Lithium			No longer manufactured
(lithiumcopper oxide)	1.7		Replaced by silver oxide (IEC-type "SR") batteries
LiCuO			
Lithium			Expensive
(lithiumiron disulfide)	1.5		Used in 'plus' or 'extra' batteries
LiFeS2			
Lithium			Expensive
(lithiummanganese dioxide)	3.0	0.831.01	Only used in high-drain devices or for long shelf life due to very low rate of self discharge
LiMnO2			'Lithium' alone usually refers to this type of chemistry
(lithiumthionyl chloride)	3.0		Expensive
		1.4-2.52	
Mercury oxide	1.35		High drain and constant voltage
			Banned in most countries because of health concerns
Zincair	1.351.65	1.59	Mostly used in hearing aids
Silver oxide			Very expensive
(silver-zinc)	1.55	0.47	Only used commercially in 'button' cells

^a<http://www.epectec.com/batteries> Visited on Dec 18th of 2014

Table 3.3: Rechargeable battery chemistry, characteristics and comments explaining the advantages and disadvantages of every specific type of battery cell ^a

Chemistry	Cell Voltage	Energy Density (MJ/kg)	Comments
NiCd	1.2	0.14	Inexpensive
			High/low drain, moderate energy density
			Can withstand very high discharge rates with virtually no loss of capacity
			Moderate rate of self discharge
			Reputed to suffer from memory effect (which is alleged to cause early failure)
			Environmental hazard due to Cadmium - use now virtually prohibited in Europe
Lead Acid	2.2	0.14	Moderately expensive
			Moderate energy density
			Moderate rate of self discharge
			Higher discharge rates result in considerable loss of capacity
			Does not suffer from memory effect
			Environmental hazard due to Lead
NiMH	1.2	0.36	Cheap.
			Not usable in higher drain devices
			Traditional chemistry has high energy density, but also a high rate of self-discharge
			Newer chemistry has low self-discharge rate, but also a 25% lower energy density
Lithium ion	3.6	0.46	Very heavy. Used in some cars
			Very expensive
			Very high energy density
			Not usually available in "common" battery sizes (but see RCR-V3 for a counter-example)
			Very common in laptop computers, moderate to high-end digital cameras and camcorders, and cellphones
			Very low rate of self discharge
			Volatile: Chance of explosion if short circuited, allowed to overheat, or not manufactured with rigorous quality standards

^a<http://www.epectec.com/batteries> Visited on Dec 18th of 2014

If it is chosen to use primary cells, the battery pack would need to consist of a lot more batteries than when using secondary batteries. From a small analysis of a typical primary battery it was found that this would result in a minimum battery pack weight of 25.5 [kg]. If the weight requirement would not be flexible this would mean that primary batteries would not be a feasible option for the energy storage since the minimum weight needed to power the motor would be more than the total allowable weight of the paramotor design.

Nevertheless primary cells are a superior choice when compared to secondary cells. The biggest advantage of these cells is the high gravimetric energy density that they have. This is also the property with which the customer was eventually persuaded to increase the weight budget to incorporate this technology. Making the the primary cells an excellent choice for the energy storage. The battery with the highest energy density was therefore selected, this is the Lithium Thionyl Chloride (Li/SOCl₂) cell. A total of 839 cells are needed for the pack when using those cells.

Battery Standards

Appendix F shows the standards which the battery has to fulfill. This table can be used to find out what standards apply for the specific battery as well as to look up the standards that the off the shelf battery might already have.

Battery Pack Development Time Line

There is not enough time or experience to develop entirely new battery packs from scratch. The battery pack development process takes up to 6 weeks, which is more than half the time available. Also, the production of the actual battery packs takes between 6 and 18 weeks, which is double the time available. So, that is just not feasible. However, not all steps should be omitted. The battery pack application review and scope development and refinement should be performed. These steps define the requirements for the battery pack and comprise the research needed to choose the right batteries. Lastly, some certification will be necessary to legally use the battery pack. Even though the pack will not be designed from scratch, part of it will be custom designed, like the configuration and assembly. Those will be discussed further in the coming sections.

3.3.3 Battery Pack Assembly

As a specific certain power output is needed and a certain potential, the cells need to be combined such that they provide these values together. Cells can be connected in two different ways. The first is called "in series" and the second "in parallel". When cells are connected in series, their positive terminal is attached to the negative terminal of another cell. With this method, the final total voltage of the battery pack is the sum of all the individual voltages of the cells. In parallel means that the positive terminals of different cells are connected and so are the negative terminals. In this case the total current of the battery pack is the sum of the currents of the individual cells.

The configuration of the system and space available for the battery pack also influence the assembly. One has to take into account how much space there is and how much it is allowed to weigh.

Next, the battery pack needs to be connected to the system. The connection between the pack and the device is usually made using vinyl clad electrical wire that conforms UL requirements. This wiring has the standard colors: red for positive and black for negative. Thermal protectors are used to prevent overheating and/or overcharging the battery. These components are connected tot the battery with a direct line circuit. The packs are spot welded together using nickel foil. Nickel does not oxidize easily and had a good corrosion resistance, furthermore it is strong.

Battery Enclosure Design

There are several encapsulation techniques that are commonly used in the packing of batteries. Some batteries are installed inside the machines which they power. Other batteries sometimes serve a mechanical function and are then for example mounted externally. When they are mounted externally a casing of injection moulded plastic is commonly used. For all battery enclosure designs there are some overall points to consider when designing the battery enclosure. One of these overall considerations are the thermal effects. Tolerance should be left to account for potential swelling of the battery pack. lithium pouch cells can for instance swell up to 10% over their lifetime. To be able to dissipate the heat and exhaust gasses of the cell vents can be used in the battery enclosure design.

Battery Potting & Encapsulating

Battery potting is used to shield the battery from the shocks and vibrations as well as against moisture corrosive agents and solvents. Potting can also be used to achieve electrical insulation, heat dissipation as well as flame retarding. Potting works by completely or partially filling or embedding an enclosure. The most common potting compounds are polyurethane, acrylic, epoxy resin, and silicone. The different potting compounds all have different properties.

Battery Cell Configuration

Different possible battery cell configurations are presented in figure 3.2.

- F-type cells
- L-type cells
- Nested type cells
- Cubic or composite F-type
- Circular type cells

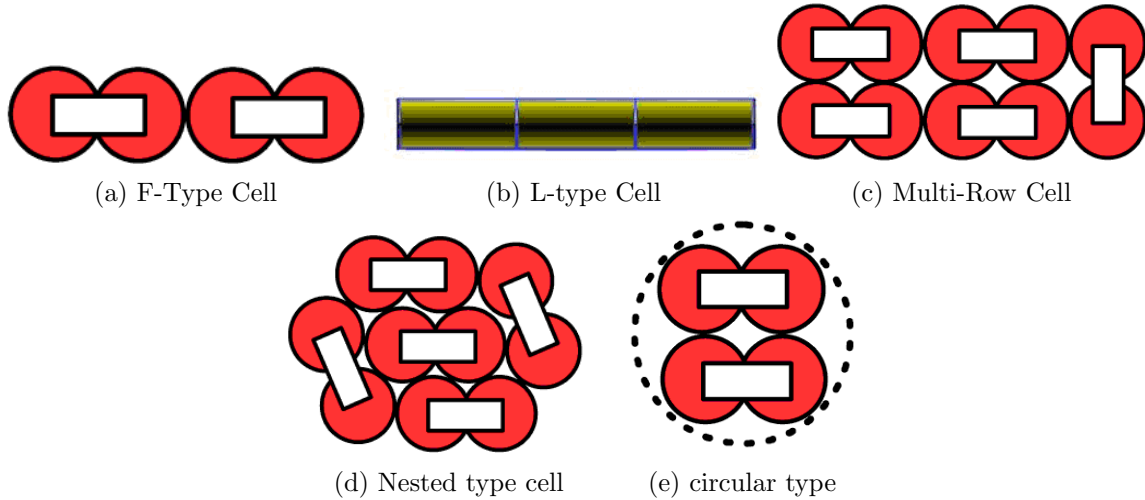


Figure 3.2: Different types of battery configurations ^a

^a<http://www.epectec.com/batteries/battery-configuration.html> Visited on Jan 6th of 2015

3.3.4 Final Battery Pack Design

In this subsection, the final design of the battery pack used for the mission will be discussed and analysed. This contains the set-up of the battery pack, but also the supporting systems such as the casings, the wiring and the supporting structure.

Final Battery Pack Configuration

As mentioned previously the configuration of the battery pack determines the output power of the pack. Four things are of importance when selecting the pack configuration.

- Maximum peak power needed (kW) - The mission requires 2.6725kW as peak power (found using mission plan program, section 2.2).
- Total energy needed (kWh) - The mission requires 5.1978kWh for the whole journey (found using mission plan program, section 2.2).
- Voltage requirements/limits by motor (V) - The motor requires 36V
- Current requirements/limits by motor (A) - The current limit is a maximum of 160A

The detailed power settings and total capacity needed for the mission were found using the mission planning program. The results of this analysis can be seen in Appendix G.

Casing

The casing consists of two parts, the casing per module and the main casing which contains the entire battery pack and provides the structural support.

Module Casing

As the complete battery pack consists of 839 cells in total as was stated earlier in subsection 3.3.2, the pack is divided into six modules in order to decrease the threat of damaging the entire pack in case only one or a few cells fail. The modules will all have their own separate thin casing made out of woven glass fibre sheets, laid up with fire retardant resin, in order to ensure the best fire retardant characteristics. In table 3.4 one can find the specifications of the type of glass fibre sheet that was chosen and the weight per square meter. $0.1342m^2$ is needed per module casing. In order to ensure proper handling and shape maintenance of the boxes, 3 layers will be laid up by hand. The total amount of glass fibre needed for the boxes is then $3.12m^2$ when taking a safety margin of 1.3 to account for production losses.

Table 3.4: Composite characteristics, total surface needed for the casings and final total weight and cost ^a

	Glass fibre	Carbon fibre
Weight resin [$\frac{g}{m^2}$]	39	184
Weight fibre mat [$\frac{g}{m^2}$]	49	160
Weight total laminate [$\frac{g}{m^2}$]	88	344
Thickness laminate [mm]	0.054	0.257
costs [$\frac{€}{m^2}$]	8.35	29.28
Layers	3	4
Thickness casing [mm]	0.162	1.028
Surface needed [m^2]	0.1342	1.56
Price [€]	4.37	237.52

^a<http://www.carbonwinkel.nl/> Visited on Jan 14th of 2015

Outer Casing

The main casing provides the structural stability and holds all the modules together. As was explained earlier, the battery pack is divided into six different modules. This configuration determines the dimensions of the casing. The biggest surfaces are the front and back plate, those are 353.5mm x 157.5mm. The sides are 157.5mm x 245mm and the top and bottom surfaces are 353.5mm x 245mm. As this case needs to provide enough strength to cope with the in-flight forces and the weight of the total battery pack, it was chosen to make it out of carbon fibre reinforced plastic. The inside will be covered with a layer of fibreglass to ensure electrical insulation. Carbon fibre is chosen for its low weight and high tensile strength. In table 3.4 one can see the characteristics of the carbon fibre type chosen. As carbon fibre is a non-isotropic material, the strength and characteristics of multiple layers of carbon fibre laid-up in different angles reach beyond the knowledge of this group and project and in the end a commonly used thickness will be chosen. Hence, this is how the amount of four layers was chosen. Four layers of carbon fibre combined with a fire retardant resin, will provide enough strength and stiffness to cope with the different loadings. The total surface of carbon fibre sheets that will be needed for the entire casing, combined with its costs and weight are shown in table 3.4.

In case the calculations of the required thickness of the walls would have been done for an isotropic material, some assumptions should have been made. The first would be the stress to be evenly distributed over the surface of the walls and the second would be that the walls are treated as fully clamped beams. With Roark's formulas (*Young and Budynas*, 2002), which can be seen underneath, the thickness would then have been calculated.

$$\sigma_{max} = \frac{\beta qb^2}{t^2} \quad (3.1)$$

With equation 3.1 one can determine the maximum stress σ . β is a dimensionless quantity depending on the ratio between the long side and the short side of the panel, t being the thickness, b is the

length of the short side of the panel and q is the distributed load which can be determined with 3.2. All SI units.

$$q = \frac{m_{battery}a}{A} \quad (3.2)$$

With equation 3.2 one determines the distributed load over a panel. Here the variables consist of the mass of the battery $m_{battery}$, the acceleration a and the surface of the panel A . All SI units.

$$y_{max} = \frac{\alpha b^4}{Et^2} \quad (3.3)$$

One uses equation 3.3 to determine the thickness of the walls by implementing E , the Young's modulus of carbon fibre, α which again is a dimensionless constant depending on the ratio of the long and short side of the panel, t and b are the thickness and the length of the short side of the panel. All SI units. It must be noted that α and β are dependant on material choice and are not the same. Both equation 3.1 and equation 3.3 should be used to determine the minimum thickness of the walls.

Support Struts

The support struts are aluminum 7075-T6 bars which secure the total battery package to the paramotor structure. They should be able to carry the weight of the entire battery pack times the highest loading case of $7g$. By using the equation for maximum tensile stress, a minimum surface of $1.15mm^2$ is found. As this is very small, a more common surface will be chosen of approximately $1cm^2$. The cross section will have a thickness of 5mm and a width of 20mm. This cross section will ensure more than enough strength. The bars are screwed to the battery casing and mostly support the forces in vertical direction. In order to also ensure more than enough security in the horizontal field, especially in the x-direction, a strap will be attached to the struts, which will go around the complete battery pack. This strap will be made of Nylon-66 as this kind of nylon is lightweight and has a good tensile strength of 60-80Mpa¹.

Wiring

The wiring of the battery is dependant on the configuration of the battery. The configuration of the battery and its sub parts are presented in section 3.3.5. The wiring needed consists of 2 types of wire, the first type is wiring that can withstand 1A connected to the 84 series packs the second wire should withstand the current of all these 84 wires from the series packs after they are combined: 84A. The choice for what type of wiring to used was based on a combination of lowest resistance together with lowest weight as well as availability. This resulted in insulated standard Copper wiring.

The resistance of the wiring can be found in equation 3.4, with R = resistance [Ω], L = length of conductor [mm], A = cross-sectional area [mm^2], ρ = resistivity [Ωmm] and $\rho_{Copper} = 1.724 * 10^{-8}$.

$$R = \rho \frac{L}{A} \quad (3.4)$$

The cross-sectional areas of the wiring is defined by gauge standards table 3.5 mentions the gauge types used as well as the lengths of the wiring needed per gauge type. A detailed overview of the wiring length calculation and the wire resistances can be found in Appendix H.

The connection of the wiring (wire type 1) to the series pack (image 3.4a)) will be by soldering. The connection of the 84 Type 1 wires to the Battery Management System (BMS) will be by directly soldering them to the PCB, on which they will be combined resulting in a Type 2 wire. The connection of the 84 Type 1 wires to the Type 2 wire which leads the current to the motor on the side without BMS will be by using a bullet connector.

¹http://www.engineeringtoolbox.com/young-modulus-d_417.html, Visited on the 18th of January 2015

Table 3.5: Wiring overview

Wire type 1 [36V, 1A] -AWG 29 [d: 0.286mm]	
Total length needed [mm]:	24066
Wire type 2 [36V, 84A] - AWG 7 [d: 3.664 mm]	
Total length needed [mm]:	1191

3.3.5 Battery Pack System Analysis

In this final subsection, the battery performance, its structural characteristics, as well as its material characteristics of the final configuration and the BMS will be briefly discussed.

Performance Analysis

Table 3.6: Performance table primary battery (ER17505M)

LiSOC12 - ER17505M	
Test current I [A]	2.8
Measured capacity [Ah]	2.8
Diameter [mm]	17.5
Length [mm]	50.5
Weight [g]	26
Price per cell [euro]	1.37
Cut-off voltage [V]	2
Voltage battery cells [V]	3.6
maximum recommended continuous current [mA]	1000
Highest discharge rate [C-Rate]	0.357
batteries in series battery pack for 36 V	10
Voltage battery pack [V]	36
Power (W) [P=V*I]	100.8
Current constant discharge [A]	1
Power constant discharge [kW]	0.036
# of battery packs in parallel	84
Safety factor [SF]	1.13
total amount of cells	840
Energy density [Wh/kg]	387.69
Power needed for engine kW [peak power *(1+SF)]	3.0199
Capacity battery pack [Kwh]	8.4672
Weight battery pack [kg]	21.84
Price battery pack [euro]	1148.792521
Price battery pack + shipping [euro]	1358.792521

Notes:

- The price of several parts of the battery are from suppliers that demand payment in dollars, and therefore the euro price in the table will change depending on the ordering date. The exchange rate used for this table is that of 18-01-2015: €1=\$1.1553.
- The price and weight of the cell were found online. ²

²http://www.alibaba.com/product-detail/A-3-6V-3000mAh-High-Quality_1146532503.html, Visited on the 18th of January 2015

- A safety margin was taken for the peak power. This safety margin consists of 7 % for difference in energy density of what the manufacturer stated compared to what was found from test results (see verification and validation chapter 4.4. Another 6% safety margin is implemented for safety, one can imagine that if the peak power needed for the mission was also the maximum power available, any decrease in power [for example due to wear or manufacturing errors] could lead to a crash. The same holds for a situation in which more power would be needed than expected. This resulted in a total safety margin of 13% ($6\%+7\%=13\%$).
- A potential of 3.6V per cell was used in calculations instead of the lowest discharge voltage because of the excess capacity of the battery, only 5.1978 kWh is needed and the battery configuration has 8.46743kWh and therefore the cell potential will not decrease during the mission.

From table 3.6 it was found that the battery pack needs 10 cells in series to achieve 36V, and 84 of these packs in parallel to achieve the peak power of $2.6725[\text{kW}] \cdot 1.13 = 3.0199[\text{kW}]$

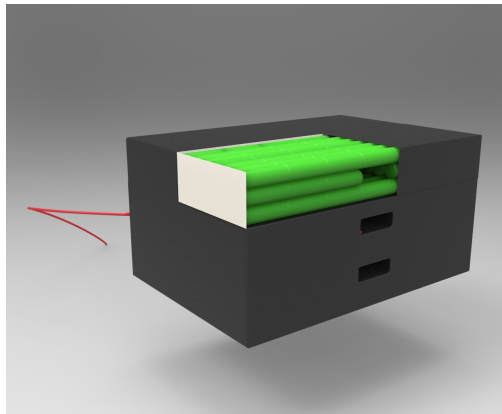
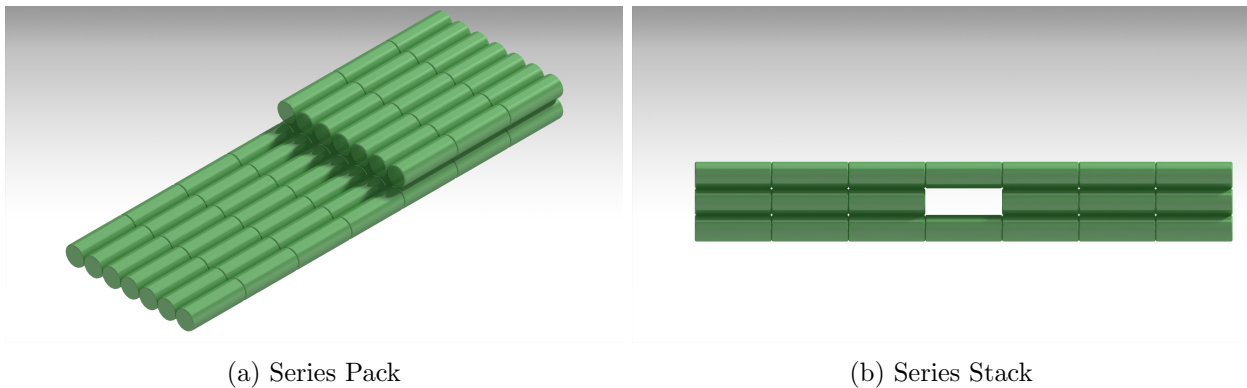


Figure 3.3: Battery pack design

The battery pack consists of series packs (figure 3.4a): seven batteries combined in L-type configuration (figure 3.2b). The extra three cells needed in series to achieve ten cells in series are also combined using the L-type configuration and this three cell combination is then connected to the other seven cell configuration using a F-type configuration (figure 3.2a). The cells connected in L-type configuration are held together using plastic wrapping this is chosen to decrease the amount of wiring needed and thereby decreasing resistance and weight. Two of these series packs (see figure 3.4a) are stacked resulting in series stacks (figure 3.4b). Seven of these series stacks are combined next to each other forming the modules. In total the battery pack will have 6 modules, two stacks of three modules next to each other. All connections between cells and wiring will be made by soldering. As can be seen in figure 3.3 the battery pack has three holes which provides some cooling, this prevents temperature increase in the battery pack. Furthermore the wiring can then pass through these channels.



(a) Series Pack

(b) Series Stack

Figure 3.4: Final battery layout

3.3.6 Battery Management System

A Battery Management System (BMS) is needed to ensure safe usage of a battery pack. The BMS has multiple functions and can be programmed according to the purpose of the mission. In this case the battery pack should ensure enough energy to fly over the Netherlands in a safe way. The function of this BMS mainly consists of the detection of improper loading of the batteries and communicating with the pilot and the motor controller. In the block diagram in figure 3.5, one can see the circuitry of the BMS.

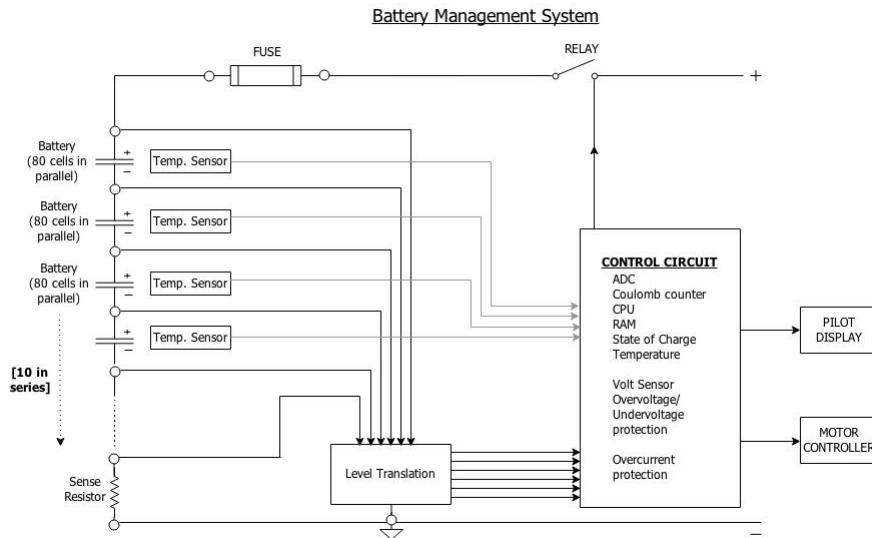


Figure 3.5: Electric block diagram of the entire BMS including all communications between the batteries and the microprocessor as well as the software and hardware connections

The block diagram shows the working of the complete BMS. When drawing the complete circuit of the BMS, this includes all battery packs connected in parallel as well as in series, all protection systems and all communication flows. The control circuit is a microprocessor that processes all data from the sensors. After that it gives commands to the relay, communicates updates to the pilot and sends data to the motor controller.

The circuit starts at the top right corner, which is the positive pole of the battery pack. From there the current flows through the relay, which is in this case a simple switch controlled by the microprocessor. Then it continues on and flows through a fuse, which is a secondary protection, which in case of a too high current or short circuit will brake and stop the current. After the fuse all batteries are connected. The potential difference of the batteries in series is measured and sent to the microprocessor via the level translation. The level translation measures the potential differences and converts those to a usable signal for the microprocessor. Next to the potential differences which go to the volt sensor in the microprocessor, temperature sensors are placed on strategic spots in the battery pack, where the temperature is expected to rise the most. These sensors provide the measured data to the microprocessor which communicates them to the pilot display and in case of overheating will open the relay. Lastly a sense resistor, or so called shunt resistor, is placed in the loop. The current is measured using a shunt resistor, the potential over the shunt is also translated to a usable signal for the microprocessor. This low resistance resistor can measure high currents by measuring the potential over it. It also provides an other extra safety measurement to the entire circuit.

3.4 Motor & Controls

In order to convert the electrical energy of the batteries into mechanical energy for the propeller a brushless direct current (BLDC) motor is selected. The process of selecting a suitable motor

is detailed in this chapter. This type of motor needs an electronic speed controller (ESC), which commutates the windings, to be able to run. To enable safe and reliable control of the motor, safety features of various speed control types are considered. For the complete system to be safe, the throttle signal that the ESC receives from the hand control needs to be reliable. Furthermore, the throttle needs to be able to give commands that put the propeller in horizontal or vertical position. To perform these and other functions a throttle control design is made specifically for this paramotor. This will be shown in the last section of this chapter.

3.4.1 Motor Selection Considerations and Final Choice

The BLDC motor was chosen as the most suitable type for our design, because of its high specific power and efficiency. It would be optimal to have a motor that is specifically designed for the exact needs of the mission, which would have a very high efficiency and power density for a low price. For example a direct drive motor could be designed which is optimally suited for the rotational speed of this paramotor, which requires a much lower rotational speed than what is generally provided by the commercially available BLDC motors. However, a lot of expertise is required for designing an efficient motor.

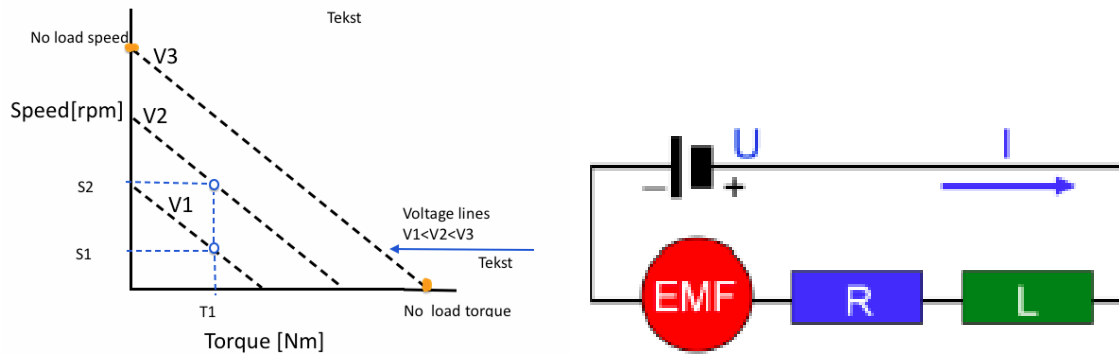
Expert advice about self-designing a motor was sought. Professor of electrical engineering and specialist in the field of electrical machines Henk Pollinder indicated that designing a motor usually is done in a nine-month graduation project. In these nine months the motor is only designed and not built or tested. It was thus decided that the duration of this project was too limited to consider this as a feasible option.

Motor selection thus comes down to comparing several off-the-shelf options. Motor options were researched while desired propeller speed, required power for the mission and maximum power available from the batteries were still varying parameters. This resulted in a list of motors which all possess favourable characteristics such as a low price, high efficiency and high power density. Both direct drive and geared motors were included. Whether a motor's higher efficiency or another motor's lower weight would result in a larger achievable range was evaluated with the equation 4.1. Furthermore, cost was considered as well as the possibility to mount the motor to the propeller and the rest of the frame. The complete list of motors can be found in Appendix I.

Speed-torque Characteristics

Not only the amount of power that the motor can deliver needs to be considered but also the amount of torque that the motor can produce and at which speed it can deliver this. The speed-torque characteristic of a BLDC motor is a linear curve between the no load operating point and the stall torque as can be seen in the dotted line in figure 3.6a³. The no load operating speed and stall torque of the motor depend on the motor design. For example motors with stronger magnets will have a steeper speed-torque curve.

³<http://www.orientalmotor.com/technology/articles/article166-1e.html>, Visited on 19th January of 2014. Figure was edited.



(a) The principle of speed control can be seen in voltage of the supply is divided over three parts, this figure. For the motor to run at a higher speed the back-EMF, the resistance of the windings and at the same torque a larger voltage is necessary. the winding induction.

Figure 3.6: To supply the torque the motor draws a certain current. A certain amount of the supply voltage is dropped over the resistance. The back-EMF increases proportionally with speed. Thus to increase the speed while the torque load stays the same a larger voltage needs to be applied to the motor.

This curve is an ideal curve. It neglects the effects of winding inductance which causes distortion at high speeds and the effect of magnetic saturation at high torque. Furthermore it only takes into account the losses in the windings. Core losses in the lamination iron and bearing friction are ignored.

The motor needs a larger current to deliver a larger torque. For an ideal motor the relationship between torque and current is described by equation 3.5. Where k_t is the torque constant. It is a characteristic of the motor design, it depends on the geometry and flux densities of the motor.

The speed at which the motor turns at a specific torque depends on the amount of voltage that is applied to the motor. For the motor to operate at the same torque with a higher speed, the voltage needs to be increased, such as can be seen in figure 3.6a.

The induced voltage of the motor is proportional to the rotational speed. For an ideal motor this can then be described by equation 3.6 (J.R. Hendershot, 1994). In this equation the constant k_e is the back-EMF constant. This constant depends on the same design factors as the torque constant and is essentially the same. Since they are often measured differently and expressed in different units they are usually seen as different constants. However when expressed in the same units the relationship is described by equation 3.7.

$$T = I * k_t \quad (3.5)$$

$$V_e = k_e * \omega \quad (3.6)$$

$$k_e = k_t \quad (3.7)$$

The motor can be considered as an electrical circuit where the supply voltage V_s needs to overcome the resistance of the motor, the inductance of the motor and the back EMF, such as is indicated in figure 3.6b⁴.

In DC motors the winding inductance can be neglected. The supply voltage is then related to the back-EMF constant, current and motor resistance by equation 3.8.

$$V_s = V_e + RI \quad (3.8)$$

⁴http://www.maxonmotor.com/medias/sys_master/root/8803450617886/maxonDCmotor-Notes.pdf?attachment=true, Visited on 19th of January 2014

Operating Regions and Efficiency

Electrical and thermal limits make it impossible to operate the motor continuously at all possible operating points. Operating the motor at the current required for stall torque is normally not even allowable for a short time, since it might either demagnetize the magnets, destroy the power transistors or burn winding insulation.

Figure 3.7⁵ visualizes the typical operating region of the motor. The motor can be operated continuously only in a small operating region, typically up to about 30% of the stall torque and can be operated for short periods up to 50-60% of the stall torque. The motor can be used in the short term operating range as long as the accumulated heating does not cause the temperature of the motor to rise above its short-term rated value. Consequently, sufficient cooling will allow the motor to run at higher current and consequently torque values.

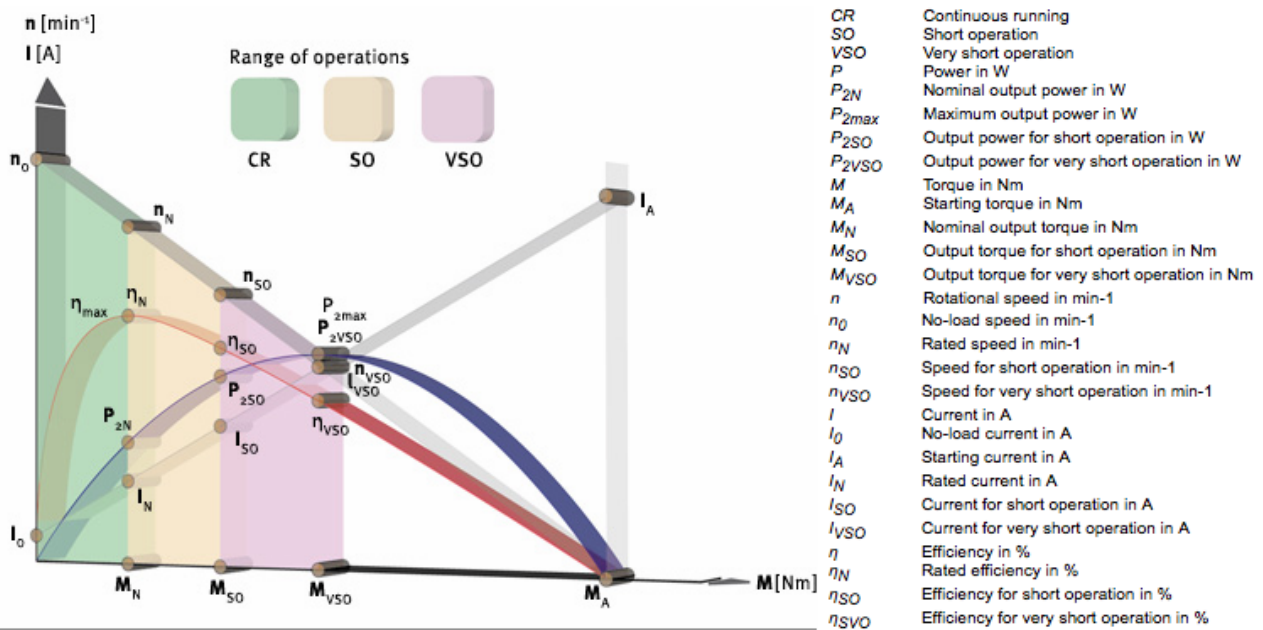


Figure 3.7: The idealized speed-torque curve, power curve, efficiency curve and torque-current curve for a BLDC motor are all shown in this figure. It can also be seen that the motor cannot be operated at the stall-torque but only at considerably lower torque values. This is indicated by the continuous, short and very short operating regions.

Furthermore the motor operates more efficient at one operating point than another. In figure 3.7 a power line and efficiency line can also be seen. The use of these graphs in predicting efficiency for a certain motor is however limited, since these again do not take into account core losses, which are a big factor in the overall motor losses and thus play a large role in the efficiency of the motor. Also certain characteristics of the motor need to be known in order to draw such a curve. Although some manufacturers publish extensive data sheets with all relevant motor constants, indications of operating regions and efficiency levels, this is not the case for most of the manufacturers of the large, cheap and lightweight BLDC type motors that were considered. Sufficient data in order to determine speed-torque and efficiency curves was not always available. Motor manufacturers often specify the k_v value. It relates to k_e by equation 3.9

$$k_e = \frac{1}{k_v} \frac{60}{2\pi} \quad (3.9)$$

It can be concluded that equation 3.5, 3.6, 3.8, 3.7 and 3.9 can be used for example to estimate the nominal operating torque when only an nominal operating current, resistance and k_v value are specified by the manufacturer.

It would be optimal if the manufacturer would supply a graph that shows the efficiency of the motor

⁵<http://nidec-ma.de/en/characteristiccurves.html>, Visited on 19th of January 2014

over its complete working range. Such as is the figure that is available for the 3kW motor from Sonceboz as can be seen in figure 3.8.⁶

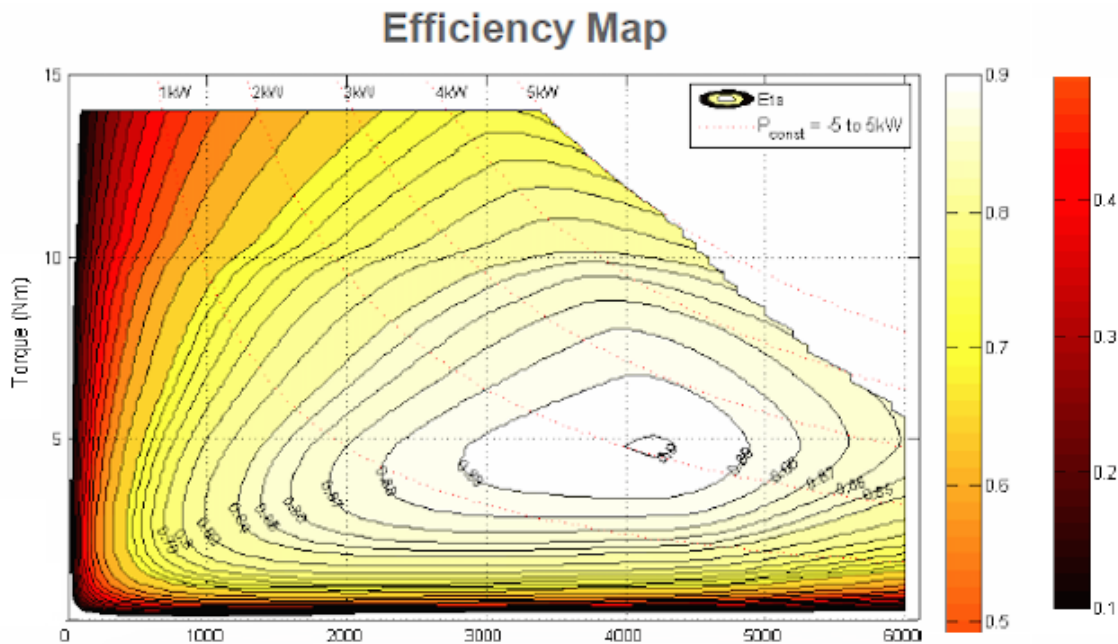


Figure 3.8: Exact mapping of motor efficiency for the 3kW continuous power motor from Sonceboz. Torque is here displayed on the vertical axis. Such an indication of the efficiency for the different operating points is unfortunately not available for the motors that were considered.

Unfortunately this motor weighs more than 3kg which makes it less suitable for our application. Manufacturers of motors in the 5kW range often do not even specify a single value for the efficiency of the motor such as its optimal efficiency. This information can also not always be obtained when contacting the manufacturer. This results in problems in making a fair comparison between the performance of different motors. Therefore, where necessary assumptions were made for the efficiency value. Scorpion was contacted about the efficiency of their motors for the Scorpion HK7050 they reported an efficiency of 87% at nominal operating conditions. Unfortunately they could not give information on the other motors considered. When efficiency data was not available for a certain motor, the motor was assumed to comply with other BLDC motors of the same size or taken close to similar types of motors of the same manufacturer for which the efficiency is reported.

Final Choice

The flight strategy is designed such that the propeller needs to receive a maximum power of $2.67kW$ during the mission and the maximum power that the motor receives from the batteries is $3.0kW$. The Scorpion SII-5535-160KV is the lightest as well as lowest priced option of the motors in Appendix I that can still provide a continuous power of at least 3kW. However, this motor has a much less reliable attachment mechanism for the gearing than some of the other motor types. It would be far easier for the gear to slip of the shaft. The difference can clearly be seen in figure 3.9. Therefore, a slightly heavier and more expensive motor with a good attachment structure was chosen. This is the Hacker A80-10 outrunner. It weighs 1.45 kg, has an efficiency of 89% and costs €483,-. Further characteristics of this motor can be seen in table 3.7.⁷

⁶http://www.sonceboz.com/medias/Products/PDFs/datasheets%20V2/CPM90_45_48V.pdf, Visited on 16th of 2014

⁷http://www.hacker-motor-shop.com/e-vendo.php?shop=hacker_e&SessionId=&a=article&ProdNr=35746019&t=7&c=2884&p=2884, Visited on 16th of 2014



(a) Scorpion motor with an unfavourable propeller connection



(b) Selected Hacker motor with a better propeller connection

Figure 3.9: In these figures the difference between the propeller connection options for two different motors that were considered can be seen

Table 3.7: Characteristics of the motor

Motor characteristics	Value	Unit
Type	Hacker A80-10	
Weight	1450	g
Cost	483	euro
Peak power	5.0	kW
Continuous power	3.3	kW
Maximum current	160	A
Operating current	100	A
Operating voltage	36	V
Motor speed constant (kV)	180	RPM/V
Diameter	89	mm
Length	107	mm
Resistance	0.023	Ω
Efficiency	89	%

It is noted that when the paramotor would be flown with rechargeable batteries and the customer would prefer to have more power than the JM1S motor from Joby Motors which provides 8.2kW continuously would be a good choice for a reasonable price.

Motor Cooling

During operation the motor will generate heat. If this heat is not dissipated efficiently then the motor can overheat. Other electric paramotors do not use additional cooling for their motors. The used motor will be inside a fairing. However, it has a large area which allows good heat transfer to the air inside the fairing. Furthermore, due to a high percentage of soaring during the mission the motor will have short periods of operation. It will cool down during the non-powered soaring phases. In case it is investigated that cooling is not sufficient additional radiators or fans could be added or incorporated.

3.4.2 Gearing

The Hacker A80-10 needs to be used in combination with a gearing system, in order for the propeller to run at its most efficient speed and to deliver enough torque to it. The nominal torque and speed

values of the motor could not be stated by the manufacturer, therefore these were estimated. The operating current of the motor is 100A and the RPM/V value is 180kV. With equation 3.5 and 3.9 the nominal torque is estimated at $5.3Nm$. At cruise speed the propeller runs most efficiently at 600 RPM (as can be seen in table 3.13 and requires a torque of $16.4Nm$. The gear ratio is then calculated with equation 3.10.

$$GR = \frac{T_{propeller}}{T_{motor}} = \frac{29}{5.3} = 5.5 \quad (3.10)$$

From this it follows that at cruise the motor needs to turn at a speed of 3276 RPM. In order to achieve this gear ratio a belt drive consisting of two pulleys and a toothed belt will be used such as is depicted in figure 3.10.



Figure 3.10: A CAD generated design of the drivetrain layout. The large gear ratio is clearly visible. The part of the drivetrain shown here will be located inside the fairing.

A toothed belt and pulleys are chosen to prevent slipping. Furthermore, synchronous belt drives generally have an efficiency of 98% whereas the typical efficiency value for (poly)V-belts is 95%⁸. This higher efficiency is achieved due to the fact that synchronous belts do not rely on friction to transmit power unlike V-belts. The diameter of the small pulley is decided to be the smallest size that fits the motor mounting points. This is $39mm$. The large pulley will then have a diameter of $214.5mm$. Both gears will be made from aluminum. A High-Torque-Drive (HTD) belt is chosen. There are different pitch options. The pitch of the belt is the distance between adjacent tooth centers. In order to select the correct belt pitch the power and rotational speed of the small pulley and the design power are considered. The belt type is then selected by making use of figure 3.11⁹.

⁸https://www1.eere.energy.gov/manufacturing/tech_assistance/pdfs/replace_vbelts_motor_systemts5.pdf, Visited on 19th of January 2014

⁹http://www.gates.com/~media/Files/Gates/Industrial/Power%20Transmission/Manuals/PowerGripDriveDesignManual_17195_2014.pdf, Visited on 19th of January 2014

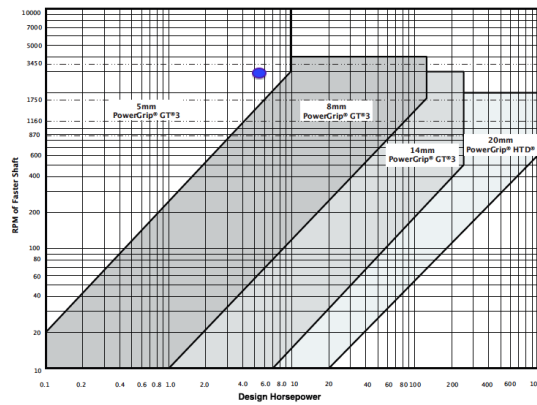


Figure 3.11: With this graph the belt type for the gearing can be selected.

A calculation tool provided by a manufacturer of timing belts¹⁰ was used to calculate the belt length and toothing of the gears. The inputs were a HTD 5M belt, a small pulley of 39mm , gear ratio of 5.5 and a center distance between the pulleys of 150mm . Since, commercially available toothed gears are not light enough for the application these will be self designed. The large gear will be made of aluminium and will have a design similar to the gear in figure 3.12a. Sufficient time was not left for a thorough calculation of gear strength. The feasibility of the design is examined by looking at existing gearing solutions for paramotors. In figure 3.12b¹¹ an aluminium gear that is used on commercially available paramotors can be seen. This gear has a weight of 0.5kg and a diameter of 180mm . It is slightly smaller than the large gear needed for the electric paramotor but is designed for a power value that is around twice the value as required for the electric paramotor design.



(a) Light weight aluminium gear for a Radne toothed belt drive



(b) Lightweight aluminium gear from the Radne Raket paramotor.

Figure 3.12: Toothed gear such as will be used in our design next to a gear that is used in a commercially available paramotor.

The gear will thus be made from aluminum by CNC with a similar design. The weight of the pulleys and belt is estimated by looking at gear sets that are available for existing paramotors of the same size. The characteristics are summarized in table 3.8.

¹⁰<http://www.maxtorque.com/calctool/centertocenterstartx.asp>, Visited on 19th of January 2014

¹¹<http://www.radne.se/sv/karting/Product/?PartNo=32401-1>, Visited on 19th of January 2014

Table 3.8: Gearing characteristics

Gearing	Weight [kg]	Diameter [mm]	Number of teeth	Cost [€]	Material
Large pulley	0.5	215	24	90	Aluminium
Small pulley	0.25	39	132	25	Stainless steel
Belt ^a	0.05	740 (length)	148	12	Neoprene black rubber and glass fibre

^a<http://www.beltingonline.com/5mm-htd-timing-belts-4575>, Visited on 16th of 2014

3.4.3 Electronic Speed Control

For the motor a controller needs to be selected. The controller needs to be efficient, lightweight, cheap and needs to perform all desired functions. The functions required from the controller will first be described. After this the cost, weight and functions of four controllers will be considered and the most suitable controller for our design will be selected. Self designing a speed controller was considered. However after a meeting with Johan Zelhorst an expert on designing speed controls it became clear that this would not be feasible in the duration of this project.

Controller Functions and Features

The center function of the motor control is to commutate the windings, such that the motor can run. Furthermore the motor control needs to control the speed of the motor. The ESC does this by adjusting the amplitude of the voltage. The effective voltage seen by the motor can be adjusted with pulse width modulation (PWM). This technique works by applying the voltage in a series of ON and OFF pulses at a high frequency. By varying the width of the ON pulse the effective voltage seen by the motor can be varied.

To be able to communicate the windings the motor needs to detect the rotor position. This can be done with dedicated sensors such as encoders or Hall-sensors or sensorless by back-EMF detection. The sensorless approach is taken since it reduces the complexity and costs of the drive shaft. The controller should thus have the capability to detect back-EMF.

The control strategy used by the controller also needs to be considered. The more conventional method is scalar control. This can be either trapezoidal or sinusoidal. Trapezoidal control is also known as six-step control. This method has the highest torque ripple and leads to the most noise and vibration. It works by having one winding at high voltage, one at low and one winding disconnected. Sinusoidal control works with a sinusoidal varying current over the windings. This reduces the torque ripple and makes the performance smoother. A more complex method which requires higher processing power is Field Oriented Control (FOC). This technique works by trying to orient the stator flux vector at a specific orientation with the rotor flux vector. In order to do this more processing power is necessary. These controllers are more complex and therefore more expensive as well. The motor performs better with FOC. The torque ripple is reduced which results in smoother performance and quieter operation.

Finally the communication possibilities which the ESC has with the input controller and the battery management system needs to be considered. All hobby type controllers use Pulse Position Modulation (PPM) signals. A safer communication could be accomplished by using for example the Controller Area Network (CAN) protocol. CAN is a two-wire differential signal protocol, used for real time control. It is used very often in the car industry.

Motor Controller Selection

Various hobby type controllers are on the market which cost around €300. The M-Spin 170 Opto

that is recommended by Hacker for their A80-10 motor is such an example. This controller was compared with the Kontronik Kosmik 200 which is a more high-end controller aimed at use in RC applications and with two industrial controllers, the MGM Compro HBC controller and the SLSi-60-240 from Sinusleistungsteller. These might be better suited for manned applications. One of the high voltage types of the HBC controller is for example used in the E-Fan Electric aircraft. In order to make comparison between these controllers their price, weight and important safety features have been summarized in table 3.9.

Table 3.9: Different ESCs characteristics such as cost, weight, communication options and voltage sensing needed to make a good choice

Features	M-Spin 170 Opto	Kosmik 200HV	HBC 18063-3	SLSi-60-240
Cost [€]	399	699	704	117.8
Weight [kg]	340	250	250	880
Back-EMF detection	Yes	Yes	Yes	Yes
Communication options	PPM	PPM	PPM, CAN, RS-485, RS-232 TTL	altered on request
Current sensing	No	Yes	Yes, current limits are configurable	Yes
Over current protection	Cut-off	Power ↓	Power ↓	Power ↓
RPM sensing	Yes	Yes	Yes	Yes
Temperature sensing	Yes	Yes	Yes	Yes, switch off & power ↓
Voltage sensing	Yes	Yes	Yes	Yes,
Commutation strategy	Trapezoidal control	Trapezoidal control	Sinusoidal control	FOC

The cheap M-Spin 170 controller, which is recommended with the Hacker motor by the manufacturer was discarded as a suitable option since it will not be possible to fly with the motor after an overcurrent situation occurs. Furthermore, only PPM communication is possible. The Kosmik controller seemed a good option, however the manufacturer explained that it could not be easily configured to be used with signals other than PPM. The HBC controller can accept CAN signals. However, it uses simple six step control. The SLSi-60-240 is the only controller which uses FOC. It can be modified to customer requirements such that different types of signals can be accepted. The only drawbacks of the SLSi-60-240 controller are the high cost and weight. Since the HBC controller already has an efficiency of 98 to 99% the added efficiency of the SLSi-60-240 would lead to less gain in range than a weight decrease of 0.63kg. Furthermore, it would better fit in the cost budget.



Figure 3.13: MGM Compro HBC 18063-3 motor controller

Therefore the HBC 18063-3 controller is chosen. It can be seen in figure 3.13. It has numerous safety features, clear instructions on configuring it with the motor and is available with CAN bus. It costs €700 and weighs 250g. The electrical diagram of the motor controller and its connections with the motor, BMS and input controller can be seen in the electrical block diagram in figure 3.14.

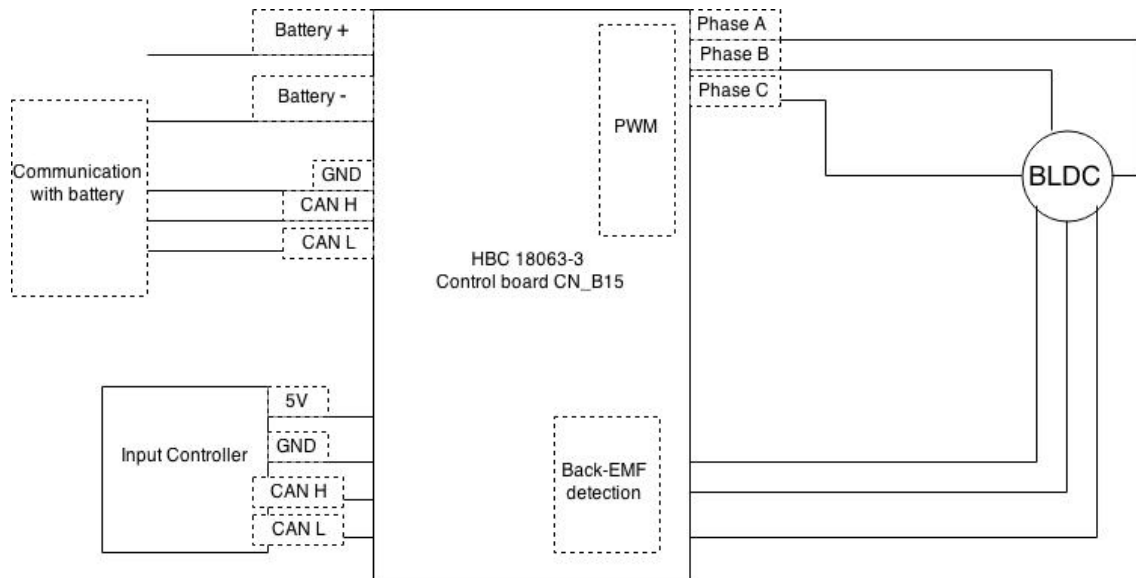


Figure 3.14: Electrical block diagram of BLDC motor, ESC and input controller

3.4.4 Input Controller and Controller Interface

The pilot needs to be able to communicate the desired throttle setting to the motor. Furthermore, it is required that the pilot is informed about data of the system such as the battery charge and RPM setting of the motor. This section first details the functions that need to be performed by the hand held throttle control. Then, various options are considered and a throttle design is presented.

Functions of the Input Controller

The input controller needs to convert the pilots hand movement to a CAN signal that communicates the throttle setting to the ESC. Additionally, the pilot needs to be able to use the hand control to disconnect the battery from the motor such that in case of emergency it is always possible to stop the motor. The option to have cruise control is desirable since the flight time will be long and it is more comfortable for the pilot to be able to fly at a constant throttle setting without having to

keep the throttle control pressed at this setting for the entire duration. It should be possible for the pilot to put the propeller in vertical position during soaring. An additional control option became necessary after the propeller design was changed such that it has a total diameter of $2m$. As a result of this change, the propeller should be locked in horizontal position during take-off. Furthermore, windmilling of the propeller should be prevented.

Take-off and Windmilling

Windmilling of the propeller can be prevented if the inertia of the propeller together with the gearing and motor are large enough. For take-off it is crucial that the propeller does not move from its horizontal position until enough height is gained. If it would, a propeller strike with the ground could occur which would lead to a crash. Therefore it was decided that to ensure no propeller movement during take-off, a bicycle type handbrake will be used that will brake the system at the propeller gear. This brake can also be used during flight to prevent windmilling. It would be undesirable if the pilot would have to time himself if the propeller stops at the correct position. He would have to look behind him while applying braking. This would distract the pilot so much from flying that it would be dangerous. It would be preferable to automatize this. In order to do this information about the propeller position is necessary. Information about the gearing ratio can be supplied to the motor controller, such that the propeller position can be known if the motor position is known. In order to detect the motor position at low speeds from the back-EMF these signals will be filtered with a Kalman filter. The manufacturer of the motor control will be contacted about implementing this custom feature in the controllers software.

Off-the Shelf Options

For conventional paramotors, numerous off the shelf input controllers are available. However, these work by moving a wire which opens the throttle valve. These controllers are thus not directly suitable for an electric paramotor. Electric paramotor manufacturer Paracell does however sell a separate hand controller for €280,-, which uses a potentiometer to supply the throttle signal, which is send to the controller with PPM. The use of a potentiometer for a critical part such as the electric throttle control is found undesirable, since the wiper contact which slides over the resistance can produce faulty readings due to wear or dirt. Furthermore as was already explained that the use of PPM for transmitting signals to the controller is also found undesirable.

Throttle controllers of other electric vehicles such as electric motors and scooters were researched but not found to be a suitable option. First of all many of these use a twist grip which is not practical to use when paramotoring. Some more suitable thumb throttles are available, however versions that can be used with CAN communication, and incorporated cruise control were not found. Furthermore, it would still be necessary to implement a functionality that can put the propeller in the horizontal position when desired.

Hand Controller & Interface design

A good off-the-shelf hand controller was not found. Additionally, to minimize weight and costs it would be favourable to integrate the controller interface with the input controller. It was thus decided to self design the input controller and interface. The handheld throttle grip will have a small screen on which system data about the motor and battery can be read. The design of the handheld grip and screen can be seen in figure 3.15.

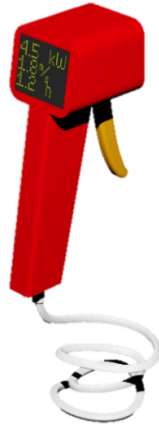


Figure 3.15: Design of the input controller and interface.(The various switches that will be on the grip are not visible in this figure).

For the throttle grip to perform all these functions a small circuit board with a micro controller, dedicated CAN micro controller, CAN transceiver and CAN PCB connector are needed.

The cruise control will be implemented with a separate switch on the hand held grip. It works by regulating the required throttle setting with the hand grip, holding it there and pushing the cruise button. The micro controller is programmed such that it will remember the throttle setting at the time that the switch is pressed. The handle returns to its neutral position after release. When the throttle handle is again removed from its neutral position then the new Hall sensor input will override the cruise control setting. This way throttle can be quickly changed just by intuitively pressing the handle and the pilot can cruise without constantly having to squeeze the hand held grip.

A separate kill switch is also implemented on the hand held controller. This kill switch is directly linked to the disconnect switch between the battery and the motor. In case of an emergency the motor can always be stopped by disconnecting it from the battery such that it will not receive any power.

In order to stop the motor in the vertical position for soaring or the horizontal position for landing the pilot first needs to release the throttle to its neutral setting and can then click on a three step switch to select vertical or horizontal stop. The hand controller knows the propeller position from the information supplied by the motor controller. The micro controllers in the hand controller processes this information together with the information about the current speed and calculates the level of electrical braking that needs to be applied to brake the propeller in the correct position. If during braking the pilot moves the throttle from the neutral position than the breaking sequence is ended and the normal throttle signal is send to the motor controller. When the braking is continued and the propeller is stopped in the correct position then the pilot puts the handbrake on the gear.

The throttle signal is converted into a CAN signal which is send to the motor controller. The hand control receives RPM, battery charge, temperature and other data through the motor controller. This data will be processed through a microprocessor and then displayed on a small OLED screen. The electrical block diagram can be seen in figure 3.16.

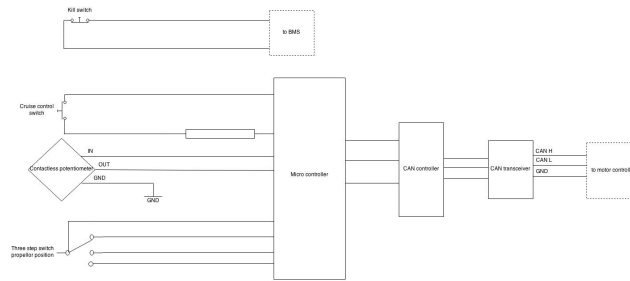


Figure 3.16: Electrical block diagram of the hand control and its connection to the BMS and ESC.

Table 3.10: Components required for the hand controller and costs

Input controller and interface parts	Cost [€]
Casing	150.00
Screen	55.14
PCB	5.00
Microcontroller	5.00
CAN transceiver	1.02
CAN MCU	4.91
CAN PCB connector	10.17
Switchers, resistors and other parts	30.00
Contactless potentiometer	140.00
Total	401.24

The hand held controller and interface will need a casing, a screen, a hall sensor, switches and a PCB with various components. The costs of professional manufactured PCB's is quite high for small volumes. A single board will cost around €50,-. Therefore the prototype PCB will not be manufactured but hand-made, which can be done for about €5,-. The expected cost-breakdown of the hand controller can be seen in table 3.10. The cost estimation is based on the parts that are mentioned in the footnotes^{12 13 14 15 16 17 18}.

3.4.5 Conclusion

In this chapter a motor and motor controller were chosen. The motor is the A80-10 from Hacker, which weighs 1.45kg, costs €483 and can provide 3.3kW of continuous power. A synchronous belt with a gear ratio of 1:5.5 is chosen. The total efficiency of the motor and gear is estimated at 85%. The HBC 18063-3 ESC from MGM Compro is chosen to control the motor. This controller costs €700,-, weighs 250g and is compatible with CAN bus. The handheld input controller was not chosen, instead a design was described which incorporates the controller interface. This design allows safe communication with the motor and incorporates extra features such as horizontal and vertical stopping of the paramotor, which are necessary for the specific large propeller paramotor.

¹²<http://dlnmh9ip6v2uc.cloudfront.net/datasheets/LCD/Color/uOLED-160-G2-Datasheet-REV1.2.pdf>, Visited on 19th of January 2014

¹³<http://www.jameco.com/1/3/copper-pcb-board>, Visited on 19th of January 2014

¹⁴<https://www.conrad.nl/nl/atmel-avr-risc-microcontroller-atmel-atmega168-20au-soort-behuizing-tqfp-32-kloksnelheid-mhz-20-m.html>, Visited on 19th of January 2014

¹⁵<http://www.microchipdirect.com/ProductDetails.aspx?Category=MCP2551>, Visited on 19th of January 2014

¹⁶<http://www.microchipdirect.com/ProductDetails.aspx?Category=dsPIC30F4011>, Visited on 19th of January 2014

¹⁷<http://www.l-com.com/d-sub-right-angle-d-sub-pcb-connector-db9-female-tray-10>, Visited on 19th of January 2014

¹⁸http://nl.mouser.com/search/refine.aspx?Ntk=P_MarCom&Ntt=132317518, Visited on 19th of January 2014

3.5 Propeller

This section describes the final design of the propeller. First the design method is described. Next the aerodynamic and structural properties of the chosen propeller will be evaluated. Finally a manufacturing method will be chosen.

3.5.1 Design Choices Synopsis

During the midterm phase a preliminary propeller design was developed.

- **Blade radius**

First it was investigated that the maximum blade radius was limited to $0.75m$, due to a required ground clearance during the take-off and landing phase. However in the detailed design phase it became clear, that the radius could be increased, when the propeller is kept in a horizontal position during the critical flight stages. This is possible, since the propeller thrust is not required during take-off and landing. The updated blade radius was determined to be $1m$ and this change resulted in an increased efficiency, going up from 69% to 79%. The increase in efficiency clearly outweighed the increase in mass for the updated design.

- **Number of blades**

Furthermore it was decided to use a two-bladed propeller over a three or four-bladed propeller, since this resulted in a 2% higher efficiency, as well as a lower weight.

- **Number of propellers**

It was investigated, if a dual propeller configuration would be favourable over the single propeller. However next to the weight penalty a decreased efficiency of the propeller can be observed, using the disk actuator theory (3.11), which states, that the disk area should be as large as possible, for maximum efficiency. Even though the dual propeller configuration could be mounted in free stream wind conditions, it would still result in worse performance data.

- **Non-ducted fan**

The idea of a ducted fan was ruled out, due to the decision not to include a safety cage between the pilot and the propeller device in the design. This has the advantage of making the structure lighter, but it also allows for a cleaner airflow into the propeller, because no netting is used.

- **Non-foldable fan**

Furthermore a foldable propeller was listed as a possible design option. However the shift in the center of gravity between the folded and unfolded propeller configurations can lead to an unstable chassis, unless the batteries would move accordingly, which would require a complex structure. Furthermore it was investigated that the drag penalty due to an unfolded propeller during soaring is not critical, since the extra drag does not prevent the paramotor from being able to soar.

- **Material choice**

Finally it was already decided in the midterm phase to use hard maple wood as material, as it provides good load carrying capabilities in combination with a low density. The biggest advantage over composite material is achieved by a severe reduction in manufacturing costs.

3.5.2 Method

The propeller of the paramotor has a big effect on the performance of the total system. Not only is a high efficiency important for an increased range, also a low mass of the propeller would leave extra room for the batteries. It is important that the propeller is able to operate efficiently over the whole flight envelope. A secondary goal of the propeller design is that it needs to be silent, though this is less important than having a high efficiency.

Although many existing propellers are already available on the paramotor market, most of them, if not all, lack specific performance data of the propeller. Since the mission is unique and a lot of aerodynamic knowledge and experience is available, it was chosen to design a new propeller from scratch instead of buying one. The main advantage of this is that the propeller can be designed specifically for a very unique flight envelope and will thus have a better performance than a propeller which is designed for a wider flight envelope.

This subsection describes the method used to design the final propeller. It explains the propeller theory and the use of MATLAB in combination with XFOIL and XROTOR to get to the final design.

Theory

Propellers typically have propulsive efficiencies in the range of 40 up to 85 percent. The power losses can be split up into three components.

- **Losses from disk actuator theory**

Disk actuator theory includes any device that creates a force by accelerating an incoming mass flow. It disregards any shape of the propeller. According to disk actuator theory the maximum ideal efficiency (no blade element losses and induced losses) can be found by equation 3.11¹⁹ which is shown graphically in figure 3.17.

$$\frac{2}{1 + \sqrt{\left(\frac{T}{A_{disk} * u_0^2 \frac{\rho}{2}} + 1\right)}} \quad (3.11)$$

Where T is the thrust setting of the propeller, A_{disk} is the total disk area of the propeller, u_0 is the airspeed, and ρ is the density of air.

- **Losses from blade element theory**

Blade element theory uses an analysis of the blade where the aerodynamic characteristics of each radial element of the blade are used to calculate the propulsive efficiency of the propeller. It is therefore of great importance that the airfoil at every station of the blade has a very high aerodynamic efficiency.

- **Induced losses**

Induced losses are increased by an inefficient lift distribution across the span of the blade. This is analogous to induced losses at wings. To ensure minimum induced losses it is necessary to generate an elliptic lift distribution across the span of the blade.

Bounding Parameters

From disk actuator theory, represented in equation 3.11, it can be seen that in order to reach the highest possible efficiency the disk area and flight speed need to be as high as possible. Moreover it is evident that the thrust setting needs to be as low as possible. In the following two figures 3.18a and 3.18b the design points for the propeller were determined using the flight simulation code. The histograms show the thrust distribution, as well as the velocity distribution during the powered parts of the mission. The mean velocity during powered flight was computed to be $11.28 \frac{m}{s}$. Furthermore the mean thrust required is $98N$. Those two values are necessary to determine the propeller design point.

The combination of 2 blades with $1m$ radius and the determined design thrust and velocity parameters result in an ideal efficiency of 91%.

It must be noted that a propeller designed on these bounding parameters may still be able to operate at a large flight envelope by varying its RPM, but will most likely have a lower efficiency at those conditions.

Airfoil Selection for Highest Aerodynamic Efficiency

Now that the general bounding parameters of the propeller are set, airfoils can be chosen for different sections of the propeller. In order to generate airfoils with the highest lift over drag ratio an airfoil optimizer tool was build which ensures that the best airfoil is found for a certain set of constraints.

¹⁹<http://web.mit.edu/16.unified/www/FALL/thermodynamics/notes/node86.html>, visited on December 10th, 2014

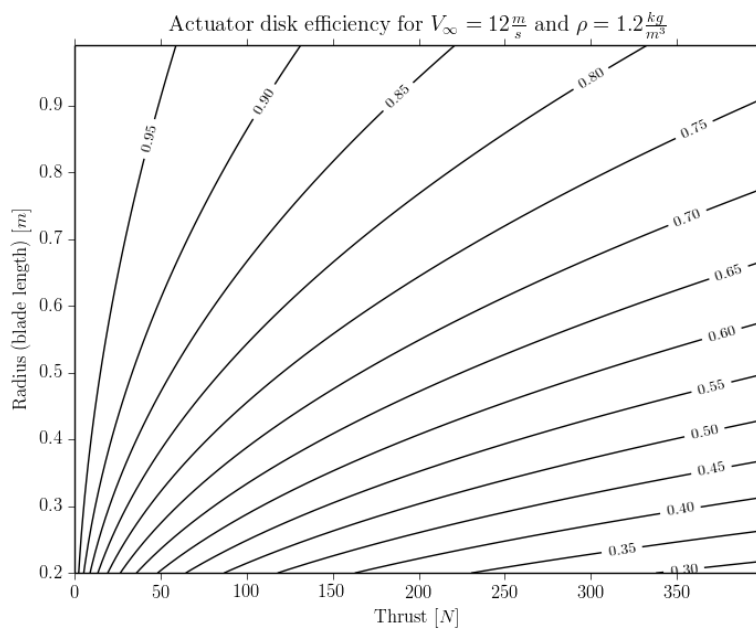


Figure 3.17: Plot of the ideal disk efficiency showing the constant efficiency lines versus thrust and speed at 12m/s cruise speed. It is obvious that having a large disk area and a low thrust setting is beneficial for the flight range, hence the large radius of the propeller.

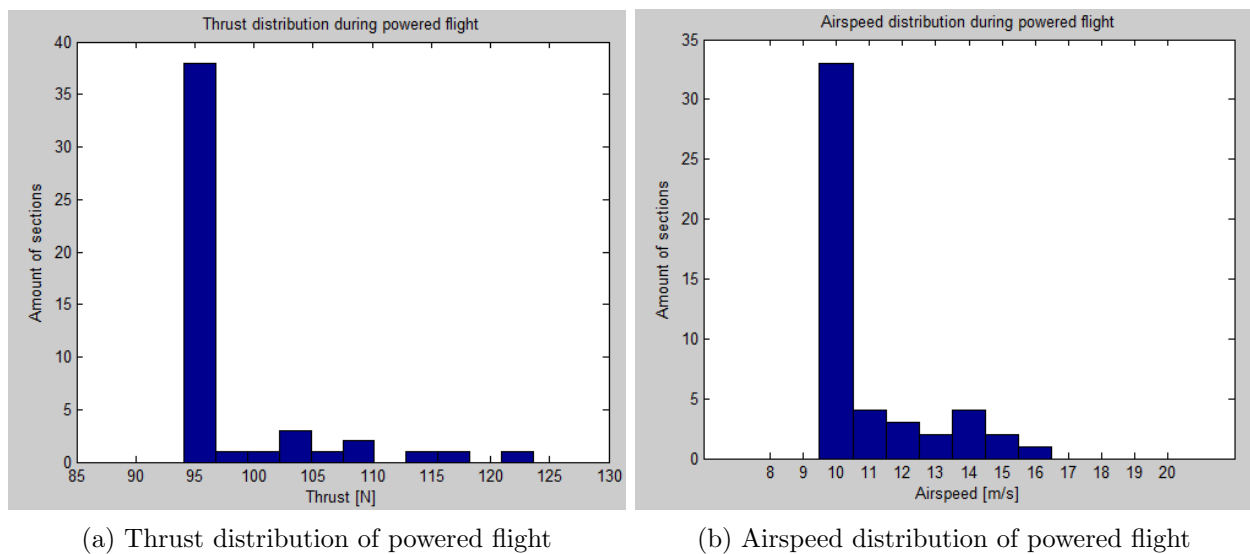


Figure 3.18: Thrust and airspeed distribution of powered flight

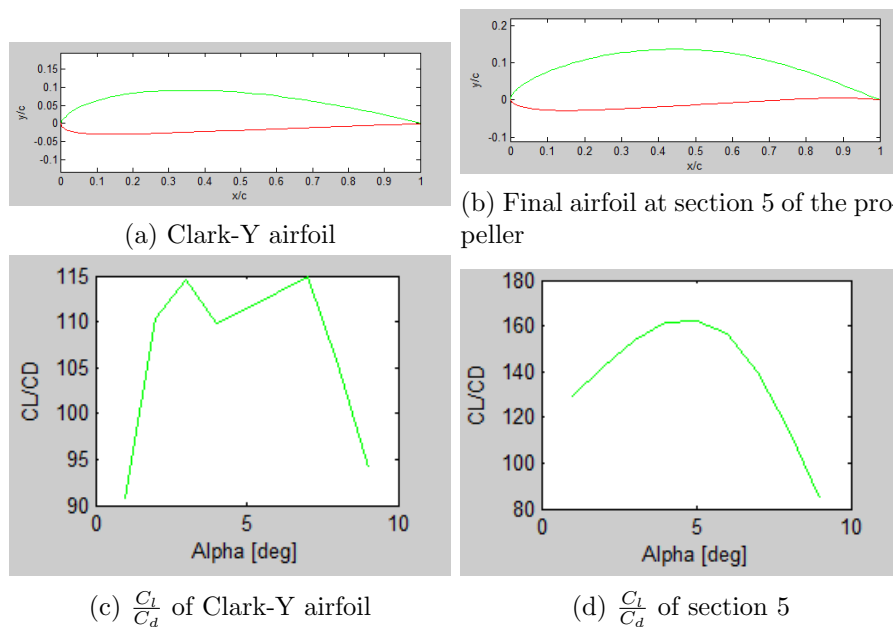


Figure 3.19: Aerodynamic comparison of existing airfoil (Clark-Y) and final generated airfoil using particle swarm optimization. Efficiency curves are calculated using XFOIL. It is clear that it is beneficial to generate airfoils for this specific case instead of using existing airfoils from internet databases.

This tool parametrizes the airfoil using b-splines and implements Particle Swarm Optimization in order to converge to a global optimum. The tool makes use of the XFOIL module written by Professor Mark Drela at MIT for attaining the lift over drag ratio's of the airfoils generated in the Particle Swarm Optimization module. More about this airfoil optimization process can be found in Appendix J.

The main advantage of optimizing airfoils instead of using existing airfoils such as Clark Y, is that they can be optimized for a very specific set of constraints. For example the Clark Y airfoil (considered having a high aerodynamic efficiency) has a typical aerodynamic efficiency of around 115 at an angle of attack range from 4 to 9 degrees, at Reynolds numbers around $1 * 10^6$. So this is an 'allround' good performing airfoil. However when the aerodynamic operating points of an airfoil are very narrow then it is more efficient to generate a new airfoil for that very specific case. The Particle Swarm Optimization tool was able to find airfoils that have an aerodynamic efficiency of up to 200. However these generated airfoils typically have bad performance at higher and lower angles of attack compared to the angle of attack at maximum aerodynamic efficiency. As a constraint for the airfoil optimization toolbox it is chosen that the airfoil must have the highest aerodynamic efficiency totaled over angles of attack ranging from 1 to 7 degrees angle of attack. This is done so that the propeller will also be able to operate efficiently and generate enough thrust at off design points. Also this range is chosen broad enough so that the effect of torsional twist due to aerodynamic loading on the propeller is accounted for. A comparison between the $\frac{C_L}{C_D}$ curve of the Clark-y and the final generated airfoil for section 5 can be found in figure 3.19

The constraints that have to be set up for the airfoil optimizer can be split up into optimization parameters and geometry constraints. A more in-depth analysis of the optimization parameters can be found in Appendix J. The geometry consists of parameters that describe a box around which the airfoil can be shaped. For example it can be chosen that the airfoil that has to be generated must have a minimum thickness of 0.2 times the chord at a chord location of 0.25 and 0.4. These thickness constraints are set to make sure that the airfoil at that section has sufficient stiffness. Also the trailing edge angle can be constraint such that the optimizer does not converge to an airfoil which is not manufacturable.

Blade Geometry Optimization for Minimum Induced Losses

When the airfoils per span-wise location of the blade are known, it is of the essence to search for the

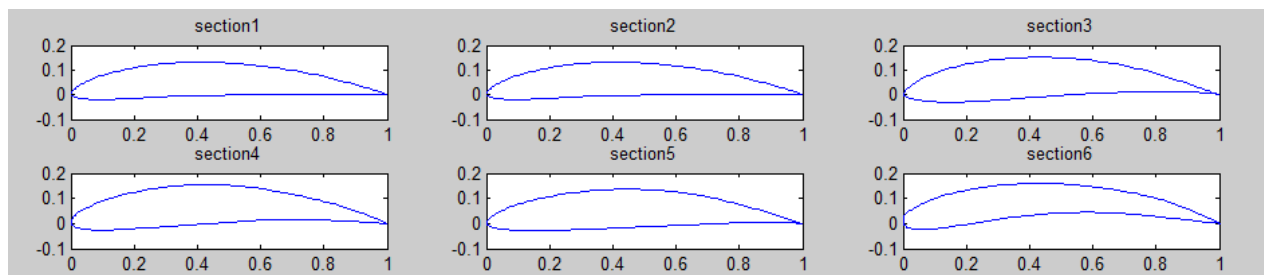


Figure 3.20: Airfoil selection after iteration 1

Table 3.11: Example airfoil characteristics used as input for XROTOR

1) Zero-lift α [deg]:	0	8) C_l at minimum C_d :	0.15
2) $\frac{dC_l}{d\alpha}$:	6.28	9) $\frac{dC_d}{dC_l^2}$:	0.004
3) $\frac{dC_l}{d\alpha}$ behind stall:	0.1	10) Reference Re number:	2000000
4) Maximum C_l :	2	11) Re scaling exponent:	-0.2
5) Minimum C_l :	-1.5	12) C_m :	0.1
6) C_l increment to stall:	0.2	13) M_{crit} :	0.62
7) Minimum C_d :	0.007		

best geometry of the blade. This geometry consists mainly of the angular distribution per span and of the chord distribution per span of the blade. These two geometry variables are optimized using the program XROTOR by Professor Mark Drela from MIT. XROTOR is a piece of code written in Fortran which allows the user to define the operating parameters and the airfoils per section. Once these inputs are defined XROTOR finds the best corresponding chord and angle distribution which ensures minimum induced losses and highest efficiency at the design point. XROTOR also has a structural analysis function where the user inserts the structural properties per airfoil and XROTOR then calculates the torsional twist and deflections of the propeller in x and z direction using a slender beam approximation.

Iteration Process

Now that every module is defined an iteration process can be set up. This process can be seen in flowchart 3.21.

First a seed propeller geometry design has to be defined in order for the iterations to start. The seed design consists out of an propeller with a constant chord of $0.1m$ over the span of the blade. Also the thickness has to be set for the iterations to start, a taper in thickness is included to make sure the blade has enough stiffness (because of the non linearity of the lift distribution over the blade also the structural loads, especially the moment around the z-axis, will be non linear). Now that the blade geometry is known, the blade can be discretized into sections. It is chosen that the blade is discretized into 6 sections. For every section, the input for the airfoil generation module is calculated, based on the chosen angular velocity, thickness distribution and chord distribution. The output of the airfoil generation module are airfoils with a very high aerodynamic efficiency for the given Reynolds numbers and thickness calculated at that section. In figure 3.20 the results from the first airfoil generation can be found.

Now that these high efficiency airfoils are generated, XROTOR can be used to ensure the best chordwise and angular distribution of the airfoils. XROTOR uses the lift polars of the selected airfoils as input and searches for the distribution of chord and angle of attack of the airfoils which ensure an elliptic lift distribution. A MATLAB script was written to transform the generated airfoil data in XFOIL to useful input for XROTOR. An example of the variables XROTOR uses to parametrize the lift curves are given in table 3.11.

With this information, XROTOR knows all the aerodynamic characteristics of each airfoil section to start calculating the performance of the propeller.

The user can specify at which C_l the airfoils must operate. Also the blade bounding parameters

Table 3.12: Input for calculating deflections in XROTOR, "i" being the blade section

R(i)	EIXX(i)	EIYY(i)	EA(i)	GJ(i)	EK(i)	M(i)	MXX(i)	XOCG(i)	XOSC(i)	RST(i)
0.15	4.06E+03	1.25E+05	5.59E+07	1.36E+04	1.30E+03	3.12	1.38E-07	8.67E-02	8.06E-02	1.01E-02
0.20	3.48E+03	1.07E+05	5.17E+07	1.17E+04	1.11E+03	2.89	1.18E-07	8.34E-02	7.76E-02	9.70E-03
0.45	1.28E+03	3.92E+04	3.14E+07	4.28E+03	4.09E+02	1.75	4.33E-08	6.49E-02	6.04E-02	7.55E-03
0.62	4.53E+02	1.39E+04	1.87E+07	1.52E+03	1.45E+02	1.04	1.54E-08	5.01E-02	4.66E-02	5.83E-03
0.82	6.99E+01	2.14E+03	7.33E+06	2.34E+02	2.23E+01	0.41	2.37E-09	3.14E-02	2.92E-02	3.65E-03
0.99	3.60E-02	1.11E+00	1.66E+05	1.21E-01	1.15E-02	0.0093	1.22E-12	4.73E-03	4.40E-03	5.50E-04

given in table 3.13 are given as input to XROTOR, which now calculates the geometry of the blade with minimum induced losses.

A nice feature of XROTOR is that the bounding parameters for the propeller can be changed at any time. Lowering the RPM generally results in a larger average chord of the blade, this is trivial since a lower RPM means the airfoil has to generate lift at a lower speed, hence XROTOR enlarges the chords of the airfoil to still generate the input thrust. It is however beneficial to lower the RPM up to a certain amount, since a bigger blade also means a bigger mass of the propeller, thus having a negative effect on the performance of the paramotor. Lowering the RPM also changes the efficiency. So after every iteration, the RPM is changed from the original input RPM to a new RPM with a higher propulsive efficiency while still keeping the blade mass within reasonable bounds.

An important step of the iterations is to check the bending stiffness and torsional stiffness. It is of great importance that the blade does not twist too much around the pitch axis due to the aerodynamic loads on the blade. A great function of XROTOR is the bend function. It needs the structural properties of each airfoil and then calculates the deflections using the lift and drag distribution of the propeller in combination with the structural properties per airfoil section of the blade. The bend function makes use of a slender beam approximation. An example input for the bend function can be found in table 3.12.

where:

- R = Radius
- $EIXX$ = In-plane stiffness
- $EIYY$ = Out-of-plane stiffness
- EA = Extensional stiffness
- GJ = Torsional stiffness
- EK = Extensional/torsional stiffness
- M = Mass density / length
- MXX = Pitch axis inertia / length
- $XOCG$ = x/c of section CG
- $XOSC$ = x/c of section shear center
- RST = Structural radius for strain evaluation

For the calculation of these structural properties the E and G modulus for hard maple timber wood were used. A MATLAB script was written to calculate the required structural properties of the propeller per section. All the parameters were calculated by taking the mid section airfoil and multiplying it with scaling factors, which are based upon chord ratio, for the other sections. For the IXX, XOCG, IYY, J and area of the airfoil, the bend function of XFOIL is used. For the calculation of the torsional stiffness, an ellipse is taken and use is made of equation 3.12. An educated guess is used for determining the location of the shear center.

$$\frac{\pi a^3 b^3}{a^2 + b^2} \quad (3.12)$$

The structural properties per radial section of the blade after iteration 1 can be found in figure 3.22.

Next XROTOR's bend function calculates the deflections in all axes and most importantly, it calculates the torsional twist due to the aerodynamic loading of the propeller. This torsional twist can

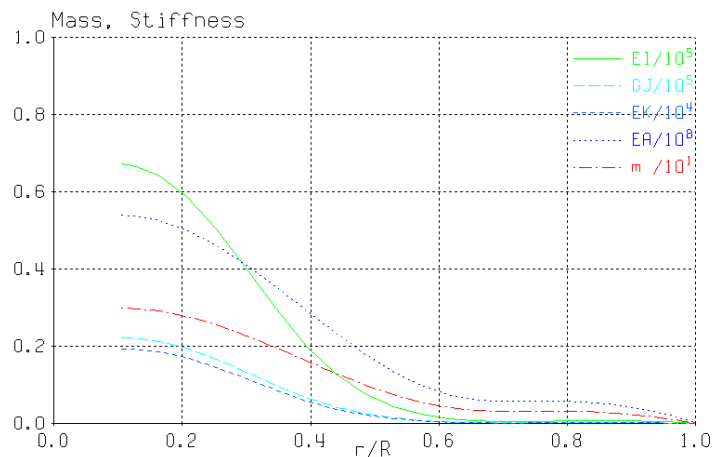


Figure 3.22: Structural properties as a function of radial station of the blade, given in SI units

have a negative effect on the propeller performance. What happens is that due to torsional twist, the different airfoil sections of the propeller start operating at a different angle of attack than in the unloaded case. This means that if the twist has a certain order, the airfoils do not operate in their highest aerodynamic efficiency zone anymore. Although the airfoils are optimized to have a high aerodynamic efficiency over a range of about 7 degrees, it is important to give the propeller enough stiffness to counteract the negative effects of twisting. It is decided that the propeller can have a maximum twist of 1 degree at design condition.

XROTOR also gives numerical output about the deflections and twist angles for different sections of the blade. If every section of the blade after an iteration does not twist more than 1 degree, a new airfoil generation can start with thinner airfoils.

At every iteration the performance of the propeller is checked at the off-design points. It is checked that the propeller is able to produce enough thrust at lower speeds while keeping the power required reasonable.

3.5.3 Performance Analysis

This subsection describes the aerodynamic and structural performance analysis of the final propeller design. It will analyse the performance at cruise speed, as well as at other operating points.

Performance Analysis at Design Points

The global, as well as the most important performance parameters of the final propeller at design speed are presented in table 3.13. The hub radius was set to $0.15m$. This decision was made to avoid extreme blade angles toward the root, which would require an oversized hub. What also can be noted is that the blade radius is $1m$. This would require an extra system which constrains the propeller in a horizontal position during take-off, and in a vertical position during soaring to reduce drag. More on this locking mechanism is explained in chapter 3.4.

In order to investigate the noise induced by the propeller blades, the XROTOR function .NOIS was used. Figure 3.23a illustrates the noise footprint at the height of the pilots head. The blue circles in the following illustrations indicate the pilot's position, which is $1.1m$ ahead and $30cm$ above the hub location. It can be seen that the pilot will be exposed to a noise of $80dB$, when the propeller is running. It must be said that the noise occurs only in 43% of the mission with numerous brakes in between, due to soaring. So the pilot is not exposed to a constant sound level over a large time span, so there is no danger of hearing damage. The noise level is comparable to heavy road traffic in $10m$

Table 3.13: Global and performance parameters of the propeller

	<i>Radius [m]</i>	<i>Hub Radius [m]</i>	<i>Material</i>	<i>Weight [kg]</i>	<i># of Blades</i>
Global	1	0.15	Hard Maple Timber	2.3	2
Design Point					
	<i>Speed [$\frac{m}{s}$]</i>	<i>RPM</i>	<i>Thrust [N]</i>	<i>Efficiency [%]</i>	<i>Power [W]</i>
Performance	11.28	600	98	78.5	1407

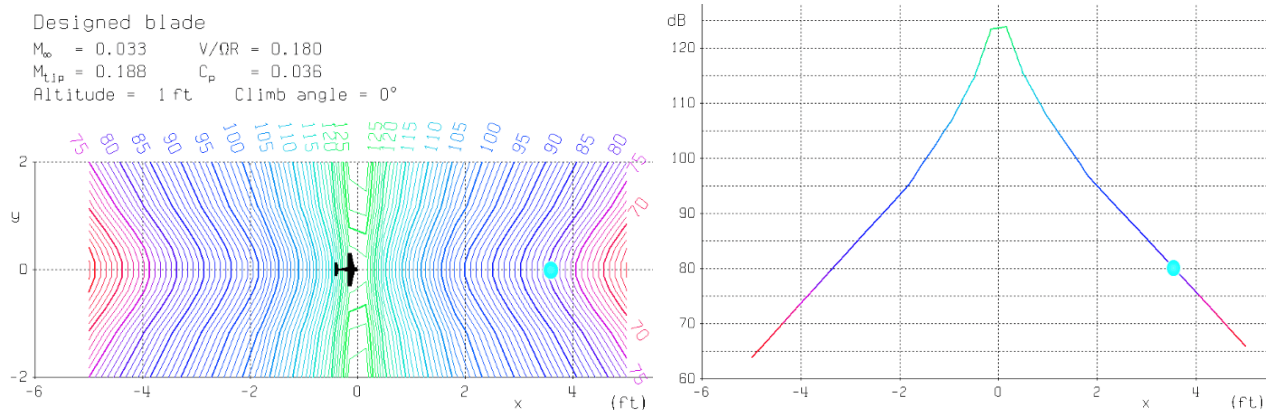


Figure 3.23: Visualisation of propeller noise at different distances

distance. Figure 3.23b illustrates the noise values in a graph for better visualisation. It can be seen that the sound right at the propeller reaches $124dB$, which indicates that long term exposure should be avoided. Furthermore it was investigated, that the sound on ground does not exceed $50dB$, when flying at $10m$ altitude.

The angular distribution of the airfoil sections can be seen in figure 3.24a. Furthermore a render of the final propeller design is presented in figure 3.24b.

Performance Analysis at Off-Design Points

Because of the fact that the flight envelope is larger than only optimum cruise conditions, the propeller also needs to be analysed at off-design points. In table 3.14 the propeller performance at the speeds encountered during the flight envelope is given. What is important to conclude from this figure is the required angular velocity of the propeller to ensure maximum efficiency.

Table 3.14: Off-design performance data

<i>Velocity [$\frac{m}{s}$]</i>	<i>Thrust [N]</i>	<i>Angular Velocity [RPM]</i>	<i>Efficiency [%]</i>
10	96.83	524	77.1
11	95.43	541.2	78.8
12	97.63	564.3	80
13	101.84	591.1	80.98
14	107	619.5	81.75
15	113.38	649.7	82.38
16	120.33	680.6	82.94

3.5.4 Material Characteristics

As explained previously, the material choice for the propeller is hard maple timber wood. The material costs, as well as the manufacturing costs outweigh the weight penalty when using wood over a carbon composite sandwich structure.

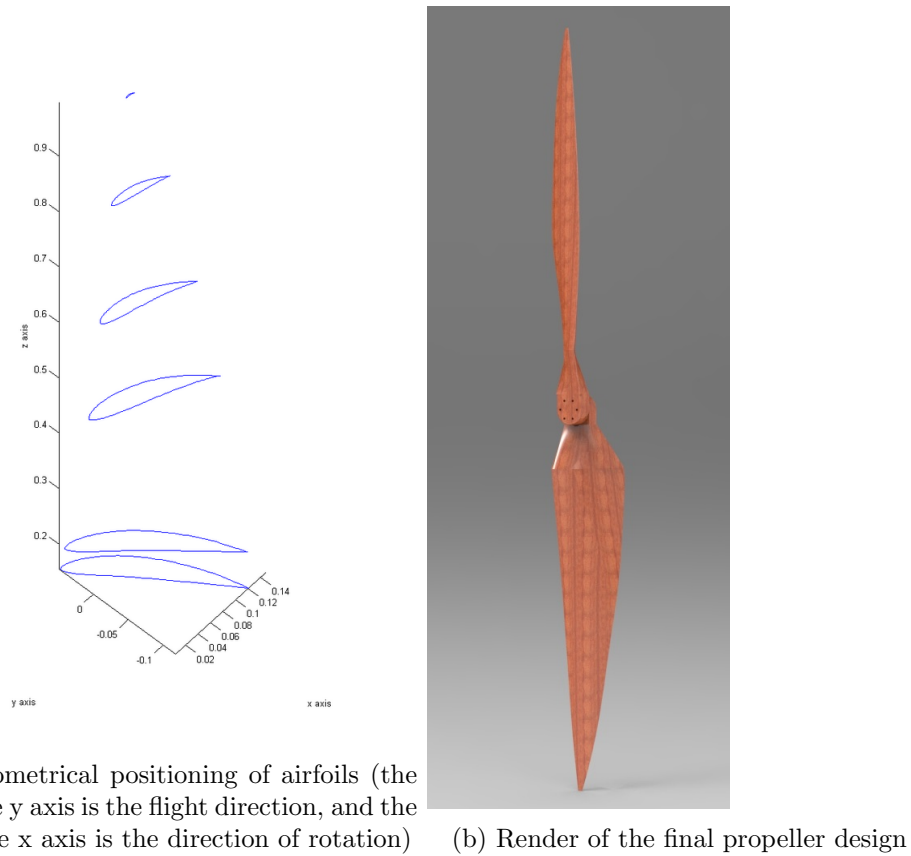


Figure 3.24: Final propeller layout

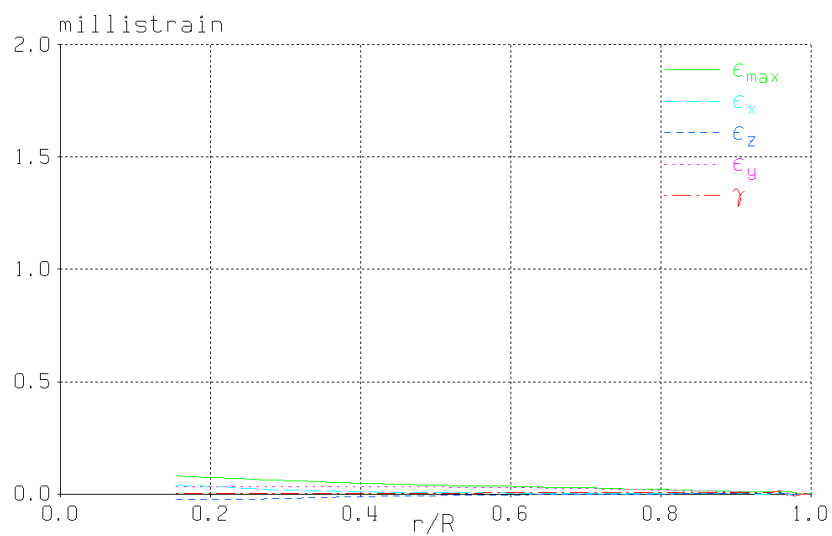


Figure 3.25: Strains on the final design of the propeller. All SI units

This material results in the deflections shown in figure 3.25. Also the torsional twist due to the lift loading peaks at 0.04 degree which is far below the limit of 1 degree. This is mainly due to the large average chord of the propeller, which gives the blade very high moments of inertia.

3.5.5 Conclusion

Extensive use of was made of MATLAB and the programs XFOIL and XROTOR during the propeller design. An airfoil optimizer tool was built for the selection of airfoils for the propellers.

The final design of the propeller has a diameter of $2m$ and an propulsive efficiency of 78.5 % . It will be made of maple timber and it will weigh $2.3kg$. A render of the final propeller design can be found in 3.24b. It generates enough thrust to maintain cruise speed and can provide a climb rate of $0.7\frac{m}{s}$ at cruise speed. The propeller is able to efficiently generate thrust at off design points. Due to the large diameter, the propeller will need to be constraint horizontally during take-off. Also during soaring to prevent an excessive amount of drag, the propeller needs to be constraint vertically. Finally, the propeller consists of two blades which are individually detachable by removing 6 bolts. These blades can easily be positioned inside the main frame to accommodate easy transportation and keep the backpack size limited.

3.6 Chassis

Following from the actions taken in earlier stages of the product development, the final chassis design was selected, of which characteristics are discussed in the following subsections. To make sure the whole system is balanced properly during all stages of the flight, it was chosen to not connect the system directly to the pilot. The pilot will sit in the harness, connected to the hang point and the system will be attached to a frame, also connected to the hang point. The only connection between the pilot and the system is via a string system to the frame and due to the fairing, covering the whole system for aerodynamic efficiency (Section 3.7). Safety is assured by placing the propeller far enough to the rear to avoid contact between pilot and propeller.

The first concept design idea was to connect all components directly to the pilot via a back plate, having a propeller attitude adjuster to control perfect thrusting during all phases of flight. This option though was determined to be much heavier and was therefore discarded. Furthermore a partial cage was planned to be added between the pilot and the propeller to protect the pilot and the lines. That option is not needed anymore, because the propeller placement is far rearward and by using assistance in the course of a zero-meter take off, the lines will not need protection anymore. This decision is very beneficial because removing the safety structure led to a much lighter and more aerodynamic efficient design.

3.6.1 Center of Gravity Optimization for System Balance

To determine where to place each component for lightest weight, smallest inertia and closest center of gravity(COG) location, a center of gravity optimization script was written. In this script, the COG in x- and z-direction were calculated for both the pilot and the system in relation to the reference point. The chosen reference point is the pilot's hip joint. Therefore everything placed ahead of the hip joint is located in positive direction and everything placed rearward is located in negative direction. If the COG of the system has minimal distance to the pilot's COG, the best fit is found, meaning that all system components are placed for optimal balancing.

To optimize for minimum COG distance, some input values were kept variable. These variables are the seat angle (45-60 degrees), the driveshaft length (400-800 mm), the battery distance (-100-1000 mm) and the drivetrain (motor and gearing) distance to the reference point, as well as the frame length and mass, since they are dependent on the placement of all other parts.

The sizes of the different body parts for an average dutch man in the age range of 30-60 years was

Table 3.15: Optimal Placement of System Components and Pilot

Output	Position [mm]	Output	Position [mm]
α_{seat}	50	$d\bar{x}_{battery}$	240
\bar{x}_{pilot}	-32.92	$d\bar{z}_{battery}$	270
\bar{x}_{system}	-32.89	$d\bar{x}_{motor}$	393.39
$d\bar{x}$	0.03	$d\bar{z}_{motor}$	0
\bar{z}_{pilot}	227.81	$l_{driveshaft}$	850
\bar{z}_{system}	228.02	l_{frame}	1,583.4
$d\bar{z}$	0.21		
m_{frame}	1.32 kg		

obtained from the ergonomics program DINED²⁰. In addition, the percentage of the whole body mass of each body part, as well as the location of the COG per body part were needed, which were gained from Graf's data in (*Charles E. Clauser*, 1969). The masses, heights, widths and lengths needed for the system components were attained respectively from the responsible engineer, who determined these values. Before calculating the COG locations, some **assumptions** had to be made:

- The reserve chute is also connected to the hang point, resting on the pilot's legs, therefore close to the overall COG
- The reserve chute's mass is negligible, since it is very light compared to the overall weight
- The leg angle is fixed to 0°, although the pilot still has some freedom to move his legs
- The frame is hollow and therefore only 1/3 of the cross sectional areas were used for calculations
- The frame material used is Aluminium 7075 T6, due to density values

Based on the assumptions and the given masses and sizes, the basic COG formula, depicted in equation 3.13, was used to calculate the pilot's and system's COG for all different possible setups.

$$\bar{x} = \frac{\sum m \cdot x}{\sum m} \quad (3.13)$$

The output of the script is given for the minimal distance between the pilot's and system's COG, which are the following:

- COG pilot
- Position of batteries
- Frame length
- COG system
- driveshaft length
- Frame mass
- Position of drivetrain
- Seat angle

To get an even more accurate result, the best height position of the drivetrain could also be optimized. In addition this could be done by fixing the driveshaft's/propeller's COG at the z-location of the overall COG and varying the drivetrain height from there. The gained result should be accurate enough though to build a prototype, due to the use of small increments in the optimization.

The optimal results for the chosen design are presented in table 3.15:

To visualize the COG locations in relation to the reference point, figure 3.26 shows a rough sketch of the placements.

²⁰<http://dined.io.tudelft.nl/dined/full>, visited on December 16th, 2014

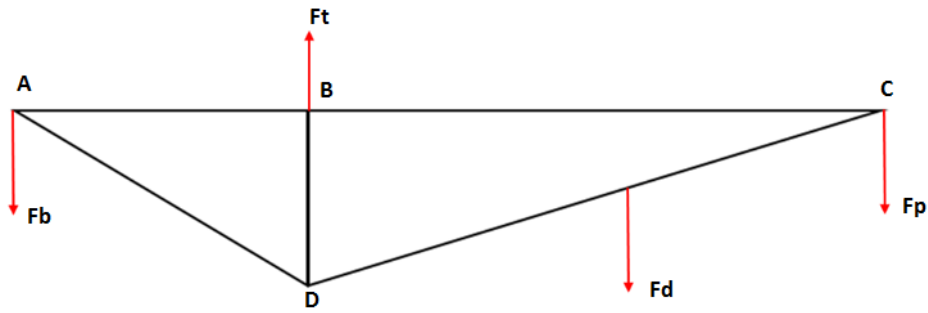


Figure 3.27: Free body diagram of the paramotor frame side view with forces due to the mass of the batteries (F_b), drivetrain (F_d), propeller (F_p) and complete paramotor system (F_t)

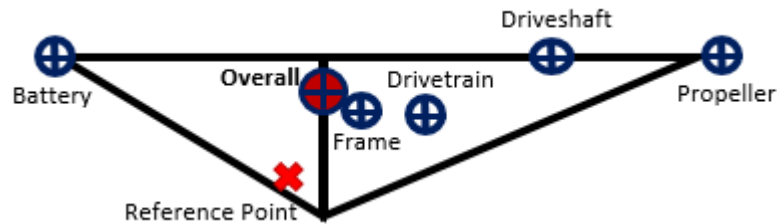


Figure 3.26: Sketch to visualize COG locations of the different parts

Based on the known COG locations, the hang point will be placed such that it is about 10-20 centimeters above the COG. This will still offer enough body maneuverability, since a low hang point was chosen, but will also give enough stability by being less affected by small perturbations and thrust inputs.

3.6.2 Frame

The frame will be used to support the batteries, drivetrain and propeller. It will be suspended from the hang points and therefore has to provide a mounting point for this. The basic dimensions of the frame are driven by the outcome of the COG calculation in subsection 3.6.1. These dimensions are the overall length, width and height of the structure. The frame dimensions are driven by the mass values of all other systems, these values became known in the late stages of the project. Therefore, there was no time left for a thorough analysis of the frame. Because of this a basic stress analysis was done for the frame by greatly simplifying the load case. This will result in a basic design for the frame.

Method and Assumptions

The free body diagram of this simplification is shown in figure 3.27. This diagram shows a side view of the frame. The analysis is done for one side of the frame which will be symmetric in the plane shown in the figure. For this reason all forces are half of the masses of each subsystem as the loads will be distributed over the frame equally. In this analysis the extreme loading case will be considered. In this loading case the system will undergo an acceleration of $7g$. This could occur when the paramotor enters a spiral due to loss of lift in the wing. All forces in figure 3.27 will therefore be multiplied by 7 for the design of the frame structure. Also, a safety factor of 2 is included to account for manufacturing and design flaws.

The forces are dependent on the weight of each subsystem. These weights are very good estimates of the final values and can be read in table 3.16. However, as the weight of each part continuously fluctuates during the optimization process of which the frame sizing is also a part, knowing a definite weight of each system is not possible at this stage. A condition for the frame is that the moment in B is zero. This will assure that the frame is balanced on point B. The COG in subsection 3.6.1

Table 3.16: Assumed weights of subsystems for frame design and geometry of frame

Subsystem weights [kg]		Beam length [mm]	
Batteries	22.5	AB	400
Drivetrain	4.2	BC	1360
Propeller	2.3	BD	191
Frame	1.3	AD	443
Total	30.20	DC	1400

generated the frame geometry needed to achieve this with the weights for each subsystem. The frame geometry is defined in table 3.16.

These weights are then translated into forces with which a stress analysis of the frame is performed. This was done by using the method of joints. Each joint is treated separately by looking what forces act in the beams connected to the joints. For this a statically determinate structure is needed. As the frame is only suspended from point B (see figure 3.27) this is not achieved. Therefore, as a simplification, it was assumed that the frame is also held in place by a pin joint in D. The forces in each of the beams were then calculated. The results are shown in table 3.17. With these values, the minimal cross-sectional area of each beam can now be determined. For this analysis aluminum 7075-T6 will be used due to its high strength and low density characteristics. This aluminum is widely applied in the aerospace industry. For the beams in tension equation 3.14 is used with a $\sigma_y = 503MPa$ for AL7075-T6.

$$A_{min} = \frac{F}{\sigma_y} \quad (3.14)$$

The beams under compression were sized based on buckling as this is almost always the first failure mode for metal beams. Therefore equation 3.15 was applied. The Youngs' modulus (E) was set to $71.7GPa$ for AL7075-T6 with $K=0.5$ as both ends of each beam are fixed. The moment of inertia (I) was then calculated. Results of these calculations are given in table 3.17.

$$I = \frac{F(KL)^2}{\pi^2 E} \quad (3.15)$$

Result

Using the attained values for the necessary cross-sectional areas and moment of inertia's of the frame the beams can now be designed. As a first design a simple hollow circular cross-section is chosen as this provides strength in all directions and can be made light weight. The outer radius (R_{outer}) for all beams is set to $15mm$, the inner radius (R_{inner}) will then be chosen such that it complies with the cross-sectional area or moment of inertia requirement from table 3.17. Aluminum 7075-T6 is used. As the beams required a very small cross-sectional area their design wall thickness would become extremely low. Therefore a minimal value of $0.5mm$ wall thickness was set for the beams. This has resulted in a total frame weight of around $470g$ per side, the total frame will thus weigh around $940g$. This frame was then created in CATIA and tested using a finite element method.

F.E.M. Analysis

In order to check the basic sizing of the frame based on the method described in subsection 3.6.2 a finite element method used in CATIA. The frame was fixed on the hangpoints and the loads were applied in their respective positions. All loads were multiplied by seven to account for the maximal expected accelerations and again by two to add a safety factor. The mesh size used on the frame was set to $10mm$. The frame was then evaluated on Von Mises stress and displacement. After a first analysis with the geometry as stated in subsection table 3.17 the frame experienced a too high Von Mises stress in the cutout location shown in figure 3.28.

The thickness of the wall in this tube was thus enlarged until the frame had no critical stress locations anymore. An increase of $1mm$, to a wall thickness of $1.5mm$ total, proved enough. The result is

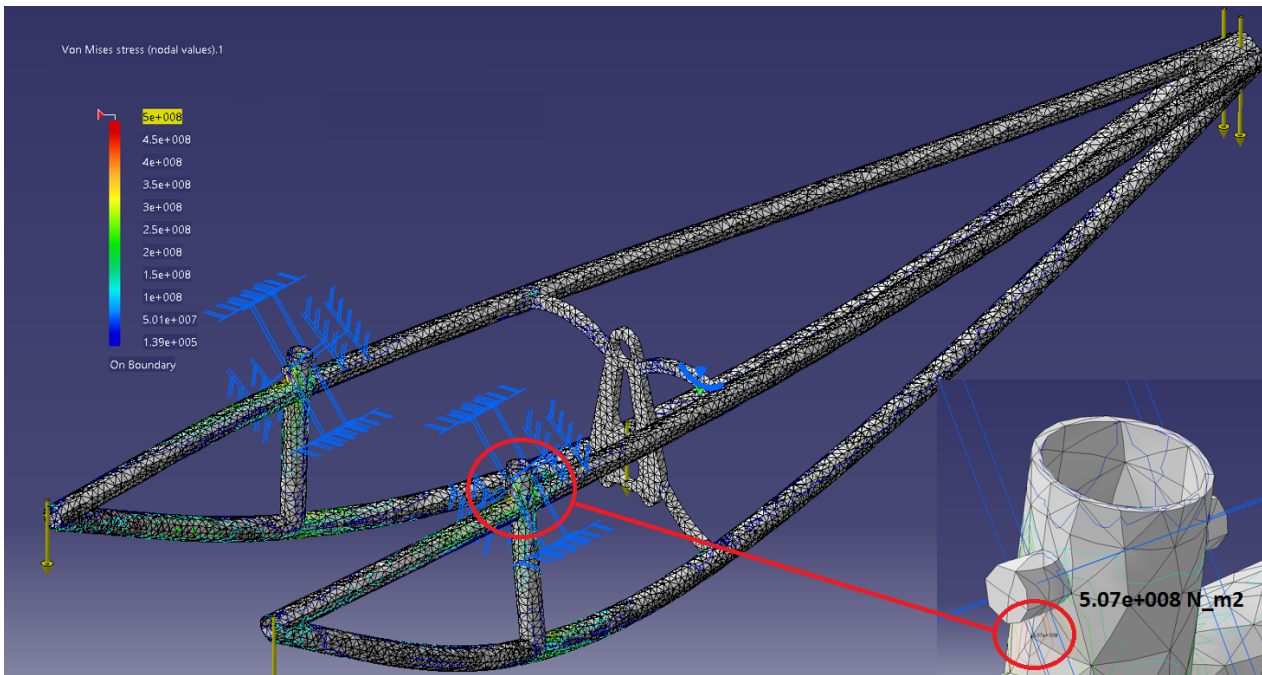


Figure 3.28: Results of F.E.M. analysis on paramotor frame. Cutout shows location of max. Von Mises stress location and value

Table 3.17: Forces, compression or tension, in each beam with minimal beam cross-sectional area or moment of inertia and corresponding cross-section geometry designed for extreme loading case ($7g+2$ S.F.).

	Force [N]	Direction [-]	A_{sec} [mm ²]	I [m ⁴]	R_{outer} [mm]	R_{inner} [mm]	Weight (AL7075-T6) [g]
AB	3236	tension	6.11		15	14.5	52
BC	61	tension	0.11		15	14.5	171
BD	1985	tension	3.74		15	13.5	69.5
AD	3586	compr.		2.49E-10	15	14.5	109
DC	61	compr.		4.07E-11	15	14.5	346
					Total		747.5 g (For one side)

shown in figure 3.28 including a cutout of the location with the highest Von Mises stress. The tensile yield strength of Aluminum 7075-T6, the material used in the frame, is $5.03e6Pa$. The frame can be considered safe under the ultimate loading case as the maximal Von Mises stress encountered in the frame is $5.07e6Pa$. This value, considering the safety factor of 2, is low enough. The inner diameter of beam AD is thus changed from $14.5mm$ to $13.5mm$. The new mass for one BD beam is $69.5g$, an increase of $13.5g$ compared to the thinner beam. The geometry for each beam is given in table 3.17. The total frame mass now becomes $747.5g$ for one side and thus $1495g$ for the complete frame constructed using aluminum 7075-T6.

The frame will not be made foldable. The frames dimensions are such that it can fit into a normal family station car without problems. A container will therefore have to be developed to safely transport the container to the mission start site. The vertical beams will be used to attach the frame to the wing. For this on each side a hole of $10mm$ is present. Through this hole a carabiner can be placed which in turn will be clipped onto the wing attachment points.

3.6.3 Driveshaft

In order to discover what size of driveshaft is necessary for the paramotor, a structural analysis was performed. The following factors were taken into account: bending stress, torsional stress, buckling

and eigenfrequency. The setup that was evaluated is depicted in figure 3.29. The driveshaft shown is mounted to the motor and supported at approximately 3/4 of the length by a bearing. The propeller is mounted at the end. The free body diagram is shown below.

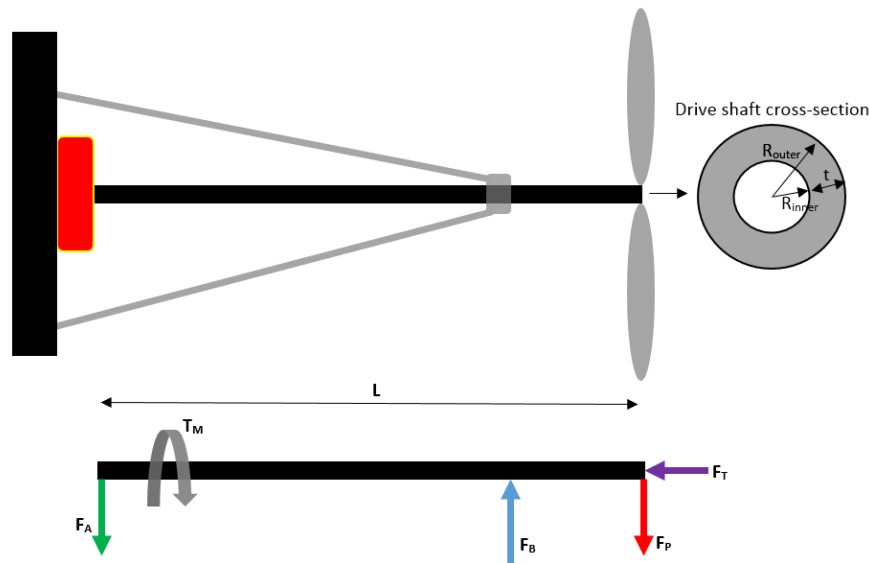


Figure 3.29: Visualisation of driveshaft lay-out and free body diagram

Method and Assumptions

To evaluate different driveshaft geometries and material options, a MATLAB script was created. In this script the bending, compressive and torsional stresses as well as the eigenfrequency are calculated for hollow cylinders of different materials with varying diameters and wall thicknesses. Hollow cylinders are chosen because they are commonly used for driveshafts as they are good at handling torsional loads. A detailed description of the method is given in Appendix K.

It is helpful to know that the driveshaft in the analysis is subjected to a maximal torsional load of $46.3Nm$ based on the maximal torsion the motor can put out multiplied with the gear ratio (see section 3.4.2).

The mass of the propeller is assumed to be $2.3kg$ (see section 3.5.3) Furthermore, the maximal thrust force is taken to be $170N$ based on calculation of thrust during cruise speed when the input power into the propeller is set to $2886W$ (see section 3.3.5) and wire losses and drive train efficiencies are taken into account.

Generally speaking, a large array of radii were considered with their minimal thicknesses in order to cope with the torsional loading. Then these geometries were tested for all other loading types. Geometries that failed due to certain loads were eliminated. The lightest remaining option was then chosen.

Materials

High performance driveshafts are made from either carbon fibre or aluminum. Materials specific properties that are important for the driveshaft of the paramotor are: shear strength (τ_y), tensile yield strength (σ_y), modulus of elasticity (E) and density (ρ). Shear strength is related to torsion, tensile yield strength deals with bending and the modulus of elasticity relates to the compression forces and density determines the weight of the driveshaft. In table 3.18 a list is given of the aluminum types considered. All types were selected based on their high performance in the required fields. In this table only isotropic materials are listed, therefore carbon fibre does not appear in this list. The analysis will first be done to see what weight will be attained using an isotropic material. If it is thought that the use of carbon fibre will deliver major benefits in terms of weight and strength this option will be considered as well.

Results

Plotting the outer radius (R_{outer}) against the mass in figure 3.30 shows that increasing the R_{outer} ,

Table 3.18: Material selection driveshaft design

	ρ [kg/m ³]	τ_y [MPa]	σ_y [MPa]	E [GPa]
Aluminum 7075-T6	2.81	331.0	503.0	71.7
Aluminum 6061-T6	2.70	207.0	276.0	68.9
Aluminum 6061-T913	2.70	240.0	455.0	69.0
Aluminum 2024-T6	2.78	283.0	345.0	72.4
Aluminum 2024-T86	2.78	310.0	440.0	72.4

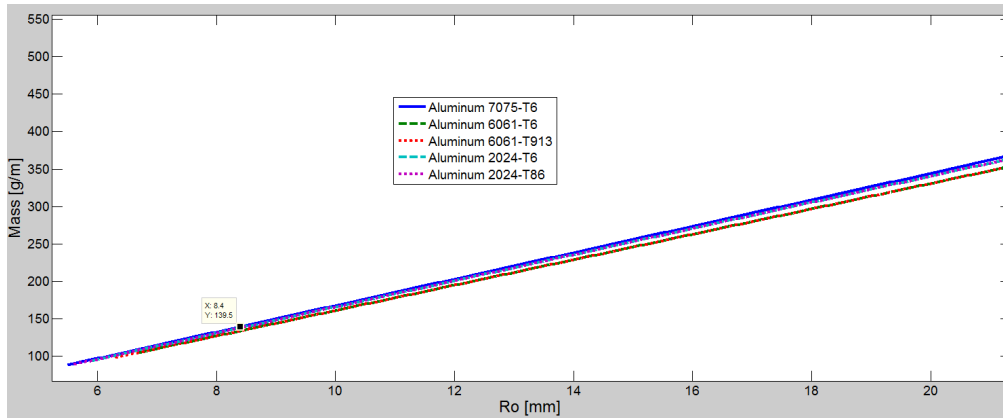


Figure 3.30: Plot showing the relation between change in driveshaft mass per meter due to changes in R_{outer} , AL6061-T6 coincides with AL6161-T913 and AL2024-T6 coincides with AL2024-T86

and sizing the thickness such that it is designed to be able to cope with $46.3Nm$ of torque, increases the mass of the driveshaft. From this one can conclude that having a low as possible R_{outer} will deliver the lightest driveshaft. Cross sections of certain materials that exceeded the shear strength of the materials were eliminated from the plot. A lower limit for the outer radius (R_{outer}) was set at $1mm$ and thickness lower limit at $0.5mm$ for practical and manufacturing purposes. The design point will thus be the cross-section that has the lowest possible R_{outer} and does not fail due to the applied loading.

The bending, compressive and torsional stresses can be combined using the Von Mises stress formula in equation K.6. This Von Mises stress should stay below the tensile yield strength of a material in order to make sure this part does not fail in tension. The Von Mises stress are plotted against R_{outer} in figure 3.31. As the R_{outer} values that have a Von Mises stress higher than the tensile yield stress are eliminated the plot only starts at the Von Mises stress value for each material. The Von Mises stress decreases rapidly for the R_{outer} values up till around $25mm$. Then the line becomes flatter. From this the conclusion can be drawn that increasing the R_{outer} above the value of $30mm$ does not provide much benefit in terms of strengthening the driveshaft.

As said before, increasing the R_{outer} has a large effect on the mass of the driveshaft, which is also shown in figure 3.30. Therefore choosing a small outer radius will result in a lighter driveshaft. It was decided to take a safety factor of 2 with respect to the Von Mises stress. Aluminum 7075-T6 shows the largest potential in figure 3.31 as it is able to sustain the highest Von Mises stress at the smallest R_{outer} of all materials. AL2024-T6 and AL6061-T6 are not visible in the graph as their values coincide with the visible line, their minimal needed R_{outer} is higher then the other materials and thus these (2024-T6 and 6061-T6) will not be considered. For aluminum 7075-T6 the tensile yield strength is $500MPa$, with a safety factor of 2 a value of $250MPa$ is thus the design point.

The data point in figure 3.31 shows this value and the according R_{outer} value of $8.4mm$. The wall thickness at this outer radius is below $0.5mm$ and is thus set to $0.5mm$ as stated before. This geometry made using aluminum 7075-T6 will give a driveshaft which is $71.9g/m$. With a length of $0.98m$ the driveshaft would weigh $70.5g$ in total. An available tube should be chosen which comes closest to these dimensions but is not smaller in thickness or radius. The other options have also been evaluated and are given in table 3.19. Carbon fibre was not considered as the weight of the

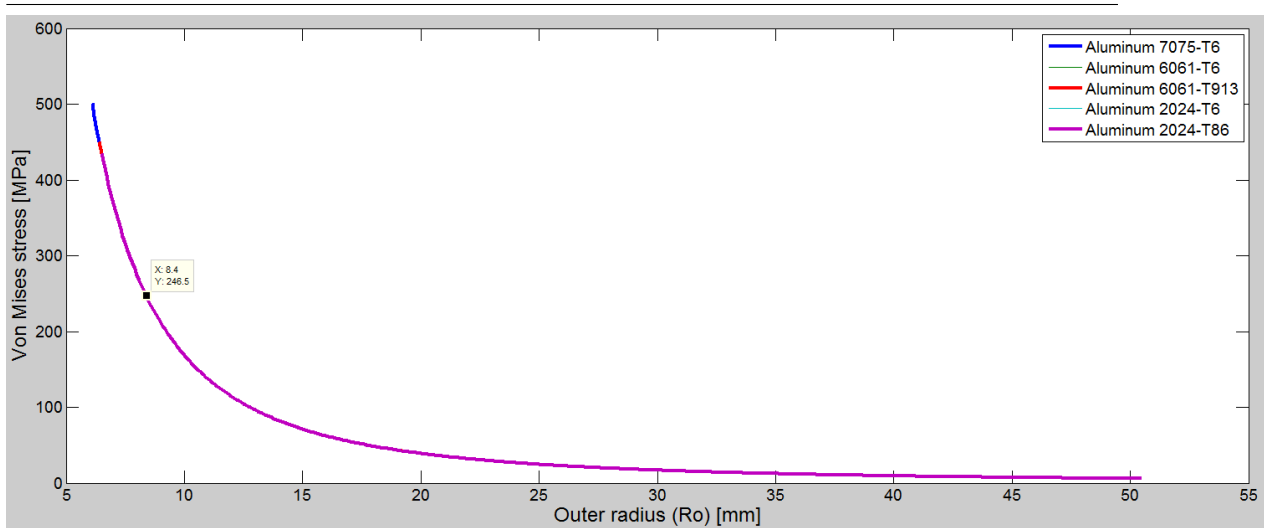


Figure 3.31: Plot showing the relation between Von Mises stress and outer R_{outer} . Data point indicates design point with safety factor of 2 for AL7075-T6.

Table 3.19: Optimal driveshaft design results for different materials with a safety factor of 2 on the Von Mises stress

Material	Ro [mm]	t [mm]	Mass/m [g/m]	Mass [g]
Aluminum 7075-T6	8.4	0.5	71.9	70.5
Aluminum 6061-T6	11	0.5	94.9	93.0
Aluminum 6061-T913	8.7	0.5	74.6	73.1
Aluminum 2024-T6	9.9	0.5	85.2	83.5
Aluminum 2024-T86	8.8	0.5	75.5	74.0

driveshaft is relatively low, no big weight benefits are expected when designing the driveshaft this way.

The lowest eigenfrequency of this design was calculated to be $72.6Hz$ (see Appendix K). The propeller will be rotating at $600RPM$, an imperfection in the blades would then create a vibration at the frequency of $10Hz$. The design can thus be considered safe with respect to its eigenfrequency based on this analysis.

3.6.4 Harness

The choice of the harness is mainly driven by weight, cost and comfort. In order to make the chance of the mission being a success as large as possible the weight and cost will be most important. For this reason a light and cheap harness has been selected.



Figure 3.32: Neo String harness

The harness of choice is the Neo string harness. This harness has an extremely low weight of 290g (excluding carabiners). Furthermore it is advertised and underwritten by users to be reasonably comfortable. The price of such a harness is around €300. By adjusting the straps the required seat angle can be attained. The Neo String is depicted in figure 3.32²¹.

3.7 Aerodynamic Fairing

A significant part of the total drag, about 20%, is caused by the pilot's body (Virgilio, 2004). If this can be minimized in any way, it might increase the range dramatically, as range is linear with drag. This means a total elimination of pilot drag would cause an increase in range of approximately 20%. Of course this is not possible, but even a decrease in pilot drag of 25% would cause an increase in range of 5%. This can be done using a specially designed fairing, an idea that will be explored in this chapter.

It was investigated that the drag of a pilot is quite high compared to streamlined bodies, no matter what position the pilot was in. The lowest drag found with XFlow for a pilot without any fairings in the most supine position was 20N (normalized to $11 \frac{m}{s}$). Interestingly, the drag of pilot in a streamlined harness was measured in a wind tunnel to also be 20N (Virgilio, 2004), although the frontal surface was larger. This indicates the advantage of using fairings to decrease drag.

To comparison, the drag of a streamlined body with a diameter of 2m (a very high value, in which pilot could stand upright) is, taking a textbook C_d value of .04 for a streamlined body, 4.5N at $11 \frac{m}{s}$. Therefore a fairing in the shape of a streamlined body might be very beneficial.

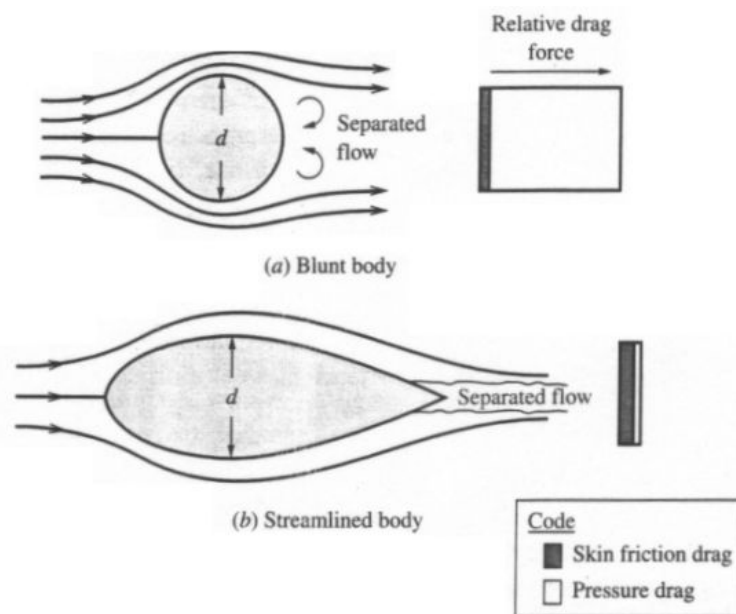


Figure 3.33: The relation between friction and separation drag.

Minimum drag is achieved by:

- Minimizing friction drag; friction drag is mostly influenced by the boundary layer (BL) being either turbulent or laminar, and by its growth downstream, influenced by surface roughness and pressure distribution.
- Minimizing separation or pressure drag; separation drag is caused by the boundary layer detaching from the surface, either in case of a laminar BL (laminar separation bubble) or a turbulent BL. This usually decreases the pressure in the zone with detached BL more than

²¹<http://www.flyneo.com/en/harnesses-neo/>, Visited on January 14 2015

with attached BL, causing a resisting force where the surface's normal longitudinal component points backwards (i.e. after the thickest point of a streamlined body).

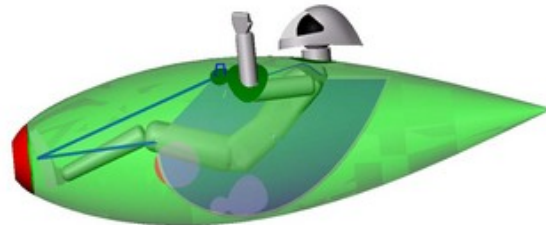
The relation between friction and separation drag is illustrated in figure 3.33.²²

3.7.1 The Cocoon Fairing

A number of years ago, some paragliding pilots experimented with axisymmetrical streamlined fairings that enclosed the pilot and harness, and were made of lightweight paraglider fabric (typically $40 \frac{g}{m^2}$), as shown in figure 3.34a. The results were promising but the practical difficulties such as getting in and out and a hard-to-reach reserve parachute prevented this invention from finding widespread use. Its working principles are quite simple: it is supported only at its nose (with the pilot's feet) and at the carabiners, which can be seen in figure 3.34b. A hole in its nose enables the dynamic pressure to pressurize it, keeping its streamlined shape.



(a) In flight.



(b) Technical details.

Figure 3.34: Lightweight axisymmetric low-drag fairing. Not in widespread use due to practical difficulties. ^a

^a<http://www.paraglidingforum.com/viewtopic.php?t=9081>, visited on December 19th, 2014

3.7.2 Lateral Stability

A problem which occurs in cocoon designing is that it is hard to ensure lateral stability, as the neutral point of the streamlined body is located in front of the pilot. When the body is at an angle it will generate lift, and this lift vector will act approximately at the body's neutral point, destabilizing the system. A solution would be to attach the fairing just at the pilot's legs, letting it act like a wind-vane, but this is not possible when sticking a prop shaft through its rear end. Another solution would be to use fins to ensure stability of the system, and add some reinforcements to avoid deformation of the fairing due to lift forces.

Thus, when designing the fairing, care must be taken to size the fins such that the entire system is stable, and to reinforce parts that would otherwise deform due to lift forces in sideslip situations.

3.7.3 Differences between 2D and 3D axisymmetric Body Drag

When comparing a 2D symmetric airfoil and a 3D axisymmetrical body, made by revolving the 2D airfoil, differences are observed, stemming from two effects:

- The minimum pressure is higher, due to the relieving effect: in 2D, the air can only go around the body in one direction, in 3D it can go around the body in two directions.

²²<http://www.aerospaceweb.org/question/aerodynamics/q0215.shtml>, visited on December 19th, 2014

- The BL thickness differs due to the body's varying circumference. The BL near the nose spreads out over a larger surface as the circumference increases. Conversely, the BL gets thicker when the circumference starts decreasing, resulting in a thick BL at the body's stern.

This also results in the transition from a laminar to turbulent BL being at a different location than on 2D airfoils.

Thus, unfortunately, using 2D analysis software like XFOIL to optimize the streamlined body shape is considered accurate enough, and there are no relatively simple codes available for axisymmetrical bodies. The only option is CFD analysis, which is far more costly in terms of computation time.

3.7.4 Optimized Streamlined Body Shapes

A considerable amount of studies have been done on optimizing streamlined bodies for drag, and interesting results have been obtained. When optimizing the fairing for lowest drag, one would inevitably end up with a shape as shown in figure 3.35a, as it utilizes laminar flow as much as possible (friction drag) while preventing flow separation (pressure drag). However, as the body has to be made out of cloth due to the weight restriction, it cannot be made very smooth, especially not at the stitches, as can be seen in figure 3.34a.

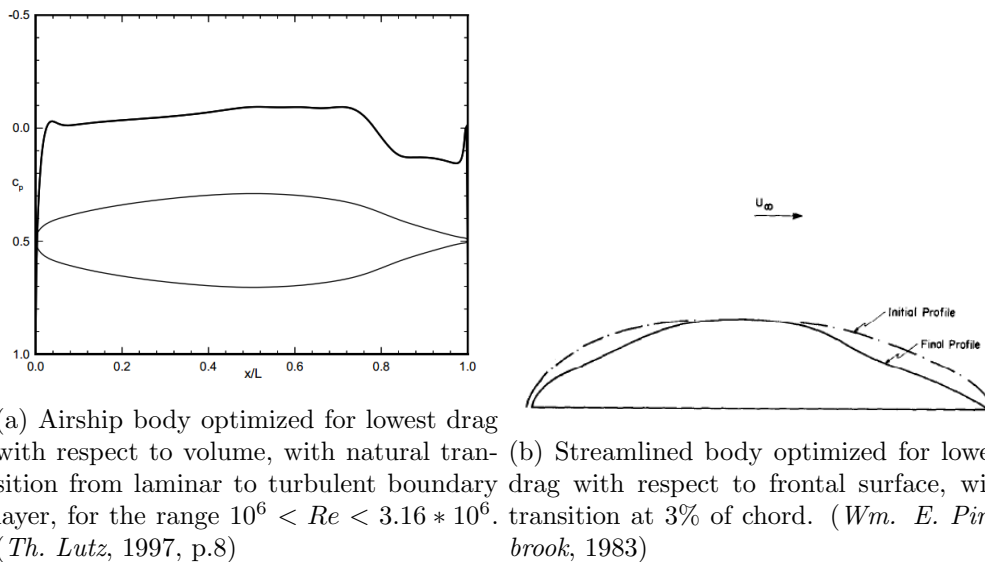


Figure 3.35: Streamlined bodies optimized for different criteria, in different ways.

It is therefore unlikely that laminar flow will be sustained for a large percentage of chord. In figure 3.35b, an almost fully turbulent body optimized for low drag with respect to the frontal surface is shown. Its shape is intuitive: if the flow is turbulent anyway, the wetted surface must be minimized. Therefore the diameter is decreased as much as possible while preventing flow separation by not letting the diameter contract too quickly.

3.7.5 Preliminary Fairing Sizing

The fairing must be optimized for drag with respect to frontal area, as a minimum thickness is needed to accommodate the pilot and the paramotor system.

To start sizing the fairing, it is important to know which fineness ratio ($\frac{length}{diameter}$) is desired. Figure 3.36 shows the drag coefficient on the frontal area of streamline bodies dependent on fineness ratio. It shows that, for any case, a relatively constant minimum drag is achieved for a fineness ratio between 2 and 4, with $C_D \approx .06$ for turbulent flow, at a Reynolds number of $Re = 1 * 10^6$. This Reynolds number is not low enough for extreme viscous effects to appear, and is close to $Re = 2 * 10^6$,

the value for a body with $2.5m$ chord length at $V_\infty = 11 \frac{m}{s}$, which are the approximate operating conditions of the fairing.

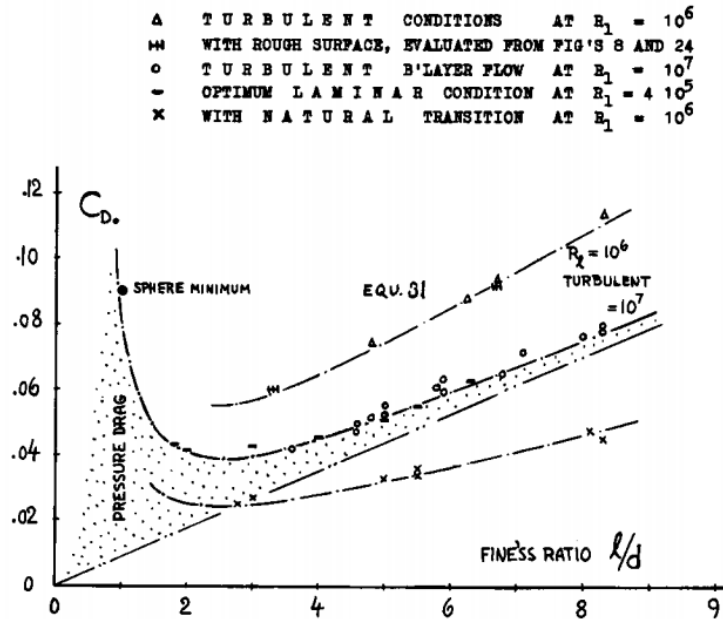


Figure 3.36: Drag coefficients on frontal area of streamline bodies as a function of their fineness ratio ($\frac{\text{length}}{\text{diameter}}$). (Hoerner, 1965, section 6-18)

However, the following should be noted: "With respect to frontal area coefficient, figure [3.36] shows a minimum at $l/d \approx 2.7$ or $d/l = 37\%$, respectively. Considering aircraft applications, it must be remembered, however, that the flow past streamline bodies is usually disturbed by interference through appendages or other adjoining parts. The optimum fineness ratio of such bodies or that of fairings is consequently higher than 2.7." (Hoerner, 1965, section 6-18)

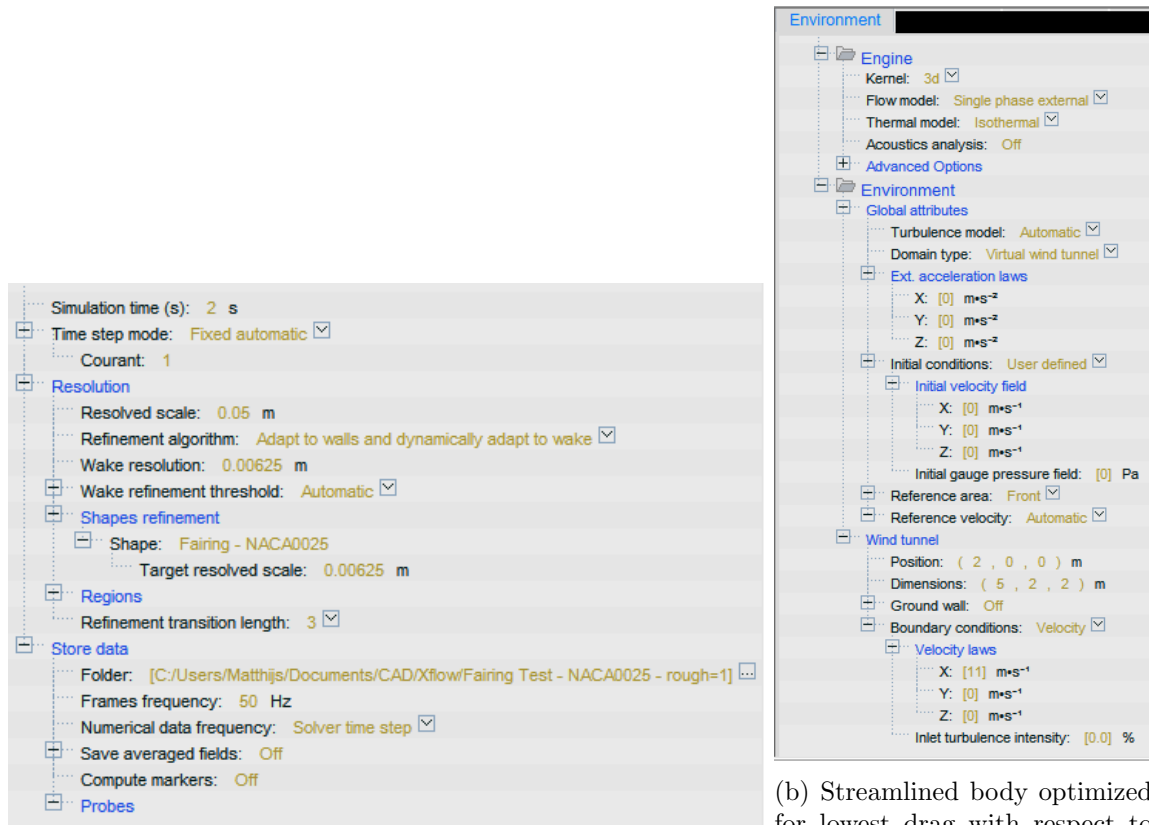
Knowing this, it seems wise to concentrate design efforts on shapes with a fineness ratio in the range $2.7 < l/d < 4$ (equivalently, $37\% < d/l < 25\%$). The final fineness ratio will be chosen based on the dimensions of the other parts, using CAD.

3.7.6 CFD Comparison of Fairing Shapes

Next to having a certain diameter to accommodate the pilot, the fairing should have a short tail end to enable a short driveshaft, lowering weight. This translates to having a maximum thickness far aft. Yet the risk of extra pressure drag becomes larger when the contours of the body contract more steeply. Therefore, XFlow simulations were done to find out the effect of thickness distribution on drag.

Four airfoils were chosen, whose outlines are shown in figure 3.38b. For the chosen airfoils a CFD analysis was performed using XFlow.

All four revolved bodies were modelled using CATIA with identical chord length of $2.2m$, after which they were imported into XFlow. A small convergence study on the mesh size was done after which a 3-dimensional wind tunnel test was simulated. All settings can be seen in figure 3.37a and 3.37b.



(a) Airship body optimized for lowest drag with respect to volume, with natural transition from laminar to turbulent boundary layer, 3% of chord. (*Wm. E. Pinebrook, 1983*)
 (b) Streamlined body optimized for lowest drag with respect to frontal surface, with transition at 3% of chord. (*Th. Lutz, 1997, p.8*)

Figure 3.37: Streamlined bodies optimized for different criteria, in different ways.

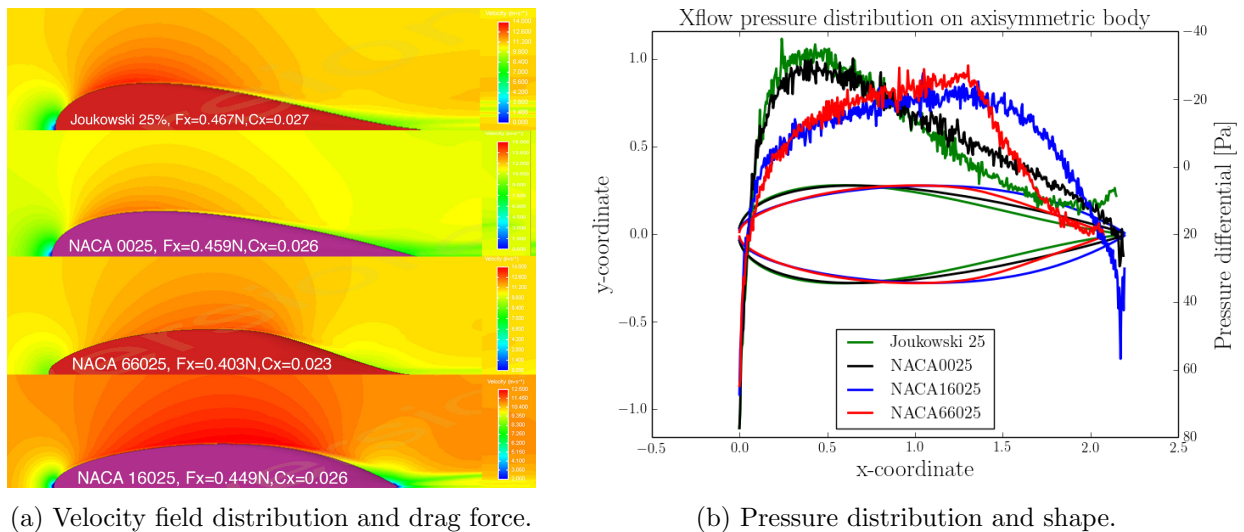


Figure 3.38: XFlow results on cutting plane in 3D simulation for four different 2.2m 25% thickness axisymmetrical bodies at $11 \frac{m}{s}$ and sea-level atmospheric conditions. The body with airfoil shape NACA66025 has the lowest drag.

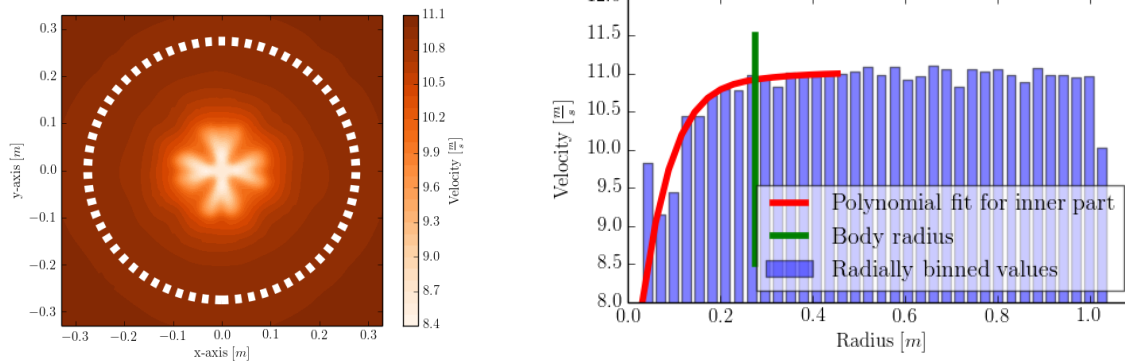
Velocity distributions and drag forces of all four airfoils can be seen in figure 3.38a, the pressure distribution in figure 3.38b. It can be noted that the axisymmetrical body with NACA66025 profile has the lowest drag, about 10% lower than the other airfoils. Looking at the velocity distribution, the wake seems to be smaller, and turbulent separation seems to happen a little later.

In addition, this shape looks more like figure 3.35b than the other airfoils; its wetted area is smaller,

which has an effect on the total drag. Adding the fact that the maximum thickness is far aft makes NACA66025 the best choice.

3.7.7 Fairing Wake Analysis

To be able to analyze the velocity field at the propeller, XFlow velocity data from a cutting plane exactly at the NACA66025 body's trailing point, orthogonal to the flow, was obtained. This velocity field is plotted in figure 3.39a. Only the NACA66025 body's wake is considered, as it was chosen for the fairing based on its low drag.



(a) Velocity field, with body contour at maximum thickness, indicated as thick dashed line. (b) Radially averaged XFlow wake velocity, with maximum body diameter indicated.

Figure 3.39: XFlow results on fairing. Length of body $2.2m$, velocity $V_\infty = 11 \frac{m}{s}$.

The rhombus shape anomaly, especially apparent at the lower flow velocities, probably appears because of a too narrow wind tunnel in XFlow. To analyze the velocity as a function of radius, these velocities are radially averaged. Figure 3.39b shows the histogram of these radial bins, a polynomial fitted to the inside region to better indicate the trend, and the body's maximum radius. Interesting to note is that the wake extends almost as far as the body's maximum diameter.

If the inflow velocity of the propeller varies, there are two factors that diminish its performance if they would not be taken into account: the blade will not see its optimum angle of attack for highest $\frac{C_l}{C_d}$ ratio, and its induced loss will be larger as the outflow velocity does not adhere to the minimum induced loss condition any more. Therefore, optimizing the twist in the inner region of the blade (where $r_{blade} < r_{max,body}$) is beneficial for propeller performance. As can be seen in figure 3.39b though, the maximum difference in velocity occurs very close to the center. It is chosen not to include this velocity profile in the optimization of the propeller since the hub radius is already $.15m$ and adding this velocity profile to the propeller design would only very marginally increase the propeller performance. However, the wake will be larger and more turbulent when taking into account the head and arms. This is not taken into account at this time, as CFD simulations are too costly regarding time.

3.7.8 Pilot Drag and Interference Drag

Due to their shape, the pilot's head and arms can be expected to be a source of substantial drag. Next to their own drag, they produce interference drag that acts on the streamlined body. In this section, this drag will be estimated, as it is of importance both in determining an accurate drag estimate, and in defining the best position of protrusions.

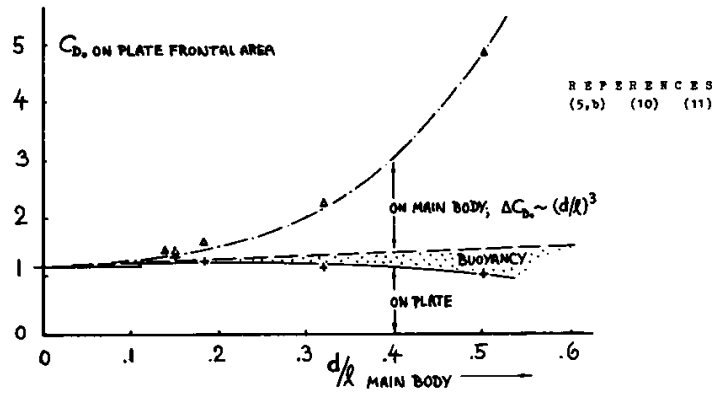


Figure 3.40: Drag coefficient on frontal surface of small plates or disks attached at 50% of chord, as a function of main-body thickness ratio, used to model interference drag of pilot’s head. (Hoerner, 1965)

The drag of the pilot’s head (including helmet) can be estimated by using empirically with figure 3.40, where drag for small disks attached around 50% chord is plotted as a function of streamlined body thickness ratio. At the design fairing thickness of 25%, The drag coefficient of the head, $C_{d_{head}}$, is 1.6. When calculating the drag in N , the local velocity value (which will be named V_{local}) must be taken, not V_{∞} . The equation for the pilot’s head drag thus becomes:

$$D = \frac{1}{2} 1.6 \rho \pi r^2 V_{local}^2 \tag{3.16}$$

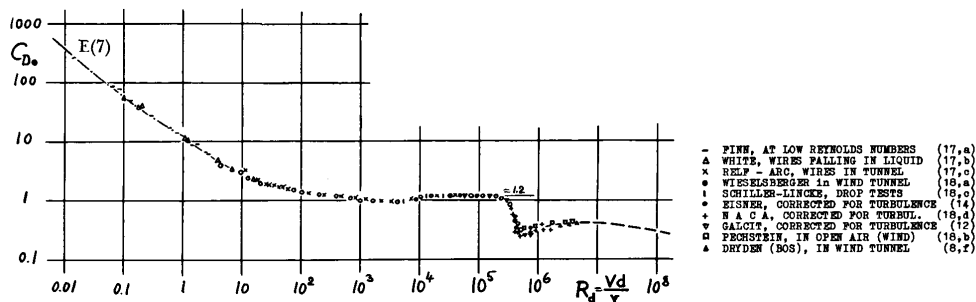


Figure 3.41: Drag coefficient on frontal surface of cylinder plotted against Reynolds number, used to model arm drag. (Hoerner, 1965)

The arms also cause interference drag, but only with the part near the body. As a rough rule only the part within 16% of the maximum main body diameter causes interference drag. The coefficient which can be found using 3.40 (Hoerner, 1965) is the same as for the head, thus $C_{d_{arms,interference}}$ is 1.6.

The rest of the arms are practically in free stream. The cross-section of the arms is approximately circular, and its Reynolds number in the order of 10^5 . From figure 3.41, it is found that $C_{d_{arms,freeflow}}$ is 1.2.

From the CATIA model, sizes of the head (including helmet) and arms were estimated using a frontal view. No increase in surface area from clothing needs to be expected, as tight jackets are usually worn to minimize arm drag. Estimated surface areas are shown in table 3.20.

Table 3.20: Pilot surface area estimates of exposed limbs.

Part	Shape	Dimensions	Surface area
Head	Circular	$r \approx 0.1m$	$S_{head} = \pi r^2 \approx 0.03m^2$
Arms within 16% of body diameter	Rectangle	$l \approx 0.1m, w \approx 0.1m$	$S_{arms,interference} = 2lw \approx 0.02m^2$
Arms outside 16% of body diameter	Rectangle	$l \approx 0.6m, w \approx 0.07m$	$S_{arms,freeflow} = 2lw \approx 0.08m^2$

Using these areas, the drag can be estimated at the flight speed of $11 \frac{m}{s}$ and ρ is 1.2 at sea level. From the velocity distribution in figure 3.38a, it can be seen that the velocity at the head and arms is approximately $12 \frac{m}{s}$, which is the value that shall be used for calculations. Results are shown in table 3.21.

Table 3.21: Drag estimate of head and arms, with interference effects on main body taken into account.

Part	Surface area	Drag coefficient	Drag ($\rho = 1.2, V_{local} = 12 \frac{m}{s}$)
Head	$S_{head} \approx 0.03m^2$	$C_{d_{head}} = 1.6$	$D = \frac{1}{2} * 1.6 * 1.2 * 0.03 * 12^2 \approx 4.1N$
Arms within 16% of body diameter	$S_{arms,interference} \approx 0.02m^2$	$C_{d_{arms,interference}} = 1.6$	$D = \frac{1}{2} * 1.6 * 1.2 * 0.02 * 12^2 \approx 2.8N$
Arms outside 16% of body diameter	$S_{arms,freeflow} \approx 0.08m^2$	$C_{d_{arms,freeflow}} = 1.2$	$D = \frac{1}{2} * 1.2 * 1.2 * 0.08 * 12^2 \approx 8.3N$
Total:			15.2N

However, this analysis assumes the arms are held wide open, while it has been shown that holding the arms closer to the body decreases drag considerably (Virgilio, 2004). In this position, interference drag is still created, but the frontal surface of the arms outside 16% diameter decreases at least half, reducing their drag to around 4N.

Figure 3.42 gives an intuitive overview of all drag values discussed in this section.

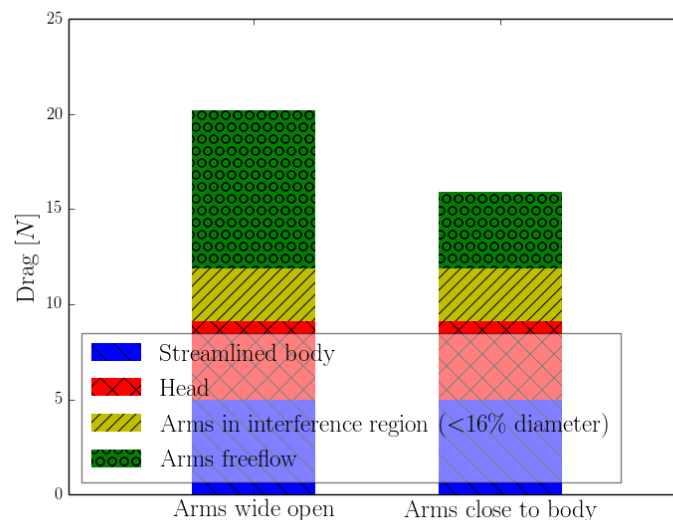


Figure 3.42: Drag estimates of entire system for $V_{local} = 12 \frac{m}{s}$ (local airspeed at head and arms is higher due to the air accelerating around the streamlined body) and $\rho = 1.2 \frac{kg}{m^3}$.

The drag is much larger than that of the streamlined body alone because of the high drag coefficient of the arms and head, but still much lower than that of a more conventional harness, which had a drag of around $20N$ (Virgilio, 2004).

3.7.9 Fin Sizing

The lateral (top-axis) moment created around the hang points by the fairing, must be counteracted by vertical fins at the stern of the body. Note that fins only have to be added to prevent lateral movement, as the centered COG provides a stabilizing moment to prevent pitch.

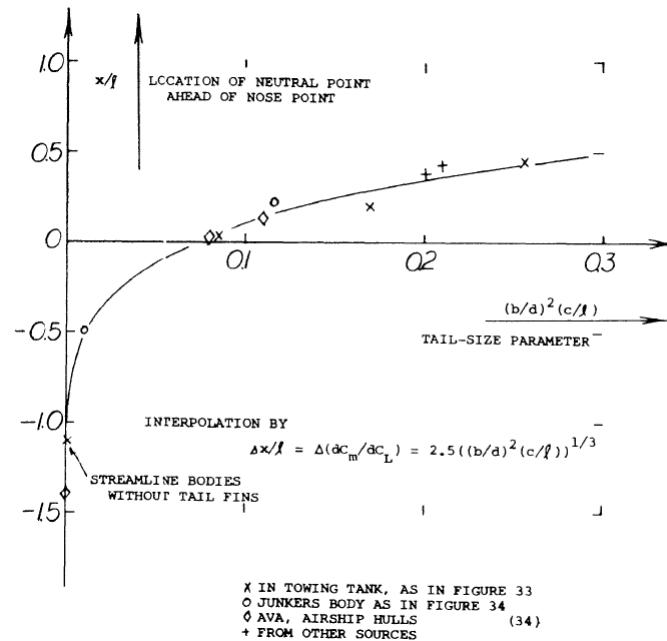


Figure 3.43: Statistical evaluation of the effectiveness of fins attached to the end of streamline bodies. (Hoerner, 1967)

The fins cannot just be seen as individual lifting surfaces, as they are influenced by the main body, and the main body is influenced by the fins. Windtunnel data of streamlined bodies with fins exists, and is shown in figure 3.43.

The length of the fairing in the current design iteration is $2.2m$, with a diameter of $.6m$, which is attached at $1.1m$ from its nose. From figure 3.43, in this case the tail-size parameter must be at least 0.3 for a neutral point at $0.5 \cdot l$. The fins must be even larger to achieve stability. A multiplication factor of 2 is chosen, which results in the following relation between fin chord and span, where b is the fin span, d body diameter, c fin chord, and l body length:

$$\begin{aligned}(b/d)^2(c/l) &= 0.3 * 2 \\ (b/0.6)^2(c/2.2) &= 0.6 \\ b^2c &= 0.5\end{aligned}$$

This relation will be used in sizing the fin. Using CFD to fine-tune fin size would be beneficial, but timeconstraints do not allow to do so.

3.7.10 Stern-Mounted Propeller Efficiency

The streamlined body shape also has an effect on propeller efficiency. One effect might be that the air is less turbulent behind a fairing than right behind a pilot without fairing, which might positively influence the propeller efficiency.

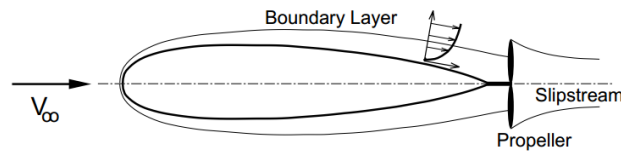


Figure 3.44: Flow around airship with stern-mounted propeller, the same configuration as the proposed fairing with pusher prop (*Th. Lutz, 1996*).

Other effects can be found by looking at the drag of airships with a stern-mounted propeller, essentially the same configuration as with the fairing proposed here. In this configuration, three effects influence drag and propeller efficiency, as described in reference (*Th. Lutz, 1996*).

1. Due to a lower pressure in front of the propeller, the back part of the streamlined body has more pressure drag. This is an inviscid effect.
2. The propeller efficiency increases due to the longitudinal velocity of the air being less at the propeller, as the air comes in at an angle due to the body's back part. This too is an inviscid effect.
3. Due to the propeller being in the lower velocity of the body's wake (and possibly boundary layer), its efficiency increases (if the propeller is optimized for this situation). This is a viscous effect, and is illustrated in figure 3.44.

It is important to note that the first and second effect practically cancel each other out. This leaves the third effect to increase propeller efficiency. In experiments with airships, required power was found to decrease between 10% and 30% (*Th. Lutz, 1996*).

If the propeller can be operated more efficiently in the body's wake, it might be beneficial to use a propeller of very low diameter. This would save weight, and be much more practical. However due to the smaller prop diameter the ideal efficiency would be reduced by a great amount (see 3.11), also the mass of the duct would be outside the propeller mass budget. For efficiency, a much larger propeller is desired. However, efficiency can be gained with any propeller size by taking into account the lower flow velocity in the fairing's wake.

3.7.11 Fairing Construction

In the final design iteration, the fairing measures 2.6m long, and is .78m (30%) in diameter. Its most forward point extends .15m forward of the pilot's feet, and the carabiners are located 1.22m behind the most forward point.

There are holes in the top surface, for the pilot's head and arms, and for the risers. It is wrapped around the rear end of the chassis, with a hole for the prop shaft. In the front, the pilot's feet are supported by a foot rest, and the fairing is connected to that foot rest.

One important practical aspect is the opening for the pilot's legs. It consists of a longitudinal slot in the bottom, with overlap in the cloth. When the pilot puts longitudinal tension on the fairing by putting his feet in the foot rest, this slot automatically closes, and the overlap makes sure no air gets out. When the pilot bends his legs, the longitudinal tension decreases, and the slot opens, so the pilot can stick his feet through the opening and make a graceful landing.

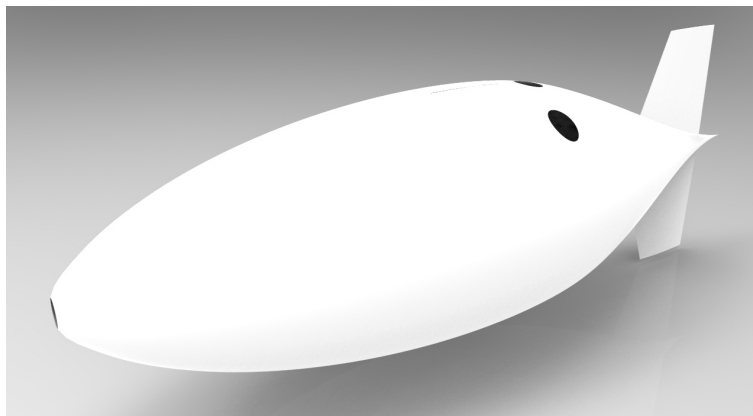


Figure 3.45: CATIA render of fairing, showing dynamic pressure port on its nose, holes for head and arms, and fins.

It was found that a fairing can significantly reduce drag compared to a normal harness, although the drag of the pilot's head and arms is relatively large still. A lightweight fairing made out of cloth, with revolved NACA66025 shape, was chosen.

A computer-generated image of the fairing is shown in 3.45.

3.8 Layout and Characteristics of the Overall System

Concluding, the final design comprises the following highlights:

Energy

The electrical energy required to accomplish the mission is stored in a primary battery pack consisting of 839 Li/SOC12 cells. This type of cells provided the highest energy density currently available. This amount of batteries in combination with the rest of the paramotor exceeded the weight budget of 22kg as set by the customer. However, the client agreed to a raise in the weight budget in order to achieve a non-stop mission. The minimum amount of battery cells was constrained by the peak power output rather than the total energy required.

Motor and Controls

The electrical energy is converted to mechanical power with the light weight and cheap Hacker A80-10 motor in combination with a gearing system consisting of two pulleys and a toothed belt, which has a gearing ratio of 1:5.5. The motor controller provides enhanced reliability w.r.t. some of the existing electric paramotors by using the CAN protocol for communication. Furthermore, the propeller can be put in vertical position to reduce drag during soaring and in horizontal position for landing and take-off. A bicycle type handbrake is attached to the gear such that even during large gusts windmilling of the propeller can always be prevented. The pilot is informed about the systems status through an OLED screen on the hand controller.

Propeller

One of the highlights of the design is the custom propeller that has been designed. An advanced optimization program was written in MATLAB which works together with XRotor and XFoil to find the best propeller design for the mission. The propeller was optimized with respect to aerodynamic efficiency and constructed using hard maple wood in order to be light and affordable. The designed propeller will perform at a propulsive efficiency of 79%.

Chassis

The designed chassis, or frame, is completely different from existing paramotor frames. The frame is attached to the wing at the hang point instead of to the pilot, and is balanced by placing the battery in the front. This keeps the frame in a horizontal position regardless of the pilot's position. The balancing of the frame has been carefully performed using a MATLAB script, to obtain the

frame's centre of gravity. The frame itself will be transportable without any folding or disassembling necessary. The final design will be constructed of lightweight aluminum 7075-T6.

Aerodynamic Fairing

The aerodynamic drag of the whole system has been greatly reduced by making use of an aerodynamic fairing around the whole system. The cocoon will be made out of lightweight fabric and uses dynamic pressure at the nose to inflate itself. The CFD program XFLOW was used to compare different cocoon shapes.

The final design of the paramotor is visualised in figure 3.46, along with an exploded view of all the parts in figure 3.47.

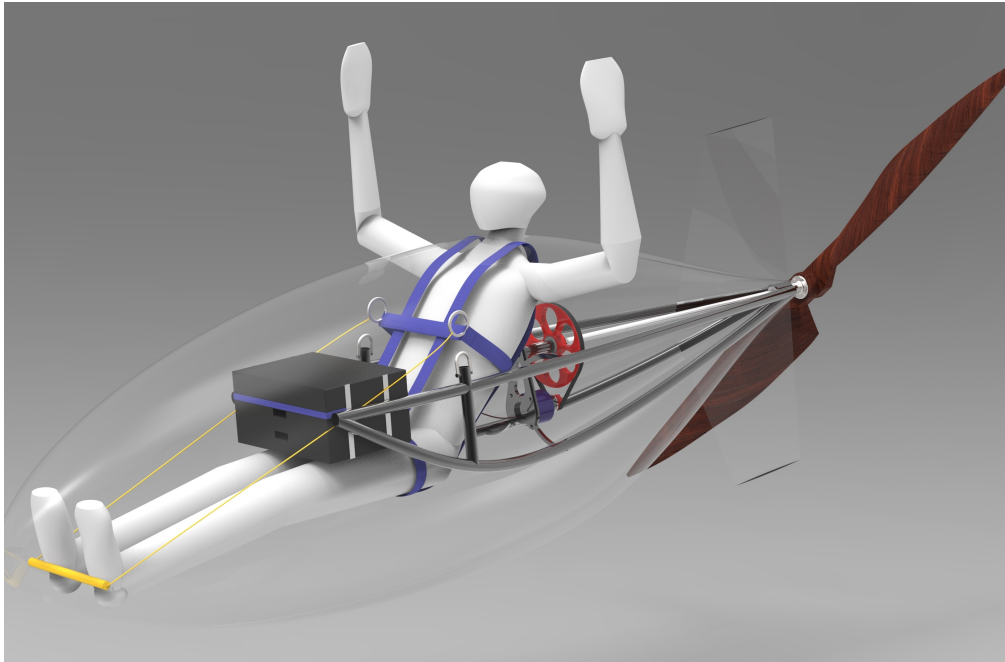


Figure 3.46: CAD visualisation of final system design

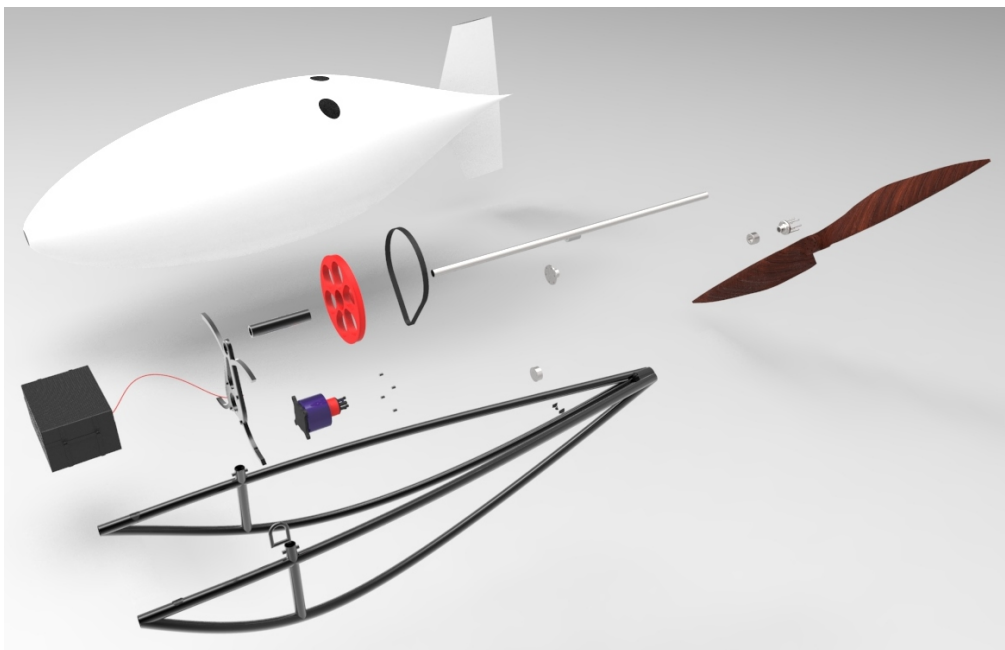


Figure 3.47: Exploded view of final system

4 Verification & Validation

In this chapter the verification and validation (V&V) procedures for every system of the paramotor design will be explained. Each section will contain the procedures for a part of the paramotor divided into their respective subsystems. Multiple types of V&V exist. It may concern the V&V of either software or a (sub)system. Software V&V will be most prominent in this chapter as many computer scripts have been used in the design. The verification of the software should check if the (sub)system is built right. In other words, prove that no errors occur in the script and show that information flows through the script correctly. Also, if problems are discretized, the software should show convergence. Software validation should check whether the script generates results that are close enough to the real world case. (Sub)System verification should prove that the (sub)system meets the set requirements, regulations and specifications. The validation of a (sub)system makes sure that the (sub)system meets the needs of the stakeholders and customers.

4.1 Verification & Validation of the Flight Simulation MATLAB Script

This section will elaborate the verification and validation of the flight simulation code written for the mission.

4.1.1 Verification of the Flight Simulation Code

The verification process proves the accuracy of the program. The code can be split up into multiple smaller functions that can be verified on their own. Choosing certain wind conditions for a fixed flight direction, it is possible to compute the airspeed analytically. Furthermore given the paramotor parameters one can calculate the thrust needed, as well as the required power and energy consumption. In order to ensure the proper functioning of the script this process should be repeated for different wind conditions and several flight paths. In the end the analytical results can be easily compared to the outcome of the MATLAB program. Since the computation of the airspeed is pure trigonometry, the error margin should be no more than 1%. After the airspeed is known the remaining parameters can be computed in a straightforward way, such that no margins of error are expected. The simple range equation that was derived for the midterm design can also be used to verify the overall mission outcome. In the following, the equation that was used is shown once more. (equation 4.1)

$$\frac{3600 \cdot \rho_e \cdot M_e \cdot \mu_{prop}}{D} \quad (4.1)$$

Where ρ_e is the energy density, M_e is the battery mass, μ_{prop} is the propulsive efficiency, and D is the drag in Newtons experienced during cruise.

Equation 4.1 is based on two assumptions:

- **Propulsive efficiency is constant over the trajectory.**

This assumption should have not that much effect since in the calculations a propulsive efficiency is taken based on the average drag and average flight speed during the mission.

- **Drag is constant over the trajectory.**

This assumption can only hold when flown at a constant velocity.

- **Steady non-climbing flight is considered**

No extra drag is created due to climb angles.

Substituting all parameters, as they are for the final design results in a total range of 217.28km with one battery pack charge. In order to verify the basic structure of the program the wind speed was set to $0 \frac{\text{m}}{\text{s}}$ in order to be comparable to the range equation. The simulation program computes then a range of 221.02km , which results in an error between the two approaches of 1.7%, which can be considered low.

4.1.2 Validation of Flight Simulation Code

The program can be validated by flying one section of the mission and comparing the energy consumption to the one predicted value from the program. An error margin of 10% is acceptable, due to constantly changing wind conditions, which are not taken into account by the program, that assumes constant wind conditions in one section. However the results can already be compared to existing paramotor performance data.

4.2 Verification & Validation of Motor and Controls

The motor, motor controller and input controller and interface all need to be verified and validated. Not only the separate components, but also their combination needs to be reviewed. The input controller will be verified and validated extensively such that it can be used when validating the motor and motor controller.

4.2.1 Verification and Validation of the Input Controller and Interface

The input control should be verified extensively before it is produced. After the PCB schematic has been developed in detail it should be checked multiple times. The behaviour of the circuit can then be simulated with a software program that visualizes its behaviour such as the program SPICE¹. Changes can still be made after which the PCB design can be produced. The software for the microcontroller also needs to be developed and verified through extensive software testing. The design can then be validated by simulating specific inputs combinations on the circuit board and checking if the output signals are as expected.

4.2.2 Verification of the motor and motor controller

The motor and motor control are bought off-the-shelf, therefore their verification mainly consisted of checking that they comply with the specifications that are desired. It has been checked with the motor controller supplier if the chosen motor is compatible with the motorcontroller.

4.2.3 Validation of the Motor and Controls

The motor and controller will first be bench-tested. Motor torque, speed and temperature will be measured as well as the voltage and current applied to the motor. In this way it can be determined if the motor provides the expected torque at the supplied current. It can also be detected if the motor becomes too hot and if extra cooling is necessary. In this way the operating range of the motor can be further investigated. If the results are as expected, then the motor and controls can be validated together with the gearing and propeller by building a test setup to which the motor and propeller are attached.

¹<http://www.ni.com/white-paper/5413/en/>, Visited on 19th of January 2014

4.3 Verification & Validation of the Propeller

Because of the fact that the propeller is a part of the paramotor that is completely designed from scratch, it is important that it is verified and validated extensively. In this chapter, these previously mentioned procedures are explained. First a breakdown of the different tools and methods used during the design of the propeller will be given. Finally the different tools and methods will be verified and validated.

Breakdown of Method and Tools

The two most important analysis tools for the propeller design are the XFOIL and XROTOR programs. They are the fundamentals of the propeller design, both airfoils and propellers are analysed using these programs. They need to be verified and validated extensively where possible. Also the particle swarm optimization module needs to be verified, both the optimization effectiveness as well as the results need to be verified. Finally the finished propeller needs to be validated in a windtunnel.

4.3.1 Verification of Propeller Design Modules

In this subsection the basic methods of verifying the most important modules used during the propeller design will be described.

XFOIL

Verification of XFOIL is an incredibly difficult process. XFOIL is based upon panel method calculations of potential flow. The solution is iteratively solved by using a full Newton method. This means the method is extremely numerical and very hard to solve by hand. Although out of the scope of this DSE, it is possible to do hand calculations on extremely simplified problems. For example it is possible to simulate the inviscid case of an airfoil with only 2 panels in XFOIL. It also must be stated that XFOIL is an extensively validated tool and widely used in the community. Hence validation for XFOIL is available and eliminates the need for verification. Validation of XFOIL can be found in (*Weisheng Chen, 2008*).

XROTOR

Analogous to XFOIL, verification of XROTOR is a very difficult process. Both the optimization process of the program needs to be verified, as well as the results. The fact that there are no publications on the workings of XROTOR make the verification process even harder. However, although extremely time-consuming, there is a possibility of verification. Since the source code for XROTOR is available online, one could try to understand the code and perform verification calculations by hand. The bend function of XROTOR is more easy to verify, since it uses a slender beam approach to calculate deflections and strains at each section.

Particle Swarm Optimization

The particle swarm optimization module verification mainly consists of verifying if the optimization process works effectively and solution converges to the lowest objective function value. This can be done by applying a simplified low dimensional problem to the particle swarm optimization module. The objective function chosen for the verification of the PSO module is two-dimensional and therefore visualisation of the dynamics of the particles is possible by plotting each particles' position against the objective function.

A good test objective function for the PSO module would be the Rastrigin function. This function is heavily multi-modal and shows a large amount of local optima as can be seen in figure 4.1.

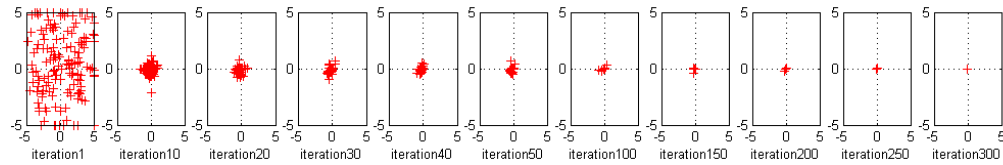


Figure 4.2: the convergence of the particles on the rastrigin function to the global optimum of (0,0)

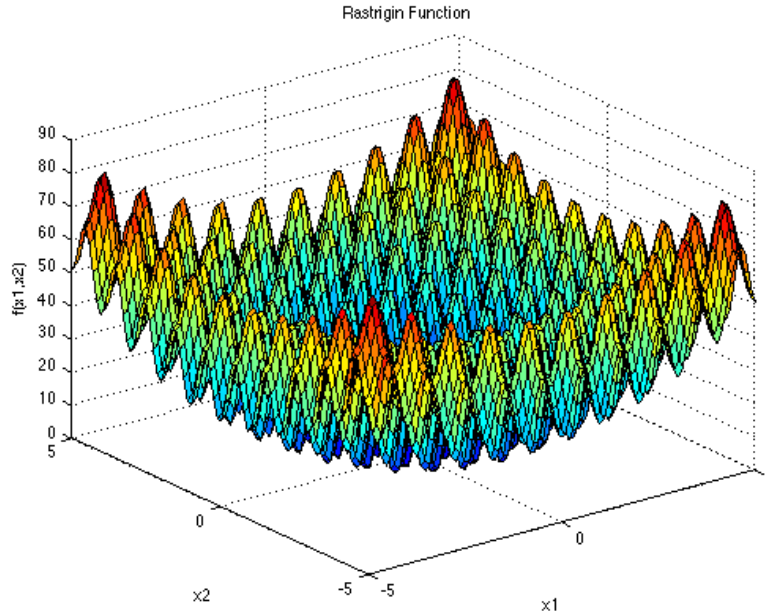


Figure 4.1: The heavily multi-modal rastrigin function, used to test the effectiveness of particle swarm optimization on multi-modal problems

The global optimum is located at $X_1=0$ and $X_2=0$ and its value is 0. The rastrigin function for a two-dimensional problem is given in 4.2.²

$$F_{obj} = 20 + (X(1)^2 - 10 * \cos(2 * \pi * X(1))) + (X(2)^2 - 10 * \cos(2 * \pi * X(2))) \quad (4.2)$$

The particle speed, particle trust factor, and global thrust factor were taken as 0.4, 0.3 and 0.8 respectively. The amount of particles was set at 150 and the number of iterations was set at 300. A visualisation of the convergence is shown in figure 4.2 and shows the behaviour of the swarm. It is clear that the minimum is approached rather quickly. It is proven that the PSO module performs as expected because it effectively finds the correct minimum of the objective function. For more information on the PSO module, please look at Appendix J.

4.3.2 Validation of Final Propeller Design

The validation of the propeller design, can be performed in a wind tunnel facility. For the investigation the propeller will be mounted in the test section and several runs will be performed. In between the runs the wind velocity varies, while keeping the RPM of the propeller fixed. Afterwards the RPM changes in a certain range, with a fixed wind speed. The torque created by the rotating propeller can be measured with force transducers, when calibrated and placed in the correct way. (*Brandt and Selig, 2011*) The produced thrust can be measured using a propeller mounting, that is connected to a load cell. This way the efficiency of the system can be obtained, since the thrust and power coefficient, as well as the advance ratio are known. The efficiency is then computed by using

²<http://www.sfu.ca/~ssurjano/rastr.html> Visited on Jan 20th of 2015

equation 4.3, where η is the propeller efficiency, λ the advance ratio, C_T the thrust coefficient and C_P the power coefficient.

$$\eta = \frac{\lambda * C_T}{C_P} = \frac{T * V_0}{P} \quad (4.3)$$

The structural properties of the propeller can be validated using a test rig, where the real-size propeller is mounted in. The thrust and drag distribution, as well as the centrifugal force over the blades can then be simulated by pulling the blade in the direction accordingly to the resultant force and therefore introducing the bending moments and shear forces. Furthermore the twist must be investigated, which is caused by the rotating of the blade towards lower blade angles. The test is being performed until the structure fails, such that a conclusion about the maximum load capabilities can be drawn.

4.4 Verification & Validation of the Batteries

This section will briefly discuss the verification and validation of the battery pack design. First the verification procedure will be elaborated on, followed by the validation.

4.4.1 Verification of the Battery Pack

The verification of the design of the battery pack mainly comprises checking all calculations that were performed in excel. The entire performance analysis of the battery pack and the structural analysis of the casing are calculated in excel. To check whether the results from excel were accurate, the same formulas that were implemented in excel have been manually worked out. This has been done two times per calculations and it could be concluded that the results from excel are accurate.

4.4.2 Validation of the Battery Pack

The validation of the battery pack will be done by testing the batteries of the final design. From these test results the same graphs will be produced as in the data sheets provided by the manufacturer. At the MAVLab, which stands for Micro Air Vehicle Laboratory, at the faculty of Aerospace Engineering a test set-up is available to test different performance characteristics of batteries. The most important graph that needs to be produced is the graph that shows the discharge rate characteristics. An example of such a validation can be seen underneath. A battery enthusiast has validated the performance of the rechargeable NCR18650B Lithium Ion battery. From figures 4.3 and 4.4 it can be seen that the manufacturers data sheet is very accurate. The manufacturer data sheet can be found online ³, while the complete self tested data sheet can be found on the forum of the battery enthusiast from where it was retrieved ⁴. A sample of such a NCR18650B battery has been bought to perform this validation and prove the accuracy of the data sheet. This test has not been performed at the moment this report is being hand in due to time constraints. Hence, if time allows so, the testing will be executed before the final symposium.

As at the moment of writing, no sample was available of the battery that will be used for the mission, all calculations will be based on the manufacturers data sheet until they are in store again.

³<http://www.bipowerusa.com/products/BP-ER17505M.pdf>, visited on january 16th 2015

⁴<http://lygte-info.dk/review/batteries2012/Panasonic%20NCR18650B%20Protected%203400mAh%20%28Green%29%20UK.html>, visited on january 16th 2015

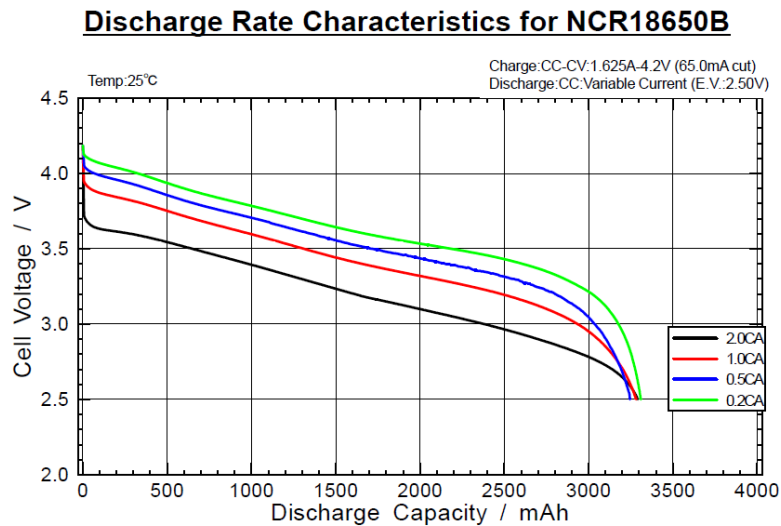


Figure 4.3: Discharge rate characteristics graph from the manufacturers data sheet

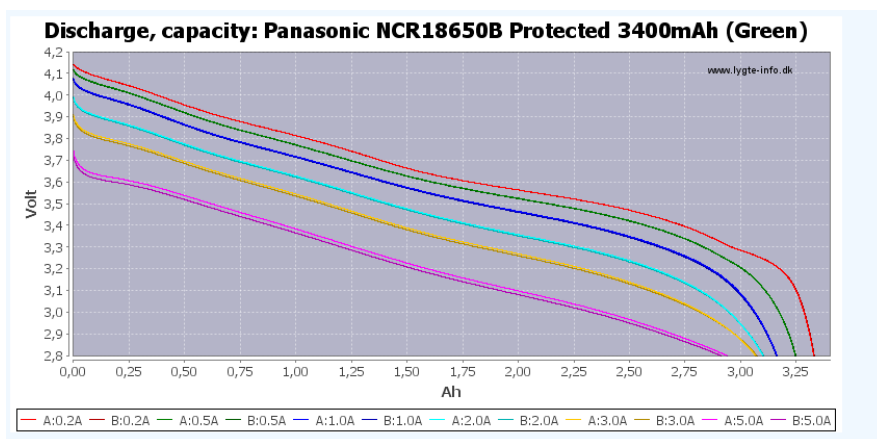


Figure 4.4: Discharge rate characteristics graph from the hobbyists data sheet

4.5 Verification & Validation of Chassis

This section will discuss the verification and validation of the chassis. The center of gravity (COG) optimization script, drivetrain and frame design will be discussed.

4.5.1 Verification of the Center of Gravity MATLAB Script

The verification is performed to check the accuracy of the script. In this case the center of gravity calculation of the pilot as well as of the system need to be tested. To test the systems COG, one can pick one seat angle and the corresponding drivetrain length, battery position and drivetrain position values and calculate the COG of the system by hand. Also the COG of the pilot should be checked by hand using that same seat angle and the given body part weights and sizes. To properly verify the script this process should be done for different angles to make sure it works for any setting. The hand calculations should be compared to the script's output to have no difference in the outcomes. If any errors occur, the script needs re-checking. Another method, which is not as accurate, is to compare the calculated COG's to the COG location Catia indicates, using the same parameters for all components. In that case the exact material properties should be used in Catia though, because else the masses and therefore the COG's will not match.

4.5.2 Validation of the Center of Gravity MATLAB Script

The only way to properly validate the COG calculations and positioning of the different components is by building a prototype and checking if the system is balanced in all flight steps. If the COG's difference stays within 10%, the system is said to be validated.

4.5.3 Verification of the Driveshaft

The verification should test the accuracy of the scripts blocks independently and as a complete unit. Each separate block should be tested by performing the calculation by hand and checking this results with the script output. This should then be done for the complete unit of blocks to check if the data is correctly transferred over each block. If errors are found, the block should be re-checked from the start. As a last check a sensitivity analysis should be performed. Each input value should be altered separately after which the results should be checked for change. If no change occurs where it is expected to appear, the script will need to be checked after which the whole procedure should restart.

4.5.4 Validation of the Driveshaft

In order to validate the method and theory used for the design of the driveshaft, one can use or create experimental data. Experimental test data could be found in literature on structural analysis. Test data that contains results on torsion, bending, buckling and eigenfrequencies in hollow cylindrical beams of isotropic material are needed. The written script in MATLAB should be set up to represent the test conditions and the results will have to be compared. If no test data is found, another option is to create a test setup. One should take a hollow cylindrical beam and put it through various loads, combined and separate, whilst monitoring the stresses that build up with the use of stress test strips. Furthermore, the eigenfrequency can be checked by exciting the beam at forced frequencies and monitoring at what frequency the eigenfrequency appears. When results of the experiment or literature come within 10% of the expected values the script can be considered validated.

4.5.5 Verification & Validation of the Frame

The verification and validation concerning the frame has been partly carried out already. This can be reviewed in section 3.6.2.

4.6 Verification & Validation of the Fairing

In this chapter the verification and validation of the fairing design is elaborated on.

4.6.1 Verification of the Fairing

Most calculations regarding the fairing are based on empirical data from (*Hoerner, 1965*), which can be consulted for further details. Further CFD analyses could give an indication as to how accurate these drag and stability predictions are.

4.6.2 Validation of the Fairing

Validation of estimated drag can be performed by making a prototype and measuring it in a wind tunnel, or in-flight. Wind tunnel tests are useful to optimize the shape of the body, and the size of the

fins. Also, measurements on the wake can be performed, which might be useful to further optimize the propeller design. In-flight tests can be used to test its drag in real-world conditions.

In-flight, the use of a wake rake, which is normally used in wind tunnels to measure drag, is very impractical. Instead, a much simpler solution exists: measuring the forces between carabiner and riser. This can even be done with just one load cell, as the weight of the system is known, thus additional forces like drag and thrust can be measured by the magnitude of the force on a one-axis (1D) load cell (which, for proper measurement, aligns itself with the load vector). However, the presence of lift from the body might complicate this measurement, something that should be investigated in the wind tunnel tests.

Such a device is placed between the riser and the hang point on the frame. It needs to automatically align the load cell with the force vector, as forces in other than the one direction are not measured. Such a device would look like illustrated in figure 4.5, and indirectly allows measurement of fairing drag and propeller thrust.

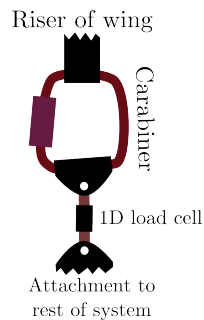


Figure 4.5: Device that can be connected between riser and carabiner, to measure in-flight loads.

4.7 Verification & Validation Conclusion

As can be seen in the aforementioned sections, well performed verifications for each part are vital before prototyping can be started. None of the MATLAB scripts nor any other calculation is properly verified yet due to the time constraints of the DSE project. Once all calculations are verified, parts will be manufactured and tested individually. Passing the system tests, a prototype is built for which test flights will be scheduled to gain experimental data. This data will be used for comparison to the theoretical results, which are proven to be validated as soon as the outcomes match.

5 System Design Support

Supportive tasks on the system design of the paramotor can be found in this chapter. Firstly a risk analysis is given in section 5.1, which describes the risks that the team has encountered and how they have been overcome. Section 5.2 analyzes four essential characteristics of this technical system: the reliability, availability, maintainability and safety. After that the communication flow within the paramotor system is mapped in section 5.3.

The sensitivity analysis in section 5.4 determines how the system is influenced by changes in major parameters and to what extent this influences the mission. To conclude this supportive chapter the sustainable approach towards the project is described in section 5.5.

5.1 Risk Analysis Assessment

Risks of all sorts are encountered when designing a technical system. These risks were assessed in the beginning of the project in order to be prepared to cope with them.

The risks that were assessed were divided into two categories; design process risks and mission risks. The design process risks comprise of team and project risks. Whereas team risks are not directly related with the technical aspects of the design or relevant for the customer, but project risks are and might influence the design process. All team and project risks are summarized in table 5.1. In addition, at the end of the section, the risks encountered during the mission itself are explained.

Table 5.1: Summary and nomenclature of team and project risks determined in the first phase of the project.

Team Risks	Project Risk
TR1: Conflict within the team	PR1: Insufficient skills
TR2: Withdrawal of a team member	PR2: Inaccurate cost estimate
TR3: Extenuating circumstances	PR3: Insufficient resources
TR4: Lack of commitment	PR4: Inaccurate planning
	PR5: Erroneous calculations
	PR6: Poor design choices
	PR7: Insufficient market opportunities
	PR8: Influences of safety on the market
	PR9: Unavailability of resources
	PR10: Change of regulations
	PR11: Market competition

5.1.1 Team Risks

The team risks that were determined in the first phase of the project as mentioned in table 5.1 are discussed in this section.

The team was confronted with risk TR1 and TR4. It was obvious that conflicts would arise when nine engineers are put together in a room for ten weeks, so people were prepared for this. Most conflicts were overcome by having group discussions, or simply by doing some more in-depth calculations to reinforce one's argument and eliminate others.

Risk TR4 was conquered by setting clear agreements within the group about making up for being late or absence. After some conflicts about these rules, they were reassessed to have everyone agree

with the terms. Although this caused conflicts, it worked out well in the end. A team member that seemed to lack commitment had some talks with the chairman, and showed more dedication afterwards. The peer evaluation was a good tool to discuss and be critical on each others commitment as well and to see where team members could improve. It can be concluded that the team worked well together.

5.1.2 Project Risks

During the project, the team also encountered quite some risks related to the development and design of the system. Those are not only relevant for the team, but also for the other stakeholders. None of the project risks was very severe and they were overcome without too much of a hassle. PR1 especially seemed the case in the beginning, as only one team member had paragliding experience. Doing a small literature study on this subject and having the experienced team member give a presentation helped a lot. For the engineering fields the team was lucky to have a very broad skilled group, so there was an expert in every field and the team complemented each other well.

The budget of €5000 was a barrier for many design options, as predicted in risk PR2. As the system had to be lightweight and aerodynamic, asking for innovative and lightweight subsystems, which are often expensive. This was overcome by engineering creativity. As soon as it was found that the mission could be flown in one go with a bigger battery, the team was given permission to extend the cost budget for the battery. However, after some research one company offered the battery for a much lower price, as described in chapter 3.3, and the whole system is again within the required budget. To the teams surprise they were not confronted with risk PR4. When setting up a project plan without being completely informed about the subject, a situation in which planning inaccuracies are likely to occur, which could delay the process. This was avoided very well by integrating periods of slack in the planning and by having regular meetings for everyone to stay up to date with the progress.

Some calculation errors were made during the project as was predicted by risk PR5. However, after double checking each others work and doing verification procedures where possible the results seem very plausible. Undiscovered minor mistakes might still exist, but their impact seems small as has been determined by the verification procedures.

As mentioned in risk PR6, due to the inexperience and the short time available to complete the project, poor design choices were made at some points in the process. These choices were discovered during team meetings as single components were good on their own, but combining these components did not always go well. An example of a poor design choice was having a leg container with a tilted propeller, which drastically decreased the propeller efficiency. After some discussion, the idea of a leg container was extended to a full body cocoon, and with some alterations and thoughts about the flight strategy, landing and take-off was still possible (which was originally the point of having a tilted propeller).

To overcome risk PR7, two strategies for the design process were determined, as thoroughly described in section 7.1. By firstly realising the mission with a dedicated paramotor system, it can be used to draw attention to the product for sales. By adapting the system in a later phase to a system that is more appealing to the market, the team hopes to have enough market opportunities. The team ran into risk PR9 during the battery design. Various articles were found about the very promising results that were obtained in energy density and mass in the development of so-called organic batteries. However, it turned out that the mission would have been a lot easier if these were already available and on the market.

5.1.3 Mission Risks

After having discussed the risks that could be encountered within the team or during the design and development of the project, the risks that could occur during the mission itself need some elaboration. As the mission has not been carried out yet, the measures that have been taken to avoid

these risks are discussed in this section.

- **MR1: Hazardous weather:** In rain, hail, thunder or other hazardous weather, one can't fly with a paramotor. This is an important risk, as the mission goal is to fly across the Netherlands which is known for its variable weather. However, as discussed in chapter 2, the date on which the mission is to be carried out will be chosen carefully with respect to the weather forecasts. In addition, during the mission the weather will also be watched closely by the ground crew.
- **MR2: Collision with other airspace users:** To avoid collision, the paraglider will avoid busy commercial airspace and stick to general air traffic regulations.
- **MR3: Turbulence and wind gusts:** Paramotoring uses a flexible wing which is very sensitive to external inputs like turbulence and wind gusts. To avoid accidents as a consequence of this, stability and controllability was an important factor in trade-off for the wing. This risk is also part of risk MR1; the mission will be carried out on a day with a nice laminar, not-too-strong wind, to avoid gusts.
- **MR4: Poor flight strategy:** The flight strategy is a big part of the success of the mission. The team has therefore prepared the mission accurately, and can easily adapt the strategy with respect to the predicted weather or other circumstances. Adaptions to the strategy can also still be made during the mission by the ground crew if they feel that it is necessary to do so.
- **MR5: Structural system failure:** A structural system failure can arise in different forms. It could be that a mistake has been made during the design, which could be a manufacturing error or for example a failure due to fatigue. Structural failures comprise all unexpected failures within any structure. These failures can be split into two categories; sure life and fail safe. The first one comprises systems that are not allowed to fail in any case, as failure would be fatal. The fail safe category comprises systems that won't cause severe consequences in case of failure. In order to avoid both kind of failures, redundancy is incorporated where possible and calculations or designs made are verified and validated where possible.
- **MR6: Pilot error:** In case of a pilot error in flight, several outcome scenarios are possible. Once again they can be categorised in two branches. Firstly the errors which have a severe consequence and secondly the errors with a less severe consequence. When a severe error occurs, the final saviour is in the safety chute. In all other pilot errors the pilot can possibly intervene and solve the situation and get back in control. Other safety features are described in section 5.2.4. The pilot that will fly the mission is a professional test pilot with adequate training.
- **MR6: Battery level low:** This risk is actually a result of risk MR1 and MR4; if the wind is stronger or in a different direction than expected, the flight strategy needs to be adapted accordingly or the mission shouldn't be carried out at all, otherwise the battery level might become too low to carry out the full mission. A small safety margin is built in the battery capacity to avoid such issues. In addition, the pilot will be equipped with a GPS device that shows exactly what direction to fly in order to fly as efficient as possible. The ground crew keeps an eye on the route flown and warns the pilot if he is going in the wrong direction.

It can be concluded that the measures taken to be prepared to cope with the team and project risks worked well, as no fatal problems occurred. Risks that the team encountered were generally dealt with well, with a good solution-seeking attitude. Good communication within the team turned out to be the most important factor in avoiding risks. A more extensive review on some mission risks and how the system reacts if they are encountered is written in the sensitivity analysis in section 5.4. However, if hazardous unforeseen circumstances arise during the mission, the mission might still have to be aborted. The ground crew will need to watch out for such cases during the mission such that it can be terminated safely if needed.

5.2 RAMS

In this section the RAMS characteristics of the electric paramotor will be analyzed. RAMS is an acronym for Reliability, Availability, Maintainability and Safety. These four properties are considered to be essential characteristics of technical systems.

5.2.1 Reliability

Reliability can be determined in different aspects of the system. Firstly, it means the system will behave in the way it should and will not react in an unexpected manner to the pilot's input. This also means the system is stable and controllable. In addition, reliability also involves the durability. This means the system has a certain resistance and strength.

For the first definition of reliability, the stability of the system is determined in section 3.6.1. A centre of gravity optimization script was written in order to define where to place each component for the lightest weight, smallest inertia and closest centre of gravity location. By having the system's centre of gravity as close as possible to the pilot's centre of gravity, optimized balancing can be achieved. The controllability of the system can be divided into the controllability of the motor and of the parachute. The motor's controllability is assured by the motor controller as described in section 3.4.4, operated directly by the pilot. As can be read, it will be a two-liner, which are known for their manoeuvrability and high glide ratio, but not exactly for their stability. However, as can be read in Appendix L, a very experienced test pilot has admitted that such a wing can be used and is safe enough to use.

The second definition of reliability, defined by the system's strength, is described for each subsystem in chapter 3. Good examples are section 3.6.3, where the structural integrity of the driveshaft is explained, and section 3.5.4, where the material choice for the propeller is justified by calculating the strains on the final design, as shown in figure 3.25.

5.2.2 Availability

In the different trade-offs the availability of the sub-parts and their materials played an important role. Whenever a certain material or technology was not available, too expensive or not on the market yet, it was not used for the system.

These choices are, among other things, illustrated in section 3.3.1, where it is explained that organic cells are not a viable option due to their unavailability. Section 3.5.4 explains that the manufacturing costs outweigh the weight penalty when using wood over a carbon composite sandwich structure for the propeller. The goal is to have the design of the system ready to build right at the end of this project. Hence, unavailability eliminates multiple design options.

5.2.3 Maintainability

The maintenance of the paramotor is discussed in section 2.3.3. In addition, the mission planning states that the paramotor is always checked before flying. During these checks it can be examined whether the paramotor components and the wing are still intact. Scheduled maintenance activities include the checking of bearings and belt tension. Furthermore the bearings should be lubricated frequently. The wing needs to be certified every two years and the safety chute should be refolded twice a year.

5.2.4 Safety

Several parts of the paramotor are critical for safe operation. The most crucial part of a paramotor to be safe is its wing. Therefore redundancy is applied in this area by taking a reserve chute, which is actually obligatory to fly with.

The battery is also a critical part considering safety, as it should be cooled and cased to prevent fire or even explosion. A carbon fibre casing as described in section 3.3.2 will be made to keep it in place. Still, if anything were to happen, the pilot and the paramotor system are both connected separately to the wing, such that the whole system, except for the wing of course, can be cut-off with a hook knife and slide off the pilot. This should of course only be the case in an emergency situation, as it will lead to a mission fail immediately and endanger people on the ground.

The propeller is placed far enough back to make sure the arms and head of the pilot can not be hit, as shown in chapter 3.6. During take-off, the propeller is locked in horizontal position to prevent propeller striking. As described in 3.4.4 the motor controller ensures the safe functioning of the motor and its speed. More safety options, like a kill switch, are assured by the input controller, which also includes a display to show all vital information.

5.3 Communication Flow Diagram

The Communication Flow Diagram (CFD) illustrates the flow of data through the system and to and from its environment. This is an essential part of the design since the need for communication between these different subsystems determines the communication techniques that can be used. Sometimes this even means that extra controllers would be needed to be able to make the different communication flow types compatible with one another. The CFD contains all elements that are part of the communication chain in blocks and represents data and command flows as arrows.

Diagram 5.1 shows the communication flow diagram for the paramotor system, where table 5.2 annotates the figure by listing the different command types of the communication flow. This diagram was created in an early stage of the project and made sure no critical communication steps would be missed in the final design process.

In addition, in section 3.3.5 the communication flow diagrams of the battery management system is discussed thoroughly.

It should be noted that the CFD shown in figure 5.1 takes regeneration into account, so it would be the CFD for the paramotorsystem that should become commercially available. As regeneration is not used in the mission, the CFD for the mission will be similar to the CFD shown, except that the Generation Control and Generation System block can be discarded. All underlined commands in table 5.2 can be discarded for the same reason, and the arrow for command 20, providing the battery status, will go directly from the battery to the display.

5.4 Sensitivity Analysis Mission

The sensitivity analysis investigates the sensitivity of a design solution for a change in major system parameters. It is used to test the robustness of design options for such a change and establishes the degree of feasibility of the final design.

For the electric paramotor, there are several system parameters that could change considerably and would result in a lower range. The consequences of these parameters are stated below and table 5.3 expresses those changes and relates them to the battery percentage left at the end of the mission. In addition, it shows the critical value for this parameter, so the point at which the battery is empty at the end of the mission.

1. **Decrease in propulsive efficiency:** A decrease in propulsive efficiency will lower range linearly, and can be caused by many imperfections, such as a higher bearing friction or the

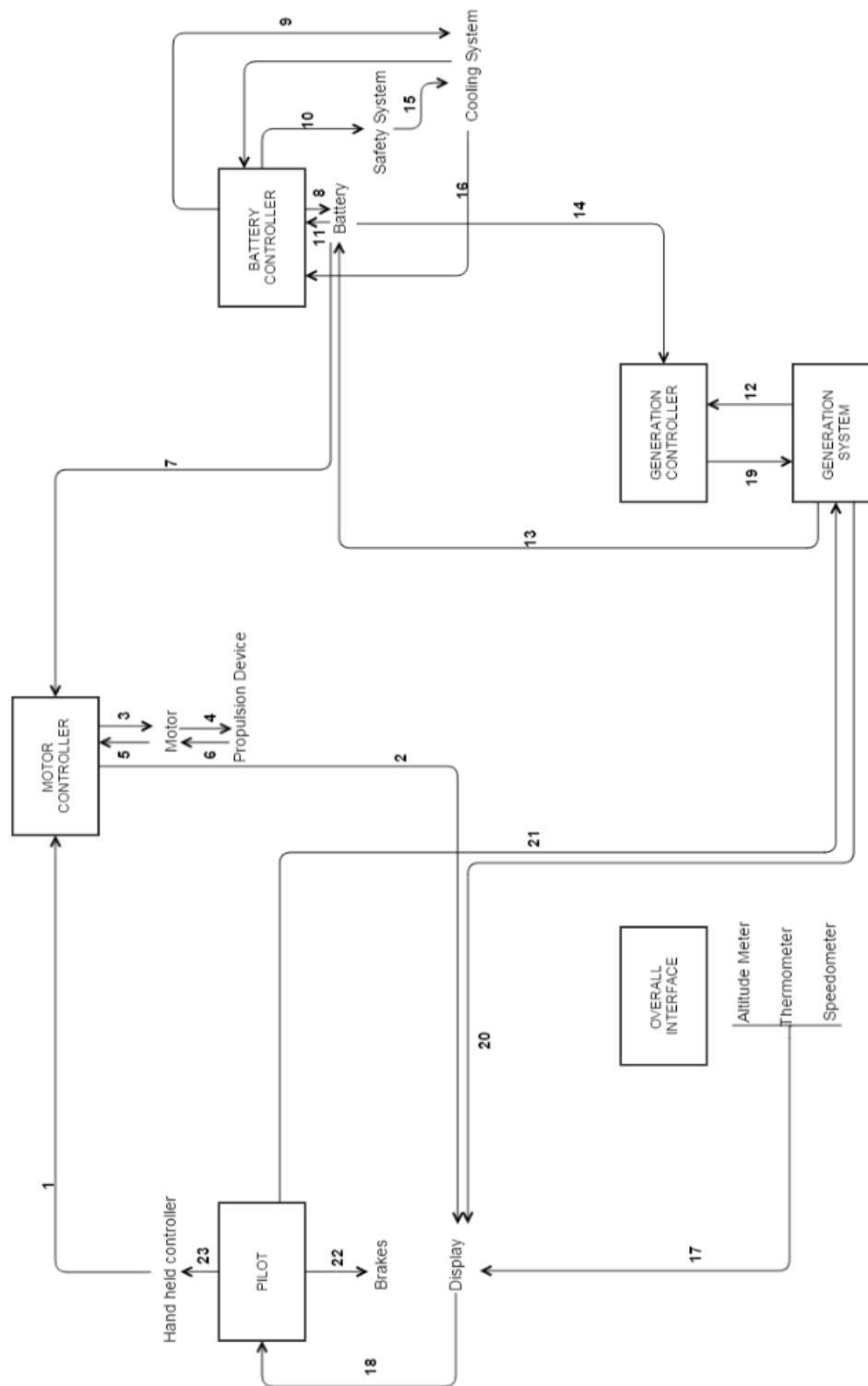


Figure 5.1: Communication flow diagram of the electric paramotor with secondary batteries.

Table 5.2: Commands CFD in figure 5.1

#	Command	#	Command
1	Command motor controller	13	Recharge battery
2	Send data to display	14	Provide battery data (energy level)
3	Adjust motor setting	15	Activate cooling system
4	Adjust propulsion setting	16	Track battery temperature+send data
5	Send motor setting to controller	17	Send data to display
6	Send propulsion setting data	18	Provide pilot with data
7	Provide energy to motor	19	Provide generation data
8	Control battery settings	20	Provide battery status
9	Control battery cooling system	21	Change generation state
10	Control battery safety system	22	Change brake setting
11	Track battery (energy level)	23	Command hand held controller
12	Status of generation system		

propeller air inflow being more turbulent.

2. **Overall increase in drag** An increase in drag also lowers range, and the propeller will be less efficient due to actuator disk theory losses and operating on an off-design point.
3. **Overall increase in mass:** An increase in mass will cause need for a higher flight speed, which may or may not be desirable. It will also increase drag, as the $\frac{L}{D}$ ratio stays approximately the same, and thus decrease range.
When considering the version for the market, an increase in mass would especially make take-off more difficult.
4. **Increase in cost:** As the maximum budget is €5000, an increase in price in certain subsystem will compromise the budget for the others. However, as described in appendix M there is a €454 margin.
5. **Battery has lower specific energy than expected:** If the battery (primary or secondary) has a lower specific energy, the range will decrease linearly. The primary battery has a 41% margin in its capacity (in the simulated mission), as it is limited by specific power, not specific energy. Thus, this parameter has some flexibility.
6. **Battery has lower specific power than expected** This is not a problem with secondary batteries, as they are limited by specific energy, not specific power, but with primary batteries this is the other way around. Currently, the maximum power needed is $2.6kW$, the battery's maximum power is $3.0kW$, so margin is low. If the power delivered is lower than expected, the mission cannot be flown for some cases, when the wind is too strong for example. In other cases the mission can be flown, but not at the optimum pace, which means that the overall drag is higher and more energy is consumed.
7. **Wind is too strong:** The wind conditions are crucial to the mission, and limit the amount of potentially successful mission days. The sensitivity of the wind conditions was investigated considering 10 different days in January 2015. From these 10 days 3 were suitable for the mission, these three had in common that the wind conditions were favourable for soaring. In all cases more than 20% of the mission could be soared, where on the best day this was 57%. In all cases more than 23% of the energy was still left in the battery pack, after reaching the final destination. On the first day of the year major parts could have been flown with tail wind, but soaring was not possible. Nevertheless the mission could have been completed, with a small redesign, since the maximum power during the mission exceeds the current design and reaches $3.5kW$. On this day 8.9% of the energy would have been left in the battery pack after the $294km$.

Thus it is probable that there are many potentially successful mission days in a year, given that 30% of all days in this small sample size are suitable for a successful mission without

having to redesign any parts.

Table 5.3: Change in battery percentage used caused by change in system parameters

	Current value	New value	Energy left [%]	Critical value
Current value	-	-	41.4	-
Decrease in system efficiency	0.66	0.56	30.9	0.40
Overall increase in drag	10 N	0 N	35.6	-61 N
Overall increase in mass	118 kg	123 kg	38.6	192 kg
Lower energy density	415 Wh/kg	315 Wh/kg	22.8	246 Wh/kg

The current value for "Overall increase in drag" defines the drag reduction due to the fairing. The critical value of this line therefore shows that the mission can still be flown even if instead of 10N reduction it gave a 61N increase in drag.

Table 5.3 actually illustrates very well that it is not the energy use that is driving for the mission, even though the design for most subsystems focused on this. The critical value for these figures shows a big increase in comparison to the current figure. As discussed in the last paragraph, the wind and power conditions are driving factors behind the success of the mission.

5.5 Sustainability Development Strategy

The general approach that was taken in this project with respect to sustainability has been outlined in the first phase of the project ((*DSEgroup6*, 2014a)). Both the LCA (Life Cycle Analysis) and TBA (Total Beauty Analysis) approach will be used to assess the environmental impact of the product through its life cycle. In order to better quantify the environmental impact as determined with the LCA, ECO-indicators can be used.

The LCA uses five indicators to assess the environmental impact of a product. These factors are: the energy efficiency of the cycle, the carbon footprint, the air acidification, the water eutrophication and the total energy consumption, which measures the consumption of non-renewable energy sources. With these indicators in mind a look will now be taken at the whole paramotor system as described in chapter 3. Components of the system for which it is clear that they have a very high environmental impact will be discussed further.

Weight savings will in the first place result in the paramotor needing less energy for propulsion, and therefore it will be more efficient and thus have less impact on the environment. Weight savings were made by choosing lightweight solutions from the various design options, which resulted in a lower environmental impact. However, it also became clear in this project that the weight budget will always be filled up completely. Since, weight saved can be used as extra mass for the battery, which increases the range of the paramotor.

The propulsion unit will consist of a propulsion device, energy supply and a motor, which will be electric. Since the motor will be electric it needs an electric energy supply. The energy that is supplied to the motor needs to be generated and stored. The motor used, as described in chapter 3.4, is a high-efficient brushless motor. Electric motors already in general have higher efficiencies than combustion engines, and from the electric motors brushless motor are more efficient than brushed motors. Furthermore they perform better in one aspect, which is not included in the LCA. That is they produce less noise, which also reduces impact on the environment.

Finally, using a lift device which is more efficient will make the whole system more efficient and consequently lessen its impact on the environment. By definition, an air vehicle that is as light and

small and flies at such a low speed has a smaller impact on the environment than other air vehicles. Especially since it produces no direct emissions as it is electrically powered. The charging power can be renewable further decreasing the footprint of the system.

5.5.1 Lithium Polymer Cells

It was decided in chapter 3.3 to have two versions of the paramotor's battery; a primary battery for the mission, and a secondary battery for customer purposes. The secondary battery will be a battery consisting of lithium cells. This is a subsystem that possibly has a large environmental impact and will therefore be analyzed using the LCA and the TBA. Table 5.4 shows the TBA of the total material breakdown of a standard Lithium cell. The different materials are assessed on their manufacturing process, total cycles analysis (Cyclic), renewable energy usage possibility (Solar), safety, efficiency and social footprint, and ugly points are awarded for general negative points.

Table 5.4: LiPo cell total beauty analysis showing the environmental impact throughout the life cycle of the cell.

Component	Material	Manufacturing process	Cyclic	Solar	Safe	Efficient	Social	Ugly
								points
Cathode (+)	Lithium Manganese Oxide (LiMnO ₂)	A manufacturing method of spinel type manganese oxide for a lithium ion polymer cell, includes pre-firing a mixture of lithium salt including lithium carbonate, manganese oxide, and heterogeneous metal, firing the mixture to 900 to 1200 °C. To form a raw material, adding in the raw material at least one of the crystal growth accelerators (lithium hydroxide, lithium sulfide or a mixture of the two) and firing the resultant compound at 750 to 850°C.	30	10	30	60	60	
Cathode collector foil	Aluminium (Al)	Natural manganese dioxide ore is mined then reduced with oil or coal to manganese oxide. Lithium carbonate ore is refined from salines/brine The aluminium oxide is obtained by refining bauxite. Aluminium oxide has a melting point of about 2000°C. Therefore it must be extracted by electrolysis. In this process, the aluminium oxide is dissolved in molten cryolite and then reduced to the pure metal.	25	10	15	50	40	
Anode (-)	Graphite (C)	Made from petroleum coke after it is mixed with petroleum pitch, extruded and shaped, then baked to sinter it, and then graphitised by heating it above the temperature that converts carbon to graphite (3000° C)	30	10	30	70	60	
Anode collector foil	Copper (Cu)	Currently, the most common source of copper ore is the mineral chalcopy (CuFeS ₂), which accounts for about 50% of copper production. The minerals are leached then smelted at 1200°C reduced and refined for copper concentrate.	25	10	5	50	40	
Electrolyte	Ethelene carbonate-solvent (C ₃ H ₄ O ₃)	An improved process for making ethylene carbonate wherein ethylene oxide and carbon dioxide are passed over an anion exchange resin catalyst and wherein the ethylene oxide and carbon dioxide reactants are absorbed from the effluent of an ethylene oxide reactor, absorbed and used as feed to the thionyl carbonate plant without further purification. In manufacturing ethylene oxide by catalytic vapor phase oxidation of ethylene, a process that consists of adding, as liquid, an organic halide as a reaction inhibitor into the ethylene raw material gas flow is provided. According to this process, ethylene oxide can be manufactured stable and in high selectivity.	5	21	30	50	60	
Separator film	Lithium Spinel	Ethylene is produced in the petrochemical industry by steam cracking. In this process, gaseous or light liquid hydrocarbons are heated to 750 - 950°C, inducing numerous free radical reactions follow by immediate quench to freeze the reactions. This process converts large hydrocarbons into smaller ones and introduces unsaturation. Ethylene is separated from the resulting complex mixture by repeated compression and distillation.	30	10	30	60	60	
Packing	Polyethelene and aluminium (Pe, Al)	A manufacturing method of lithium spinel for a lithium ion polymer cell, includes pre-firing a mixture of lithium salt including lithium carbonate and heterogeneous metal, firing the mixture to 900 to 1200 °C. To form a raw material, adding in the raw material at least one of the crystal growth accelerators (lithium hydroxide, lithium sulfide or a mixture of the two) and firing the resultant compound at 750 to 850°C.	27	15	27	60	50	
Electrode tabs	Aluminium (Al)	Lithium carbonate ore is refined from salines/brine Polyethylene is made from ethane, which is found in natural gas. Natural gas is found deep under the surface of the earth usually in pockets of crude oil. Before the process of making polyethylene can begin, the oil must be pumped up to the surface, and the natural gas must be separated from the oil. Ethane is converted into ethylene and then finally into polyethelene polymer. For the manufacturing process of Al see process above.	25	10	15	50	40	
Average	Score	See manufacturing process above	24,63	12,00	22,75	56,25	51,25	-50

Table 5.5 shows the conclusion of the total beauty analysis, based on the characteristics analysis that has been made in table 5.4. The total system received fifty ugly points, because of the fact that the production of all the different parts of the cell costs too much energy. This is mainly due to the production processes of the metal components, and therefore this is where there may be some room for improvement in the future. Chapter 3.3 describes some of these future possibilities.

Table 5.5: Results Sustainability analysis LiThio Cell

Cyclic	score: 24.63%
Low Result	Very low recycles content, but recycled material available
Challenge	Multi:level bill of materials (BOM) and processes
Opportunity	Increase use of recycled content for Al and Cu (40% of pack weight)
Solar	score: 12%
Low Result	High use of fossil fuel energy for furnaces and smelters
Challenge	Determining embodied renewable energy content from municipalities
Opportunity	Increase use of renewable energy in production processes
Safe	score: 22.75%
Low Result	Low non-toxic lifetime release due to front end manufacturing cycle and fossil fuel use
Challenge	Re-active chemical process output gasses difficult to identify
Opportunity	Identify more non toxic materials to substitute
Efficient	score: 56.25%
Average Result	complexity of the manufacturing processes and efficiency increases over 20%
Challenge	Some of the processes are relatively new
Opportunity	Increased durability of battery design
Social	score 51.25%
Low Result	Workers have bad working conditions, their treatment is not totally clear.
Challenge	Identifying stewardship sourcing of raw materials
Opportunity	Increase local production (manufacturing base and recycling)
Ugly points	score: -50
Very low result	Battery manufacturing
Challenge	N/A
Opportunity	New design with less metal content

5.5.2 Disposal of Lithium-Thionyl Chloride Cells

It was said that for the mission a primary battery will be used due to its high energy density as described in chapter 3.3. These batteries embody a non-aqueous thionyl chloride solution which contains lithium aluminum chloride.

Even though these cells are primary, they can be disposed without lasting toxic environmental effects. This is because once the end products are neutralized, the end products of this battery are not toxic. This again is due to the fact that the cells do not contain heavy metals or organic solvents, which are malicious components that are hard to decompose. The result of this are lasting toxic environmental effects.¹

Remaining components of the cell after discharge consist of the carbon cathode, lithium chloride,

¹[http://www.tadiranbat.com/0111.-_Guidelines_for_Disposal_of_Lithium_Cells_and_Batteries%20\(5\).pdf](http://www.tadiranbat.com/0111.-_Guidelines_for_Disposal_of_Lithium_Cells_and_Batteries%20(5).pdf), visited on the 10th of january 2015.

aluminum chloride, metallic can, cover and current collector.

The lithium chloride is formed during discharge as the thionyl chloride is converted into lithium chloride and in addition some sulfur and sulfur dioxide is formed. Approximately 95% of the thionyl chloride reacts during full discharge of the battery, the remaining bit will eventually discharge after disposal.

Using a shredder, the contents of the cells can be exposed. The electrolytes can then be neutralized using a caustic solution, so ferrous and non-ferrous metals can then be recovered, and the clean scrap can be sold to metal recyclers.

Filtering the caustic solution, the lithium hydroxide is converted to lithium carbonate which can be used to make lithium ingot metal and battery foils or provide lithium metal for resale or to produce sulfur dioxide batteries. In additions, the carbon that is recovered from the solution is pressed into sheets of carbon cake to recycle with cobalt.²

5.6 Conclusion of System Design Support

This chapter clearly described all design supporting processes that were performed over the course of this project, as stated below. All of them evolved throughout the project and their final outcomes were presented in this chapter.

- **Risk Analysis Assessment:** From the final risk analysis it appeared that all project risks were analysed and prepared for on time and hence could be avoided timely throughout the entire course of this project. From this assessment a good idea of how risks should be forecasted and prepared for has been acquired. This will result in a well prepared and safer mission.
- **RAMS:** It was illustrated that the four variables; reliability, availability, maintainability and sustainability, have been insured throughout the specific design of the various subsystems.
- **Communication Flow Diagram:**The need for communication between the different subsystems was determined by drawing the flow of data through the system and to and from its environment.
- **Sensitivity Analysis Mission:**The sensitivity analysis showed that the energy source is slightly overdesigned as its capacity is higher than the energy needed to accomplish this mission. However, the power needed for this mission is driving for the battery sizing and therefore, the high energy capacity, makes the driving parameters that have a major influence on accomplishing the mission, less sensitive to changes. This was illustrated by the fact that it was determined the mission could be flown in three out of the ten past days.
- **Sustainability Development Strategy:** The section on sustainability presented the life cycle analysis of the whole paramotor. The main results from this analysis were that the use and recycling of materials is of importance in decreasing the ecological footprint of the paramotor. Secondly, the energy source is of importance. If it is chosen to use renewable energy when using the product, the ecological footprint can be reduced even further. Finally, it was concluded that the most ecologically unfriendly subpart is the battery, but recycling options are still possible.

²<http://www.allbatterysalesandservice.com/browse.cfm/2,1096.html>, visited on the 15th of january 2015.

6 Production Plan

6.1 Manufacturing

For Prototyping, first all separate components need to be manufactured. Those parts can be seen in Table 6.1. For each part listed in the table, the chosen material is shown as well as the selected manufacturing process. The choice of material and manufacturing was mainly based on weight and cost, is further described in the respective section of the part characteristics.

Table 6.1: Used material and manufacturing process for all manufactured parts

Part	Material	Manufacturing Process
Brackets for driveshaft	Aluminium 7075 T6	CNC-Milling
Fairing	SkyTex Fabric ($40 - 45 \frac{g}{m^2}$)	Cutting & Sewing
Frame	Aluminium 7075 T6 tubes	Welding
Propeller	Maple timber wood	CNC-Milling
Battery Casing	Carbon/Aramid & Glass fibre Composite	Vacuum Infusion
Battery Module Casing	Glass fibre composite with fire-resistant resin	Vacuum Infusion
Big Gear	Aluminium 7075 T6	CNC-Milling
Small Gear	Aluminium 7075 T6	CNC-Milling
Drivetrain Connection Plate	Aluminium 7075 T6	CNC-Milling
Input Controller Casing	Plastic	3D printing

Some of the components were too complex or expensive to manufacture though, wherefore they will be purchased.

6.2 Name and Type of Purchased Parts

The parts that will be bought were investigated into great detail and chosen with caution to perfectly match the product's requirements. Which components were chosen to be purchased are depicted in Table 6.2, which also indicates the exact product name/type.

Table 6.2: Purchased Parts

Part	Product Name
Harness	NEO String Lightweight Paragliding Harness
Reserve chute container	High Adventure Front Container Size M or L
ESC	MGM Compro HBC 18063-3
Interface display	1.7 Zoll microOLED GOLDELOX Display OLED-160-G2
Input controller PCB	Single-Sided Pre-Sensitized Circuit Board
Input controller CAN transceiver	MCP2551
Input controller CAN MCU	DSPIC30F4011-30I/P
Input controller microcontroller	Atmel 168
Input controller CAN PCB connector	Right Angle D-sub PCB Connector
Input controller contactless potentiometer	ETI Systems HSM22 Series
Motor	Hacker A-80-10 (3kW)
Gearing Toothed Belt	Rubber
Gearing 2nd Shaft	Aluminium 7075 T6 Rod
Battery Cells	Fanso ER17505M (for market: Panasonic NCR18650)
Battery Cell Connectors	Copper
Wires	AWG 29,AWG7
Bearings	different sizes from Koyo
Bolts	different sizes (M4-M8) Imbus

After manufacturing and purchase of all necessary parts, the paramotor can be assembled.

6.3 Assembly

The assembly will be performed in three main subsequential steps, in which some parts can be assembled simultaneously. The assembly process is displayed in Table 6.3. The simultaneous process are shown in each row, whereas the sub-sequences are represented in the columns.

Table 6.3: Assembly Process

		Sub-sequential →	
Simultaneous ↑	Motor & Gear	Motor+Gear & Controls (= Drivetrain)	Frame & Drivetrain & Driveshaft & Propeller
	Controls		
	Battery		
	Frame		

After the assembly of the paramotor is done, the final step is to program the motor controllers and the BMS and to attach the fairing around the system. Finishing the last steps, the first prototype is ready for its flight tests.

7 Business & Marketing

This chapter describes the future possibilities of this product. The development of the product is discussed in section 7.3. An overview of the the cost break-down structure of the electric paramotor is given in Appendix M. A final market analysis is performed in section 7.1, referring to the preliminary market analysis performed in the Baseline Review ((*DSEgroup6*, 2014a)). and using the results of a questionnaire filled in by more than 200 air sport practitioners. The chapter then concludes with how all these factor lead to a return on the initial investment and the operational profit that can be expected in section 7.2

7.1 Market Analysis & Planning

The objective of the Market Analysis is to establish the competitive cost and volume of the market for the product or for services that the product can provide. This is derived from the current market for comparable products or services and an assessment of the added value of new technology or solutions that could be implemented.

The focus areas that were determined in the SWOT analysis in the first phase of the project are evaluated. In addition, a questionnaire has been carried out to determine the customer's wishes. The questions can be found in the midterm report (*DSEgroup6*, 2014b).

7.1.1 Current Market

The first electric paramotor was built in 2006, and since then, various manufacturers have been working on electric paramotors. The technologies used are without exception a brushless DC motor (due to its high efficiency and possibility of direct drive without reduction), and some variations of lithium-ion batteries. Electric paramotors are very appealing to paraglider pilots, as they are more silent than gasoline-powered ones, and could enable pilots to launch from low places like a valley floor, avoiding the hassle of winching or driving up a mountain. This can also be done with petrol-based paramotors, but next to the aforementioned reputation, some cannot be restarted in-flight, thus the pilot will have to deal with the idling engine's noise. Also, electric paramotors have low maintenance costs and do not have the gasoline smell.

At the moment only a few electric paramotors are commercially available and they can roughly be divided into three categories:

- Paramotors that have a normal paramotor conversion (i.e. they look like a paramotor with combustion engine, complete with cage and netting) are the cheapest with a price starting at €9,800, but with their 20 minutes of battery time they also have the shortest range.
- Paramotors that use a foldable prop and a stirrup to have the pilot position himself a little more reclined to have a more aerodynamic position, while the motor, propeller and cage swivel to stay horizontal.
- Paramotors that use a hard monocoque shell, with the propeller mounted far in the back, and the battery in the front. However, the stiff cocoon makes the whole system quite heavy and expensive; there is only one product of this type and it is available at €12,800.

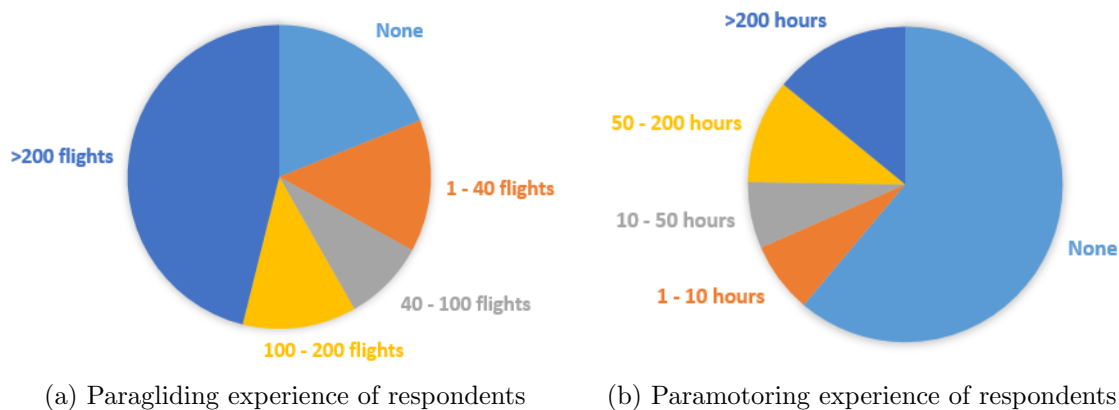
Interesting to note is that all commercially available electric paramotors use the same drivetrain, developed by Geiger Engineering, consisting of a 10kW continuous-power direct-drive brushless DC

motor, ESC, and some optional components.

7.1.2 Market Research

It would also be interesting to know how great the interest of people that currently paramotor is to change from a petrol-based paramotor to an electric one and which factors influence this decision. In order to investigate this further and to find out what factors would influence whether or not an electric paramotor would be something they buy, a questionnaire was performed. It was distributed through several Dutch and English paramotor fora, and put in the newsletter of the KNVvL. A total of 206 responses were received. It addressed questions on how a reduction of paramotor noise levels as well as other factors such as sustainability and costs influence the decision to fly a paramotor. As well as questions on what would either stop people from flying a paramotor or convince them to take up the sport. Additionally, questions on expected flight duration and pricing were asked.

Figure 7.1a and figure 7.1b show the experience of the respondents in paragliding and paramotoring respectively, to know what point of view the respondents have. It should be noted that only eighty respondents had paramotoring experience, and from their comments on the various questions it was obvious they were more realistic on what to expect from an electric paramotor. The answers from the respondents with and without paramotoring experience will therefore be treated separately in some cases.



The reasons for 126 respondents for not using a paramotor are illustrated in figure 7.2. This first question was asked as an open question, but most respondents gave similar answers. It can clearly be seen that acoustic noise is a big issue. It is clear that the team should focus on noise reduction when bringing a paramotor on to the market, but having an electric motor instead of a shaky and noisy gasoline motor already helps. This also applies to the smell and the fact that a gasoline motor can be quite bulky. If the weight budget is kept strictly for the customer requirements, it would be very light compared to a gasoline motor which generally are around 35 kg. Similar conclusions can be drawn from the other part of figure 7.2, where it was asked what would convince those who didn't have paramotor experience to do so. Respondents could fill in more than one answer for this second question.

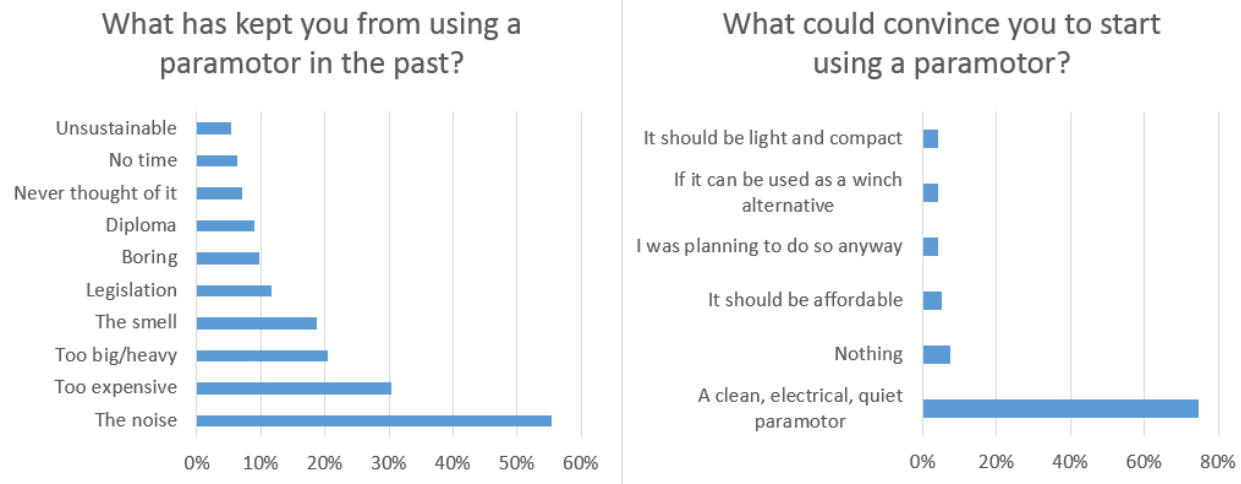


Figure 7.2: Reasons for paragliders not to paramotor, and reasons to be convinced for starting with paramotoring

What can also be noted from the questionnaire, is that the average price respondents are willing to pay (€4,030) is quite low. In addition, the range that respondents gave on the price they were willing to pay varied strongly, from €500 to €12,000, and 37% of the respondents mentioned that a price of €5,000 would be acceptable.

Keeping within the €5,000-budget would also still account for a market price when producing more than one that is closer to the desired customer price than the current range of €9,800 to €12,800. Interesting to note is the difference in expectations on what they would find acceptable between respondents with and without paramotoring experience. The average price respondents would like to pay for the paramotor system is €4,030, while those who do have paramotoring experience thought a price of €4,566 would be acceptable, and those without experience were willing to pay only €3,465. This difference can be explained by the assumption that those with paramotoring experience know what they have to pay for a petrol powered set, which is also approximately €5,000.

A similar situation applies to the desired flight time. On average, a desired flight time of 65 minutes was found, but those with experience would like to have 79 minutes and those without experience thought 55 minutes would be acceptable. Once again the more experienced pilots have more realistic desires.

This might be explained by the fact that those with experience are used to their gasoline powered motor, which can stay in the air for a couple of hours with a full tank, and they expect similar results for an electrically powered motor.

Those who do have paramotoring experience were asked what they use their paramotor for, as illustrated in figure 7.3. It is also shown in this figure what those who would like to start paramotoring in the future, what they would like to use it for. These two graphs look quite similar, the main difference being that a lot of respondents who would like to have a paramotor would use it to find some thermals, but in practice only 27% of the respondents who have paramotor experience use it to do so. An average of 70% for both categories would use their paramotor to just fly small tours. As described in chapter 3.3, with the battery used for the customer dedicated paramotor, the paramotor can still fly for approximately two hour, which is plenty for flying small tours.

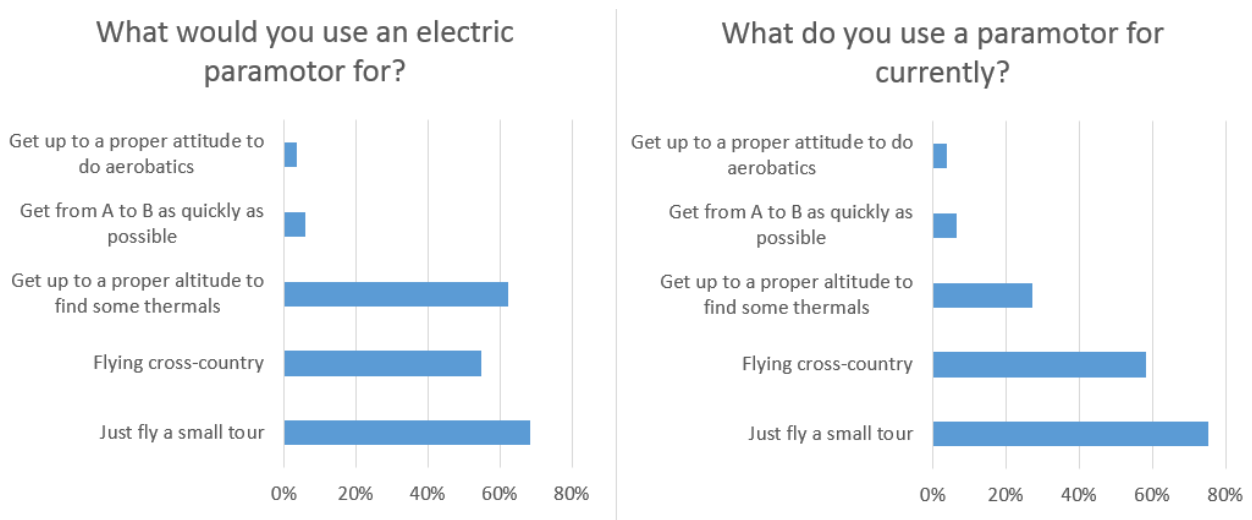


Figure 7.3: Bar chart showing what respondent would like to use a paramotor for and what current paramotor gliders use their paramotor for

These respondents gave a good overview of the the potential market for electric paramotors, 64% of them answered that they would be interested in a quiet and clean electric paramotor. Therefore the potential of this market is quite good. However, the respondents with paramotoring experience were a bit more sceptical; only 53% answered with: "Yes, very interesting!", in comparison to 75% of the respondents without paramotoring experience. It should also always be kept in mind that the market for paramotors is still a niche market, even with such a high percentage of potential buyers.

7.1.3 Market Profitability

The market profitability can be investigated using the Porters five forces model, which takes the market size and deducts all the profitability threat factors to result in the final market profitability. In the following paragraphs these profitability threats will be mentioned.

Threat of Substitute Products or Services

As described in section 7.1.1 there are currently several market solutions. The biggest threat to the team's paramotor are standard paramotors with petrol engines, because this technology is cheaper than the current electric paramotor market solutions. The scepticism of current paramotor pilots was also illustrated in section 7.1.2. However, since the cost of the electric paramotor will be within the same price range as petrol paramotors, this will not necessarily be a reason. The electric paramotor does win from the petrol paramotor in terms of noise, smell and sustainable appeal, the latter becoming more and more important in the future.

Threat of new Entrants

The threat of new competitors entering the (electric) paramotor market is not very high, as will be discussed in section 7.2. The only new potential entrants that can be expected are companies that develop an electric paramotor which is of similar price as the current petrol fuelled paramotors and with a similar flight time as petrol fuelled paramotors. This threat is found to be moderate. The reason why this threat is not high is because of the high start-up costs that come with the development of such a state-of-the-art machine.

Threat of Established Rivals

The threat of established rivals is low as the product brought to market fulfils all requirements that have been stated in the the first phase of the project.

Bargaining Power of Suppliers

The bargaining power of the suppliers is not very high as most subsystems consist of off-the-shelf components. All materials mentioned are producible and widely available, and where possible designing was done using open source software. The only component where the supplier has some bargaining power is the motor, as this is one of the more expensive components and a dedicated product. However, although the motor that has been selected is the best option, there are other options that are very close to that one. One could say the same about the bargaining power for the battery supplier, as there are also numerous battery suppliers.

Bargaining Power of Customers

The customers will not have a very strong bargaining position as the paramotor will be the only electric paramotor with a decent range and an appropriate price to match these specifications.

7.1.4 Preliminary SWOT Evaluation

This section presents the results of the preliminary SWOT analysis. This analysis was done in the beginning of the project. The specific results found can be found in the baseline report (*DSEgroup6*, 2014a) that was presented in an earlier stage of this project. The SWOT analysis resulted into seven challenges, which can roughly be categorised in two main focus areas. One of which was using the strength of the low price to attract the opportunity of new markets. The second focus area was to use the strength of the hands-on project experience of the group within a technological favourable environment to achieve a good design and thereby attract more customers.

It can be concluded that both focus areas have been fulfilled. The paramotor is within the desired financial budget, and the market research shows that customers find it an attractive product when it meets all requirements set.

7.1.5 Opportunity for New Markets

As mentioned before, the current environment is mainly the hobby environment for personal flight machines. This is also the market that was focused on in the design, several opportunity markets for the preliminary market strategy were mentioned in baseline report (*DSEgroup6*, 2014a) that was presented in an earlier stage of this project.

7.1.6 Potential Market for the Electric Paramotor

Currently very few paramotors are sold and the market for petrol-based paramotors is also a small market. The number of people that paraglide is much larger than the number of people that fly with a paramotor. It was considered that an electric paramotor, which significantly reduces noise levels and smell issues, might remove some of the main reasons that prevents people from taking up paramotoring. People that have never flown a paramotor might give paramotoring a try when they are not deterred by the paramotor noise, as determined in section 7.1.2.

7.1.7 Market and Business Plan After Detailed Design

The possibilities for the market and business plan have severely changed in the course of this project, the reason for this is that the team has accumulated several new skills, programs and data. For this reason the decision has been made to re-evaluate the SWOT analysis, the re-evaluated SWOT analysis is presented in Appendix N.

SWOT Analysis After Detailed Design

Appendix N presents the SWOT analysis (internal and external analysis) for the detailed design. This analysis resulted in five challenges that can be categorised in two main focus areas. One of these focus areas was to use the strength of the hands-on project experience of the group within a technological favourable environment to achieve a good design and thereby attract more customers. The second focus area is to use the self created paramotor design programs and system engineering program in combination with all the accumulated data and experience to overcome the threat of the competition and the high prices of current (electric) paramotors.

Challenges

The second focus area was chosen to be used for the marketing plan. The programs that have been made for the design of the electric paramotor that will be used to fly the mission (mission explanation: chapter 2) can then be reused. There are four programs that are referred to in strength three (S3) and strength four (S4) (which can be found in Appendix N). Apart from these programs some data sheets with paramotor sub parts have been assembled which can be used for the system engineering. The specific details about these programs and datasheets will be presented in the following paragraph.

The following challenges were found in the second focus area:

- Challenge 4: How can the paramotor design programs be used to attract new markets be attracted for the product group. (S4+O2)
- Challenge 5: How can the teams experience in system engineering be used to overcome the threat of the competition in the gasoline powered paramotors industry which are cheaper. (S4+T1)

Paramotor Design Software

Table 7.1 shows the input and output variables of the three different programs that have been made to design the paramotor.

Table 7.1: Paramotor design program characteristics

	Input -by user programme	Output
Propeller design program	Cruise speed Thrust setting Prop diameter	Propeller design
COG determination program	Dimensions of sub parts Weights of sub parts	Final Location of all sub parts Frame dimensions + weight
Mission planning program	Route	Power requirements Battery requirements Mission duration Soaring conditions Thrust settings All of the above as prediction

These programs were used in combination with all the different data that was gathered about separate sub parts of the paramotor system. The quantity and quality of the data of the different sub parts increased constantly due to the iterative design process that was used to design the endurance paramotor. These iterations resulted in a very complete lists of the different paramotor subparts. Examples of sub parts are the different types of batteries, different types of motors and a variation of possible materials.

Actions

Appendix N mentions some actions for the challenges. The following chapter will combine these actions with some more detailed specific actions that can be taken for the marketing planning.

- Design do it yourself (DIY) paramotor designs for clients using the paramotor design programs.
- Open source the paramotor design programs to create a community and enable the community to contribute to the development of these programs.
- Use paramotor design programs to connect clients (i.e paramotor pilots) to paramotor suppliers (for a premium which suppliers will pay to the platform).
- Use paramotor design programs to connect clients of different product groups to paramotor suppliers for a premium.
- Optimize the system engineering program to select designs of specific characteristics (ex: light weight, cheapest solution).

To summarize, the plan is to provide the developed programs to the public and in this way to get an enthusiastic active community together who would use the to be developed platform with the paramotoring programs to design their own paramotors. The way in which this could be monetized is by getting a percentage of the total orders that are made by users of the to be developed platform at the suppliers and manufacturers. Furthermore the business would start by offering a customer friendly paramotor version of the paramotor that has been designed for this DSE. In which the primary battery would be replaced with an affordable high performance secondary battery.

Sensitivity Analysis

There are several threats that could occur with the actions named in the previous paragraph. In this paragraph these threats will be identified accompanied with possible solutions to circumvent these threats.

- **Database and programs get outdated-** Solution: Add a suppliers and manufacturers input tab on the platform through which they can add new data.
- **Clients think that cheapest solution are not presented since the platform benefits from higher priced sub parts-** Solution: Periodic website inspection by trusted community member. And public feedback on platform forum.
- **Persuade people to come to the forum-** Solution: Provide the paramotor design software for free, and show the paramotor that has been designed with these programs for this DSE as an example product resulting from the platform.
- **Not enough clients come to the platform-** Solution: Negotiate with suppliers and manufacturers to persuade them to give discounts to clients that come to them through the to be developed platform.
- **Paramotoring community is too small for an active community as described above-** Solution: Do more research and develop the programs such that they can be used for different use cases than the paramotoring community. examples could be by providing the propeller design software to other communities such as for example the UAV community which is a good example of an active community. The mission planning program could also be implemented in different situations than the paramotoring use case, examples could be to use it within an app for cyclists or sailors/wind&kite surfers (in which the program would predict wind conditions at their chosen location and display this on the users mobile device).

7.2 Return on Investment & Operational Profit

In order to establish the Return on Investment (RoI) the market price, market volume, achievable market share, development cost, production cost and direct operational costs are determined. The RoI is defined as the positive balance between the number of products sold and the total cost. In the end the RoIs of the different market opportunities are compared.

7.2.1 Development Cost

Up until now, the development cost have been very low. The only investments that have been made is a ShareLatex account for €36 and one testing battery for €9. As the project is an obligatory part of all team members' bachelor, there have been no labour costs. If the team members choose to continue with the project after the DSE is finished, no wages or anything can be paid in the start-up phase.

There will however be higher development costs when the project is continued and a paramotor is built. Of course a prototype of the chassis will need to be built, and probably a second one to account for design errors in the first one. The motor and battery will need to be tested. This is especially costly for the primary battery to be used in the mission. Development cost in the initial phase will therefore consist of the cost of; two primary batteries, a rechargeable battery, two times the chassis, a motor and a wing. It is assumed that as the whole group are students from the TU Delft, the facilities such as working space, software licenses and basic machinery from the TU Delft can be used. A detailed cost break-down is given in table M.1 in Appendix M, from which it can be deduced that the development cost will be at least €12,000. It could be more if design errors are found when building the prototype or when subsystems don't work according to plan.

To provide the set as a DIY paramotoring kit, no more costs will be made since the whole process will have been taken to be able to make the prototype. The only extra costs made will be the development of the website. These costs will not be very high but are predicted to be within €3,000

7.2.2 Production Cost

The material cost of one paramotor will be €5,000, as this was a requirement set in the first phase of the project. Assuming team member own some small machinery and machinery from the TU Delft can be used in the first phase, the production cost of a paramotor will also be €5,000.

The production costs for a website are considerably lower, the only costs made for this will be the operational costs.

7.2.3 Direct Operational Cost

The direct operational cost of the paramotor will not be for the account of the development team. Once the paramotor has been sold, its cost are for the customer.

In order to carry out the mission, there are some operational cost; a car and a boat will need to be rented resulting in gas costs, a good internet connection is needed in the following-vehicles and the pilot and his gear and the ground crew will need to be transported to the take-off site and from the landing site. Some additional costs like nutrition will also be made. The direct operational costs for the website will consist of server costs and maintenance. In the beginning it would even be possible to start using a free web server site such as "www.webs.com" which could decrease the costs to €0.

7.2.4 Market Price

As mentioned in section 7.1.1 the price of the current market solution is between €9,800 and €12,800. In order to still have the benefit of attractive pricing, this paramotor will be sold for €8,000. The price of the DIY kits can be priced even more competitively since there is not yet a market for this.

7.2.5 Market Volume

An attempt at making an estimation of the market size has been made in the first phase of this project. Several authorities have been approached to get reliable numbers, but this was very hard. The KNVvL estimated the number of people flying a paramotor to be 300, but also found it very hard to estimate this as not all paramotorers are members of the KNVvL. In addition, they thought there were about 1500 paragliders.

However, it was investigated that with a clean, quiet electric paramotor also people who are not paramotoring yet might be interested in buying one. Using the data from the questionnaire in section 7.1.2 one does know that 64% of the respondents answered that they would be interesting in buying such a paramotor, and all respondents were members of the KNVvL. The KNVvL, The British Hang Gliding & Paragliding Association (BHPA), de Belgische ParaMotor Federatie (BPMF), the European Hang Gliding and Paragliding Union (EHPU) and United States Powered Paragliding Association (USPPA) together have approximately 48,000 members, which means there are about 31,000 potential customers worldwide.

In addition, market research on the paraglider market has been performed by the Paramotor Manufacturer Association (PMA). The annual sale of paragliders per type is described in this report. They found that the amount of active pilots worldwide was 98,120 in 2010¹, but again, no figure on paramotoring were given. These 98,210 pilots would form a potential market for the electric paramotor. Again, in the questionnaire, 67 out of the 106 people with paragliding experience who answered this question, said they would be interested in having a quiet electric paramotor. This means that the potential market worldwide would be approximately 62076. However, it should be taken into account that paramotoring might be more popular in the Netherlands than for example France where a lot of mountains make the environment much more suitable for paragliding. It is thus possible that the worldwide number is considerably lower. A conservative number for the potential market size is therefore taken of half the number calculated. This gives us a market size of approximately 30,000, which is very close to the number determined in the first paragraph, and will be taken as the potential market size.

7.2.6 Achievable Market Share

It is clear that the market for paramotors is not a very big market and with the current market solutions this market seems saturated. However, as the product that will be introduced has some new, desired features such as the low-pricing and low noise this enables the potential to create a new market. Due to the high cost and small market, there are only a few competitors and barely no new entrants.

In addition, with no information present on replacement rates of paramotors it is still hard to make a reliable estimate of the financial market size. It is assumed that a paramotor is renewed every five years. If it is also assumed that about 10% of the customers from potential market actually buy an electric paramotor, this means that there are 600 annual sales. As there are only three other options commercially available on this market, and the paramotor designed by the team has the best specifications and is the cheapest, it is reasonable to assume to get a 10% market share fairly quickly.

The platform can possibly achieve a much larger market size since it will be very easily accessible,

¹URL <http://www.p-m-a.info/news/article/pma-paragliding-market-study.html> [cited 19 November 2014]

and it will provide a lot of sharply priced upgrades for people that currently own paramotors. It is therefore realistic to assume that a market share of 10% of global electric paramotor sales is possible in combination with a market share of 20% of all paramotor subsystems is possible through the to be developed platform.

7.2.7 Conclusion RoI

At this moment in time the return on investment depends on two parts of the business strategy. First off the prototype, which is a consumer-friendly version of the paramotor that was designed for this DSE will be sold as a DIY kit. According to the estimate for the achievable market share this could yield enough profit in the first year of sales to cover all cost for the prototype production and platform development. This moment could be seen as the moment of return on investment. After this the operational costs of the website will be covered by any additional sales of the prototype, and the new systems that will be designed using the open source platform. The extra income that flows in through the supplier and manufacturers agreements will be used to invest in the platform and its community as well as development of new products that make use of the design programs.

7.3 Project Design & Development Logic

The Project Design & Development (PD&D) logic shows the logical order of activities to be executed in the post-DSE phases of the project. It is shown in figure 7.4. The activities specified are specific to the project, reflecting the technical characteristics of the design.

7.4 Conclusion Business & Marketing

A final market analysis was performed in section 7.1. The market analysis performed in the Baseline Review (*(DSEgroup6, 2014a)*) was referred to and adapted to the new internal and external characteristics of the project. The main results from this new market analysis were to use the new strengths. These strengths have been developed in the course of this project, namely the paramotor design programs. To use these strengths several actions were mentioned. These actions can be summarized as being the development of a platform for the paramotor community that uses the work done in the course of this project to develop paramotors.

The chapter then presented an explanation on how all these actions lead to a return on the initial investment and that an operational profit can be expected, as presented in section 7.2. An overview of the the cost break-down structure of the electric paramotor was given in Appendix M. The chapter concludes with the development timeline of the product and the previously mentioned platform, as was done in section 7.3.

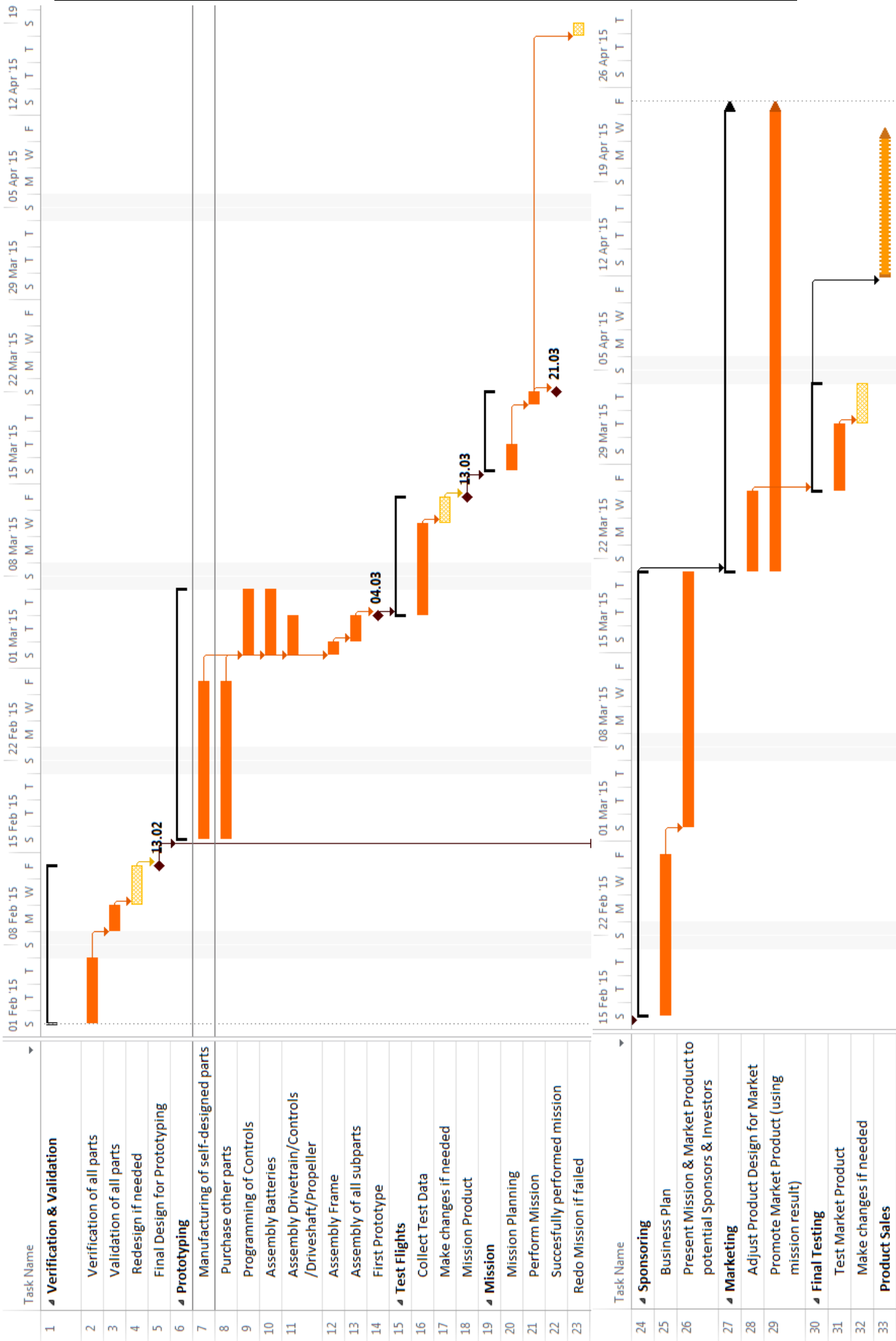


Figure 7.4: Gantt Chart representing Post-DSE Activities, needed to be performed for mission and sales

8 Conclusion

The goal of this report was to design a machine capable of crossing the Netherlands in one single day, whilst giving the pilot the sense of pure flying, by taking away the noise, smell and strong vibrations that combustion motors induce.

This goal was achieved by designing a light-weight and highly efficient paramotor and by setting a route that made use of the natural possibility to soar along the Dutch coast to increase the machine's range even further. Efficiency was achieved by designing a propeller dedicated for the paramotor's flight envelope, reaching a propeller efficiency of 79%. Placing this propeller far enough back so it is out of range of the pilot's arms allowed for losing the heavy and drag-causing safety cage. The mission was designed to be flown at a low power, at the motor's most efficient RPM. In addition, a fairing was designed to reduce the pilot's drag and to allow a clean air flow into the propeller.

The low-weight property of the paramotor was achieved by setting weight budgets for the different subsystems in a very strict manner. Every system was critically analyzed to see where more weight could be lost. The fairing for example consists of a light-weight aluminum frame and a light cloth that inflates in flight due to a hole in the stagnation point.

The light-weight construction also had to allow enough room in the weight budget to account for the battery to be taken along. A 22.5kg primary battery pack consisting of high energy density Li/SOCl₂ cells is taken along in order to accomplish the mission in one go.

The pilot's safety is assured by several measures, the most important one being the fact that the paramotor system and pilot are attached separately to the glider's hang-point. This is done to make sure the paramotor system balances itself independently of the pilot's position, but also such that in case of emergency, the pilot can cut the paramotor system loose.

The whole system will be transportable inside a protective casing by only detaching the propeller and batteries from the frame. The propeller blades are placed alongside the frame inside this casing. The batteries and wing will also fit inside this container. A set-up time of 5min should be possible in this manner.

The paramotor will be combined with the high performance Ozone Mantra R11 wing allowing for the highest possible glide ratio. This way, when using a 22.5kg of primary batteries, with an energy density of $415\frac{\text{Wh}}{\text{kg}}$, the 294km along the coast of the Netherlands can be flown without any stops in approximately seven hours. A total of 5.65kWh of energy is consumed with a maximum power of 2.67kW .

An important part of the design process was defining the verification and validation procedures for every system of the paramotor, by checking if the results generated were close enough to the real world case. This validation procedure makes sure that the to be built paramotor will meet the needs of the stakeholders and customers as set in the detailed requirements.

Customer requirements were also analyzed in depth by carrying out a market analysis and creating a subsequent business plan to allow for continuing developing the paramotor and its accompanying development software after the DSE has officially finished.



Figure 8.1: Visual representation of the PZero electric paramotor design

The process was concluded with the creation of an appealing design and name for the paramotor. With pride we present the PZero. A high-performance, low-cost, electrically powered paramotor capable of crossing the Netherlands. Finished in striking green showcasing its sustainable nature.

8.1 Recommendations

In order to actually complete the set mission of crossing the Netherlands using the designed paramotor several steps will have to be taken.

Firstly, a team should be gathered which is willing to continue with the process of design and mission execution. All subsystems that have been designed should of course be validated. After this, a completed prototype has to be produced, where each has to be tested separately as well as combined into the final system. Improvements and updates will be made where needed.

In order to complete all these tasks, funding is required. Financial support could be sought in crowd funding, sponsors or TU Delft financing. Only then, completing the mission as stated is a viable option.

In addition, completion of the mission can serve as a stepping stone for launching the paramotor platform, as it would serve as a proof of concept for the developed system. This could comprise of setting up an online forum and starting the sales of paramotor subsystems and a DIY electrical paramotor design kit.

Furthermore, the platform should be kept up to date by incorporating technological advances in all paramotor subparts. Batteries have been identified as the subpart showing the most promise for future development and improvement, so this especially applies to them.

Keeping in contact with the paramotor community as well as the manufacturers and suppliers is of vital importance in making this platform a succes.

Bibliography

Brandt, J. B. and M. S. Selig

2011. *Propeller Performance Data at Low Reynolds Numbers*. University of Illinois at Urbana-Champaign.

Charles E. Clauser, e. a.

1969. *weight, volume, and center of mass of segments of human body*. Aerospace Medical Research Laboratory.

DSEgroup6

2014a. *Base line*. Delft University of Technology, Faculty of Aerospace Engineering.

DSEgroup6

2014b. *DSE - Electric Paramotor, Midterm Report*. Delft University of Technology, Faculty of Aerospace Engineering.

Hoerner, D.-I. S. F.

1965. *Fluid-Dynamic Drag*. Hoerner Fluid Dynamics.

Hoerner, D.-I. S. F.

1967. *Fluid-Dynamic Lift*. Hoerner Fluid Dynamics.

J.R. Hendershot, T. M.

1994. *Design of brushless permanent-magnet motors*. Magna physics publishing and clarendon press.

Th. Lutz, S. W.

1997. *drag reduction and shape optimizatino of airship bodies*. Institute for Aerodynamics and Gas Dynamics University of Stuttgart, Germany.

Th. Lutz, D. Leinhos, S. W.

1996. *Theoretical Investigations of the Flowfield of Airships with a Stern Propeller*. Proceedings International Airship Convention and Exhibition, Bedford, Great Britain.

UML

unknown. *Natural frequencies for common systems*. University of Massachusetts Lowell, Modal Analysis and Controls Laboratory.

Virgilio, N.

2004. *Study of aerodynamic efficiency Free Flight equipment (translated from Portuguese)*. Department of Mechanical Engineering, Faculty of Science and Technology, University of Coimbra.

Weisheng Chen, L. P. B.

2008. *Design and Performance of Low Reynolds Number Airfoils for Solar-Powered Flight*. University of Michigan.

Wm. E. Pinebrook, C. D.

1983. *drag minimization on a body of revolution through evolution*. University of Houston, Houston.

Young, W. C. and R. G. Budynas

2002. *Roarks Formulas for Stress and Strain*, 7th edition. McGraw-Hill.

A Requirements

The requirement discovery tree (RDT) was one of the most important steps in the design of the system, to identify and organize the requirements that are significant for the system. It orders all requirements that represent the wishes of all stakeholders hierarchically. The RDT was created, based on all functions of the system and its subsystems shown in the FBS, driven by the customer requirements and the mission profile. The RDT can be found in figure A.1.

The top level requirement of the system is the performance of the mission. To closer define the top level requirement, it was divided into two major branches. One branch presenting all requirements necessary to perform the mission within constraints whereas the other branch states all the requirements the system has to provide to perform the mission technically.

The constraints to perform the mission are mainly set by the customers' needs and wishes. These constraints can be further subdivided into design related and development related requirements, as described below.

- **Design related requirements:**

- Constraints imposed on the design itself, including performance, usage and ergonomics of the design, as well as the budget limit and schedule.
- Regulations on the design to be able to get the design approved.

- **Development related requirements:**

- Driven by the DSE limitations, such as the given time frame and number of engineers allowed to work on the project.
- Driven by the technical functions that must be performed by the paramotor. These depend on the mission profile discussed earlier.

The first level of the technical requirements in the RDT can be broken down into four main branches, as discussed below. Those are in their turn split into more specific requirements. This process continues until verifiable requirements are set.

- The **structural** aspect comprises of the materials and the loads acting on the system and within the system. Here, one needs to take into account the payload, aerodynamic loads and external loads. Also impact loads during ground operations and transportation are important to take into account
- The requirements on **propulsion** consist mainly of the requirements set by the customer. To be more precise, the paramotor shall be electric, it will have a low noise level and it should be able to cross the Netherlands from north to south in one day. From this it follows that next to the noise level and the electric part, the two other main branches in the propulsion part of the RDT are the power and endurance.
- The **controllability** of the system is one of the four technical top-level requirements, which is split into input controller and motor controller, and a controller interface, to visualize paramotor data.
- The last subbranch is the **aerodynamic** design of the paramotor. This comprises choosing a wing and the aerodynamics design of the propulsion system and the chassis. To choose a wing, a trade-off between different, already existing wings needed to be done, whereas the aerodynamic design of the propulsion system and the chassis were done from scratch.

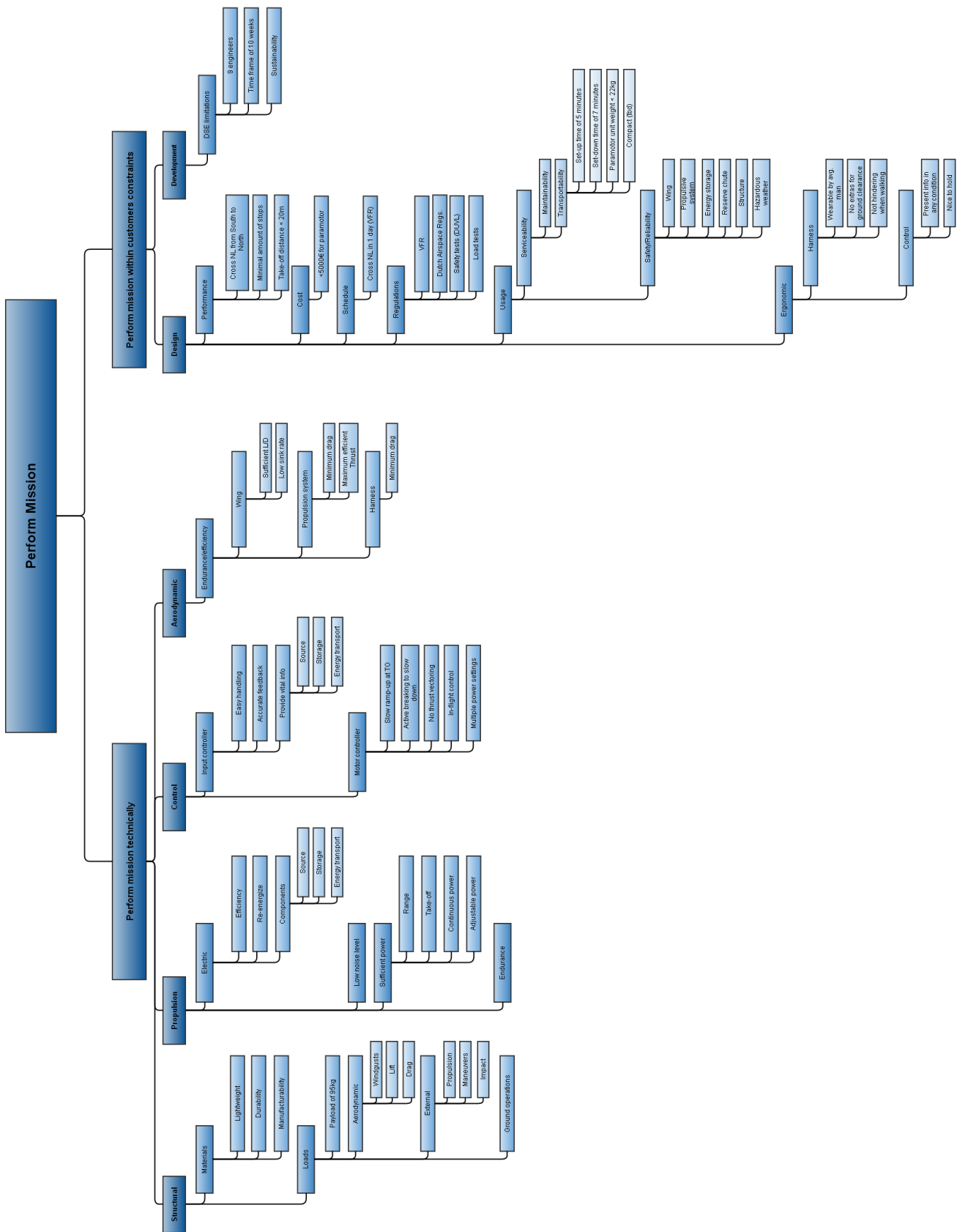


Figure A.1: Requirement Discovery Tree

Requirements Compliance Matrices

This section consists of all requirement tables defined for the mission in an earlier phase of the project, and discusses which requirements have not been reached. The tables have been updated for mass, weight and financial budgets, according to the resource allocation in Appendix B.

As all tables, except for the flight strategy, had the stakeholder requirements as depicted in table A.1, these are not mentioned separately for every subsystem. In addition, how manufacturability, safety and durability were achieved is discussed in the RAMS analysis in section 5.2, and sustainability is elaborated on in section 5.5.

Table A.1: General Stakeholder Requirements

Identifier	Requirement
EP-Ast-XX-01	The system shall be manufacturable.
EP-Ast-XX-02	The system shall be safe.
EP-Ast-XX-03	The system shall be durable.
EP-Ast-XX-04	The system shall be sustainable.

A.0.1 Requirements Flight Strategy

Chapter 2 directly refers to the requirements in table A.2 when defining the mission. It can be concluded that the flight strategy meets all requirements.

Table A.2: Requirement List Flight Strategy

Identifier	Requirement
EP-Ast-FS-01	The electric paramotor shall be able to cross the Netherlands from south to north in one day.
EP-Ast-FS-02	The electric paramotor shall be able to cross this distance with a minimal amount of stops.
EP-Ast-FS-03	The electric paramotor shall be able to take-off within 20m of running.
EP-Ast-FS-04	The electric paramotor shall be certified by the DULV.
EP-Ast-FS-05	The flight strategy shall obey the Dutch Airspace regulations.
EP-Ast-FS-06	The flight strategy shall avoid hazardous weather.

A.0.2 Requirements Energy

Table A.3 shows all requirements for the energy storage, and sets all requirements for the energy regeneration system. The second part can actually be discarded for the biggest part, as the mission will be flown in one go and no regeneration is needed during the mission. The batteries used are primary batteries, so they will be delivered generated and ready.

In the first part of the table, the sustainability requirement is endangered by using a primary battery. However, a primary battery makes the mission achievable and it does still have quite some recycle possibilities, as described in section 5.5.

Requirement EP-Ast-ES-07 has not been achieved, evolution of the mass budget for the battery is described in chapter 3.3 and explains that the mass of the battery is over budget because it suited the mission best, and all other systems are as lightweight as possible. Requirement EP-Sys-ES-06 is also slightly over budget, but this doesn't matter as the battery pack is inside the cocoon, so no additional drag is produced.

Table A.3: Requirement List Energy

Identifier	Requirement
Energy Storage System	
EP-Ast-ES-05	The energy storage system shall be easy to use.
EP-Ast-ES-06	The energy storage system shall be silent.
EP-Ast-ES-07	The energy storage system shall, together with the energy generation device, not exceed a budget of €1954,-.
EP-Sys-ES-01	The energy storage system shall, together with the energy storage device, not exceed a mass of 13kg.
EP-Sys-ES-02	The energy storage system shall be structurally sound.
EP-Sys-ES-03	The energy storage together with the energy generation system shall create no more drag than 20N while inoperative.
EP-Sys-ES-04	The energy storage system shall be safe.
EP-Sys-ES-05	The energy storage system shall be accessible for recharging.
EP-Sys-ES-06	The energy storage system together with the energy generation system shall not exceed a volume of 0.0034m ³ .
Energy Generation Method	
EP-Ast-EG-05	The energy generation method shall be easy to use.
EP-Ast-EG-06	The energy generation method shall be silent.
EP-Ast-EG-07	The energy generation method shall, together with the energy storage device, not exceed a budget of €1954,-.
EP-Sys-EG-01	The energy generation method shall, together with the energy storage device, not exceed a mass of 13kg.
EP-Sys-EG-02	The energy generation method shall be structurally sound.
EP-Sys-EG-03	The energy generation method shall create no more drag than 20N while inoperative.
EP-Sys-EG-04	The energy generation method shall together with the energy storage system shall not exceed a volume of 0.0034m ³ .

A.0.3 Requirements Motor

Table A.4 shows the requirements set for the drive train, which consists of the motor and the gearing, and the controller. The mass of the motor, the gearing and the motor controls together is 3.35kg, which complies with requirement EP-Sys-DT-03. The financial budget has been updated. Requirement EP-Sys-DT-05 was not taken into account as, after some research, only a very low climb rate was needed and the mission will be flown at moderate wind conditions. This means a much lower power is needed, so the current motor only produces a power of 2.8kW.

Although requirement EP-Sys-IC-01 was not reached as it weighs 0.45kg, the light motor compensates for this. The requirements for the input controller interface have all been achieved.

Table A.4: Requirement List Drivetrain and Controller

Identifier	Requirement
Drivetrain	
EP-Ast-DT-05	The drivetrain shall fit in a backpack.
EP-Ast-DT-06	The drivetrain shall be easy to set-up/down.
EP-Ast-DT-07	The drivetrain shall be silent.
EP-Sys-DT-01	The drivetrain shall not exceed a budget of €1778,-.
EP-Sys-DT-02	The drivetrain shall have a minimum efficiency of 85%.
EP-Sys-DT-03	The drivetrain shall not exceed a mass of 4kg.
EP-Sys-DT-04	The drivetrain shall be structurally sound.
EP-Sys-DT-05	The drivetrain shall generate a power of 11kW.
Input Controller	
EP-Ast-IC-05	The input controller must be immediately accessible in any circumstance.
EP-Ast-IC-06	Selection of power level must be precise, smooth and stepless.
EP-Ast-IC-07	The pilot must be able to stop the propeller immediately in any circumstance (kill switch).
EP-Sys-IC-01	The weight of the input controller must be less than 0.11kg
Input Controller Interface	
EP-Ast-ICI-05	The input controller interface shall be readable in sunlight.
EP-Ast-ICI-06	The input controller interface shall have a low energy consumption.
EP-Ast-ICI-07	The input controller interface shall be reliable.
EP-Sys-ICI-01	The input controller interface shall have a low energy consumption.

A.0.4 Requirements Propeller

Table A.5 shows the requirement list for what was originally called the propulsion device, but became the propeller quite quickly. Requirement EP-Ast-PPD-08 was not exactly achieved, as silent was not well defined. A noise footprint at the height of the pilot's head is given in figure 3.23a and figure 3.23b illustrates the noise values in a map. It was shown that the sound on the ground does not exceed 50dB, while the pilot is exposed to a noise of 80dB when the propeller is running. However, as 57% of the the mission is being soared, the pilot is not exposed to a constant sound level. The team did not have time to make an extra XFlow simulation to investigate requirement EP-Sys-PPD-06. However, the propeller is locked when it is inoperative to ensure it creates as little drag as possible.

Table A.5: Requirement List Propulsion Device

Identifier	Requirement
Propulsion Device	
EP-Ast-PPD-05	The propulsion device shall have a packed volume of less then $0.012m^3$.
EP-Ast-PPD-06	The propulsion device shall not be 'windmilling'.
EP-Ast-PPD-07	The propulsion device shall be easy to set-up/down.
EP-Ast-PPD-08	The propulsion device shall be silent.
EP-Ast-PPD-09	The propulsion device shall not incorporate thrust vectoring.
EP-Ast-PPD-10	The propulsion device shall not exceed a budget of €150.
EP-Sys-PPD-01	The propulsion device shall generate a minimum of $250N$ of thrust.
EP-Sys-PPD-02	The propulsion device shall have a minimum efficiency of 25%.
EP-Sys-PPD-03	The propulsion device shall not exceed a mass of $1.4kg$.
EP-Sys-PPD-04	The propulsion device shall be structurally sound.
EP-Sys-PPD-05	The propulsion device shall not exceed a blade length of $1.5m$ during takeoff.
EP-Sys-PPD-06	The propulsion device shall create no more drag than $20N$ while inoperative.

A.0.5 Requirements Chassis

The first part of table A.6 gives the requirements for the harness, for which all requirements have been achieved, just like the requirements for the hang point. The safety system that was originally ment in the table was a (partial) safety cage, maybe even including netting. The current safety system consists of the propeller being placed far enough back, in order to have a safe clearance from the pilot. This implies that all requirements for the safety system have been achieved. All requirements for the reserve parachute container have been achieved. The reserve parachute is right at the top of the cocoon, on the pilot's belly and can easily be reached. In addition, instead of having a back plate as described below, a structure inside the cocoon is used to keep everything in place. The battery is packed in a fire retardant box to ensure the achievement of requirements EP-Sys-CBP-04 and EP-Sys-CBP-01.

A.0.6 Requirements Lift Devices

All requirements for the lift device, as given in table A.7 have been achieved. This applies to the requirements of the main lift device, the suspension lines and suspension lines geometry. It was chosen to fly with a two-liner. The requirements for the wing control can be discarded, as it was chosen not to have an automatic pilot. However, all requirements given in this table also apply for the regular wing control, and have been achieved. To conclude the requirements set for the lift devices, the requirements for the reserve parachute as given in the last part of the table, and have also been achieved.

Table A.6: Requirement List Chassis

Identifier	Requirement
Harness	
EP-Ast-CH-05	The harness shall be easy to put on/off.
EP-Ast-CH-06	The harness shall not exceed a budget of €1098.
EP-Ast-CH-07	The harness shall be comfortable.
EP-Ast-CH-08	The harness shall allow for walking.
EP-Ast-CH-09	The harness shall be wearable by an average man/woman.
EP-Ast-CH-10	The harness shall not exceed a volume of $0.15m^3$.
EP-Sys-CH-01	The harness shall be structurally sound.
EP-Sys-CH-02	The harness shall be able to cope with all forces in all flight scenarios.
EP-Sys-CH-03	The harness shall not exceed a mass of $2.4kg$.
Hang Point	
EP-Ast-CHP-05	The hang point shall be easy to connect/disconnect.
EP-Sys-CHP-01	The hang point shall be structurally sound.
EP-Sys-CHP-02	The hang point shall be able to cope with all forces in all flight scenarios.
Safety System	
EP-Ast-CSS-05	The safety system shall be easy to set-up/down.
EP-Sys-CSS-01	The safety system shall not exceed a mass of $3kg$.
EP-Sys-CSS-02	The safety system shall be structurally sound.
EP-Sys-CSS-03	The safety system shall create no more than $20N$ drag.
EP-Sys-CSS-05	The safety system shall protect the pilot from the propulsion device.
EP-Sys-CSS-06	The safety system shall protect the suspension lines from the propulsion device.
EP-Sys-CSS-07	The safety system shall not exceed a volume of $0.1m^3$.
EP-Sys-CSS-08	The safety system shall not exceed a budget of €800.
Reserve Parachute Container	
EP-Ast-CRPC-05	The reserve parachute container shall not exceed a volume of $0.002m^3$.
EP-Ast-CRPC-06	The reserve parachute container shall be placed in reach of the pilot.
EP-Ast-CRPC-07	The reserve parachute container shall be attached to the harness/chassis .
EP-Ast-CRPC-08	The reserve parachute container shall be easy to attach/detach.
EP-Sys-CRPC-01	The reserve parachute container shall protect the reserve parachute from impacts.
EP-Sys-CRPC-02	The reserve parachute container shall tuck the reserve parachute.
EP-Sys-CRPC-03	The reserve parachute container shall not exceed a mass of $0.3kg$.
EP-Sys-CRPC-04	The reserve parachute container shall open quickly.
EP-Sys-CRPC-05	The reserve parachute container shall have minimum drag.
Back plate	
EP-Ast-CBP-05	The back plate shall be lightweight.
EP-Ast-CBP-06	The back plate shall allow for easy subsystem attach and detachment.
EP-Ast-CBP-07	The back plate shall be comfortable.
EP-Sys-CBP-01	The back plate shall be fire resistant.
EP-Sys-CBP-02	The back plate shall be structurally sound.
EP-Sys-CBP-03	The back plate shall sufficiently strong to support all subsystems.
EP-Sys-CBP-04	The back plate shall not conduct electricity.

Table A.7: Requirement List Lift Device

Identifier	Requirement
Main Wing Design	
EP-Ast-LMW-05	The main wing shall be silent.
EP-Ast-LMW-06	The main wing design shall be attractive to customers.
EP-Ast-LMW-07	The main wing design shall be controllable.
EP-Ast-LMW-08	The main wing shall have comparable flight characteristics to already existing paramotor/paragliding wings.
EP-Ast-LMW-09	The main wing shall have a maximum volume of $0.07m^3$.
EP-Sys-LMW-01	The main wing shall generate a minimum of $1250N$ of lift.
EP-Sys-LMW-02	The main wing shall not exceed a mass of $7kg$
EP-Sys-LMW-03	The main wing shall create no more drag than $100N$.
Wing Control Unit	
EP-Ast-LWC-05	The wing control unit shall be intuitive.
EP-Ast-LWC-06	The wing control unit shall fit on a paramotor/paraglider wing.
EP-Ast-LWC-07	The wing control unit shall give feedback to the pilot.
EP-Ast-LWC-08	The wing control unit shall not exceed a budget of $\text{€}100$.
EP-Ast-LWC-09	The wing control unit shall be redundant.
EP-Ast-LWC-10	The wing control unit shall not exceed a volume of $0.0002m^3$.
EP-Sys-LWC-01	The wing control unit shall not exceed a mass of $2kg$
EP-Sys-LWC-02	The wing control unit shall create no more drag than $10N$.
EP-Sys-LWC-03	The wing control unit shall not consume more than $100W$.
Suspension Lines	
EP-Ast-LSL-05	The suspension lines design shall not exceed a budget of $\text{€}800$.
EP-Ast-LSL-06	The suspension lines design shall be attractive to customers.
EP-Ast-LSL-07	The suspension lines shall have comparable flight characteristics to already existing paramotor/paragliding wings.
EP-Sys-LSL-01	The suspension lines shall withstand a maximum tension of $10kN$.
EP-Sys-LSL-02	The suspension lines shall be flexible under compression.
EP-Sys-LSL-03	The suspension lines shall not exceed a mass of $1kg$
EP-Sys-LSL-04	The suspension lines shall not stretch more than 2% .
EP-Sys-LSL-05	The suspension lines shall create no more drag than $40N$.
Suspension Line Geometry	
EP-Ast-LSG-05	The suspension line geometry shall ensure safe flight.
EP-Ast-LSG-06	The suspension line geometry shall provide solid control of the wing.
EP-Sys-LSG-01	The suspension line geometry shall produce little drag.
EP-Sys-LSG-02	The suspension line geometry shall match the main wing.
Reserve Lift Device	
EP-Ast-LR-05	The reserve lift device shall have a packed volume of less then $0.002m^3$
EP-Ast-LR-06	the reserve lift device shall be deployed like a regular paramotor safety parachute.
EP-Sys-LR-01	The reserve lift device shall not exceed a mass of $2.1kg$

B Resource Allocation

A comparison between the first and the latest resource allocation is performed in this Appendix. Its outcome is shown in Table B.1 and Table B.2 respectively. They depict the choices made on which component of the system shall receive what level of funding. Budgeting is done to allocate sufficient resources for accomplishment of the mission. The basic resource budgets were set, based on market research and the final resource budget was based on the detailed design and iterations.

The basic resource allocation was performed as a preliminary determination, which did not take into account any future design decisions. A margin was therefore appointed to fix how much each overall resource budget is allowed to vary during the design selection process. The only resources with a margin of zero were the mass and the cost of the system, which were preset by customer requirements. In this way it was assured that the fixed budget is not going to be exceeded. In the final resource allocation no margin is assigned anymore, since the budget has to be as accurate as possible for the detailed design, as from here prototyping starts.

It can be seen that quite some major changes were made. The biggest changes are in the mass and cost of the battery (power provider), which needed a lot more mass assigned to be able to fly with the minimal amount of stops. To be able to purchase such an amount of batteries also more money expenses were assigned to them. The motor controller and input controller also got assigned a higher price, because they are directly linked to safety and no money wants to be saved there to make sure to have a reliable product. Therefore the mass of the controls is decreased by almost half. The biggest mass and money savings could be made during the motor choice as well as in the propeller and chassis design. The last prominent difference that can be depicted comparing the two tables is the power consumption and output. After more detailed mission planning, the result was that clearly less power is needed to fulfill the mission without any stop, resulting in a very low power consumption. Therefore the batteries also need to deliver noticeably fewer power output.

Table B.1: First Budget Breakdown

Unit	$Power_{use}$ [W]	$Power_{output}$ [W]	Mass [kg]	Lift [N]	Drag [N]	Thrust [N]	Volume [m ³]	Maint. cost [€/week]	Total cost [€]	Maint. time [hrs/week]
Total budget	11,107.00	15,000.00	117.00	1,719.90	192.71	363.64	0.355	14.72	5,000.00	2.72
Motor	11,000.00	-	4.00	-	-	-	0.003	-	1,500.00	-
Motor control	80.00	-	1	-	-	-	0.004	-	500.00	-
Input controls	10.00	-	0.11	-	-	-	0.0002	-	40.00	-
Reserve chute	-	-	2.10	-	-	-	0.002	-	(500.00)	0.04
Safety structure	-	-	3.00	-	20.00	-	0.10	0.65	800.00	0.06
Propulsion	-	-	2.00	-	-	363.64	0.012	0.80	300.00	0.80
Interface	5.00	-	0.20	-	-	-	0.00005	0.10	40.00	0.10
Wing	-	-	(4.50)	1,719.90	100.00	-	0.07	0.90	(2,850.00)	0.30
Lines	-	-	(1.00)	-	40.00	-	0.01	1.00	(800.00)	0.60
Harness	-	-	3.4	-	5.00	-	0.15	0.30	590.00	0.30
Power provider	-	15,000.00	5.69	-	-	-	0.0034	10.87	1,130.00	0.50
Power distributor	2.00	-	0.10	-	-	-	-	0.10	50.00	0.01
Drive system	10.00	-	0.40	-	-	-	-	-	50.00	0.01
Pilot	-	-	95.00	-	27.71	-	0.07	-	-	-
Margin	200	7500	0	172	19.3	36	0.05	0.2	0	0.2

Table B.2: Latest Budget Breakdown

Unit	$Power_{use}$ [W]	$Power_{output}$ [W]	Mass [kg]	Lift [N]	Drag [N]	Thrust [N]	Volume [m ³]	Maint. cost [€/week]	Total cost [€]	Maint. time [hrs/week]
Total budget	2,809.00	2,866.20	117.00	1,146.60	131.30	286.00	0.192	18.02	4,546.00	2.15
Motor + Gear	2,719.00	-	3.35	-	-	-	0.003	-	688.00	-
Motor control	80.00	-	0.45	-	-	-	0.004	-	700.00	-
Input controls	10.00	-	0.25	-	-	-	0.0002	-	335.00	-
Reserve chute	-	-	(1.37)	-	-	-	0.002	-	(1,190.00)	0.04
Reserve container	-	-	0.35	-	-	-	0.01	-	79.00	-
Safety structure	-	-	-	-	-	-	-	-	-	0.00
Cocoon + Structure	-	-	1.69	-	2.6	-	0.020	0.50	600.00	0.10
Propulsion	-	-	1.40	-	-	286.00	0.012	0.80	150.00	0.80
Interface	-	-	0.10	-	-	-	0.00005	0.10	55.00	0.10
Wing+lines	-	-	(6.10)	1,146.60	91.00	-	0.07	1.90	(2,850.00)	0.30
Harness	-	-	0.65	-	25.30	-	0.00	0.30	344.00	0.30
Power provider	-	2,866.20	13.12	-	-	-	0.0079	14.42	1,500.00	0.50
Drive system	-	-	0.46	-	-	-	-	-	75.00	0.01
Bolts	-	-	0.30	-	-	-	-	-	20.00	-
Pilot	-	-	95.00	-	12.4	-	0.07	-	-	-

C Functional Breakdown Structure

The Functional Breakdown Structure (FBS), which can be seen in figure C.1, was created to state all functions the design needs to fulfill the mission.

The primary objective statement is the following: 'Fly an electric paramotor across the Netherlands from north to south'. In order to fulfill this mission the system is split up in three subsystems:

- **Flight**

The sub-branch flight contains all the functions of the mission with regard to keeping the paramotor in the air. The paramotor must be able to generate lift, propel itself, and provide stability and control for the pilot.

- **Electric Power**

One of the main requirements of the mission is that the paramotor must be electric, meaning it should provide electrical power. Moreover, electricity must be controlled and distributed into systems that consume electricity.

- **Human operation**

This sub-branch is split up into pilot interaction and ground operations. Pilot interaction contains all the functions required because the system is operated by a pilot. Ground operation contains all the functions that require human interaction while not in-flight.

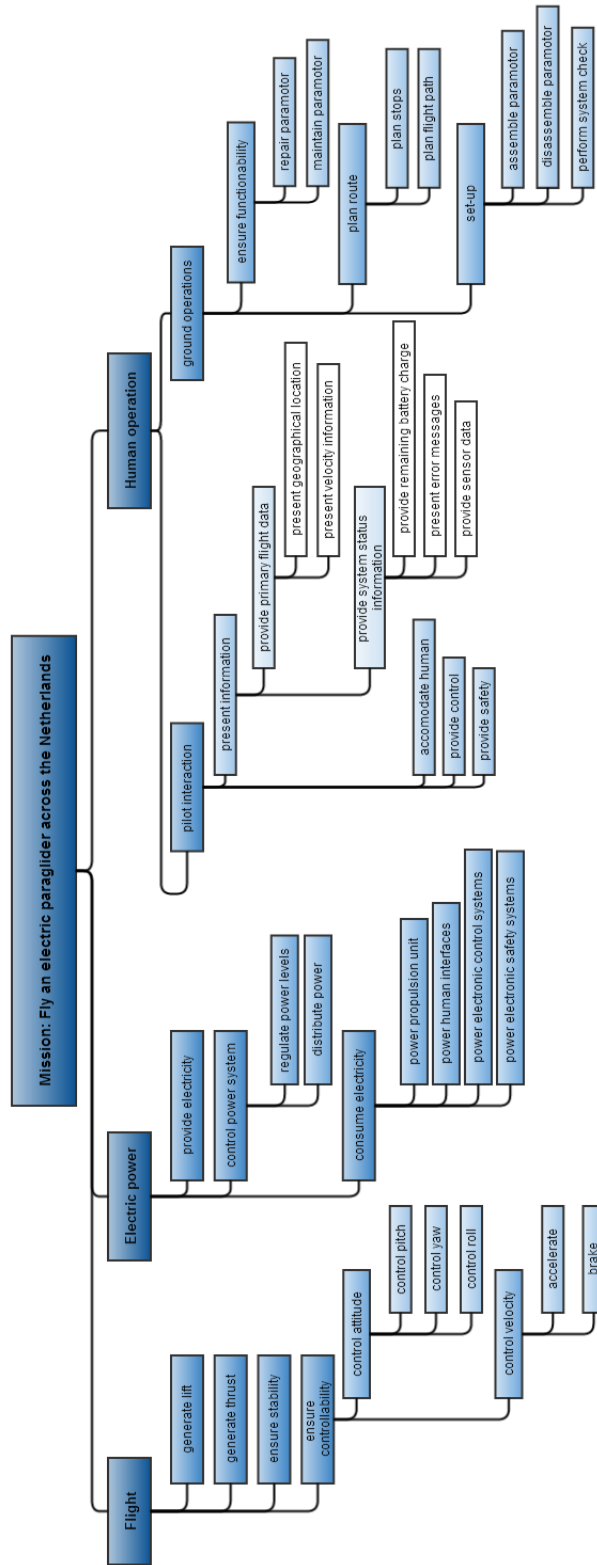


Figure C.1: Functional Break-down Structure

D Functional Flow Diagram

The Functional Flow Diagram (FFD) provides a chronological overview of the procedure that needs to be executed in order to perform the mission successfully and is presented in Figures D.1 and D.2. Furthermore, the diagram includes conditions, which are shown as G and \overline{G} . G representing a positive outcome, whereas \overline{G} indicates a negative outcome. The mission is split up into five main parts, namely: Preparation, Take-off, Cruise, Landing and Post-Landing.

- **Preparation**

The first phase describes the preparation of the mission, as well as assembling the paramotor at the start site and performing a complete system check.

- **Take-Off**

In the second phase the take-off procedure is explained, which covers the time span from getting strapped in the paramotor until reaching cruise altitude. During this phase the pilot has to check the environment for appropriate starting conditions. Furthermore the FFD elaborates on the procedure while climbing, which includes the control of the vehicle, as well as checking sensors and flight path data. The take-off phase ends when cruise altitude is reached.

- **Cruise**

During the cruise phase, all steps that are required to cover distance between stops are presented. Again the paramotor has to be controlled and sensors need to be checked. Excluding the emergency case, there are two events that will end the cruise phase. One being that the charge/fuel status is too low to continue or that the next stop has been reached.

- **Landing**

The landing phase covers the period from leaving cruise altitude to descend until touching the ground. In this time span an appropriate landing site is chosen and approached by steering the vehicle and adjusting the thrust level. The final phase of the descent is initiated, when the paramotor is close to the ground and the pilot moves himself into the recommended landing position, before touching the ground.

- **Post-Landing**

All post-landing activities are listed in this phase. The electric system is switched off right after landing. If this landing is only a stop for recharging/refueling, the procedure continues in the preparation phase at the system check. In case the paramotor has landed at the final destination, it needs to be disassembled and packaged.

The functional flow diagram was used to generate the requirement discovery tree and the design option tree, since it gives a clear view of which functions the design needs to be able to fulfill within the constraints.

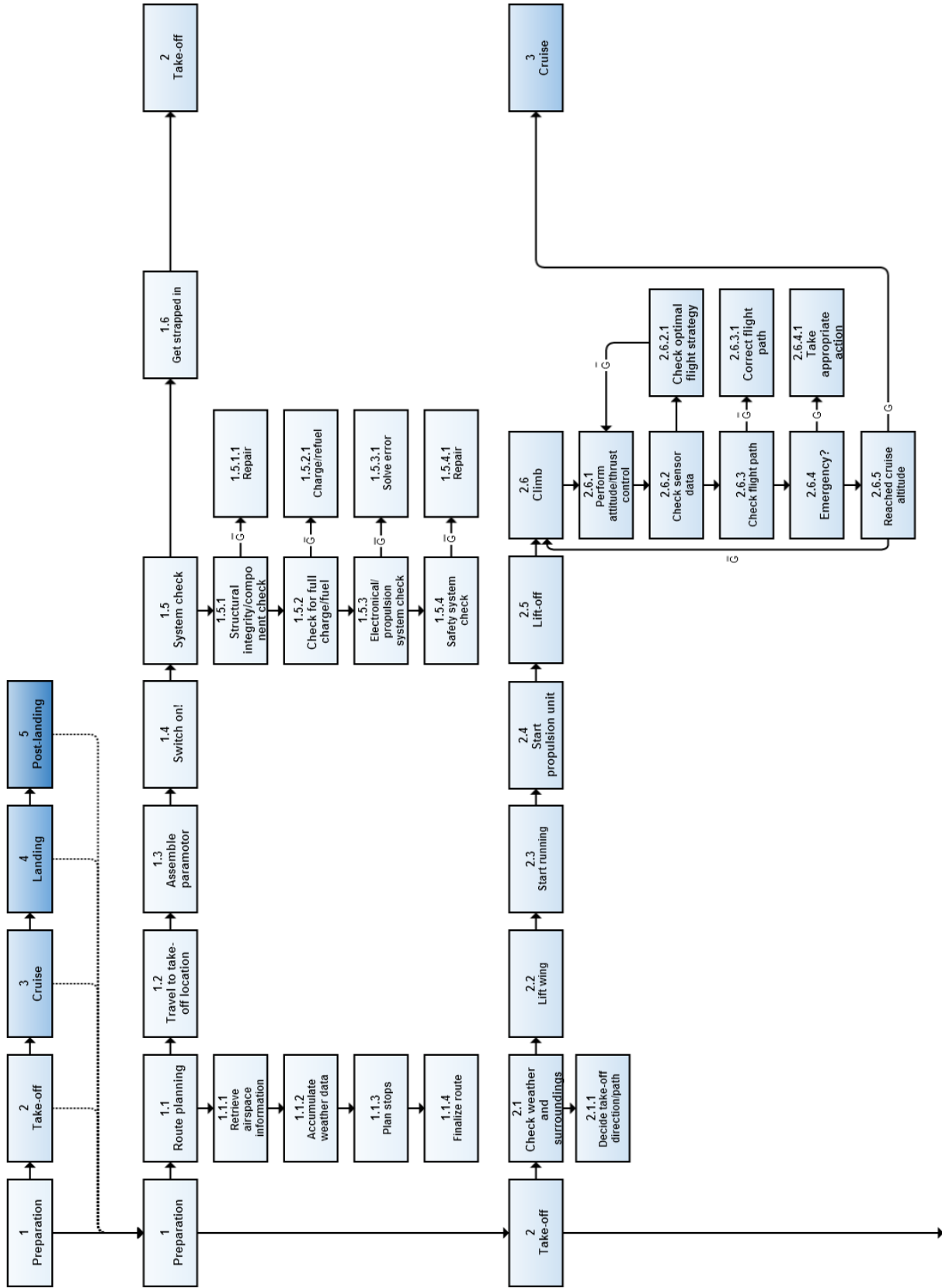


Figure D.1: Functional Flow Diagram Part 1

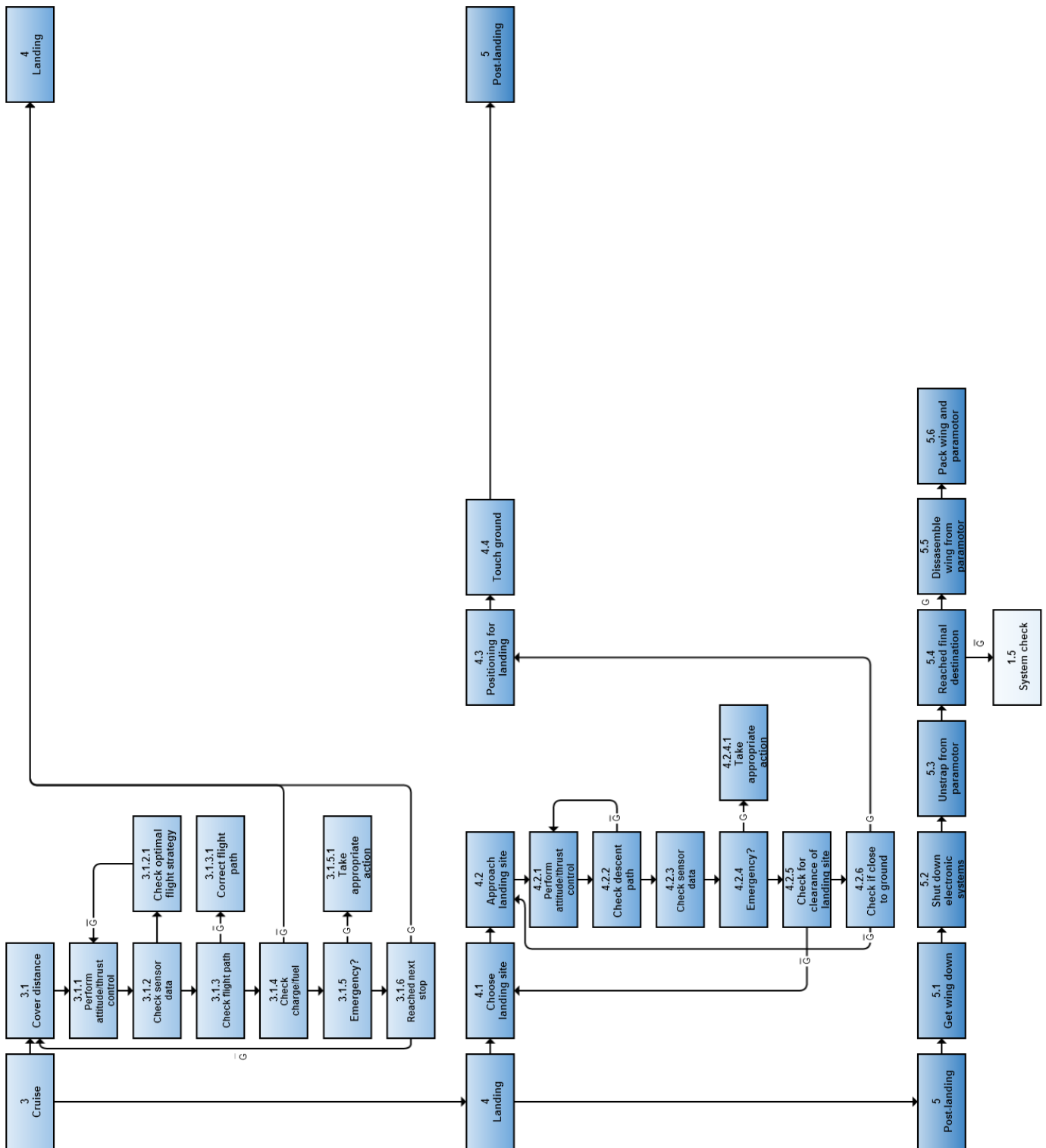


Figure D.2: Functional Flow Diagram Part 2

E Battery Terms

Table E.1: Battery Terms 1 ^a

Anode:	The negative electrode of a cell.
Button Cell:	A small round or elliptical cell whose diameter is greater than its height.
Capacity:	Capacity is the product of the discharge current Amps (A) or milli Amp (mA) and the discharge time (h) at a given load and is expressed in Amp-Hours (Ah) or milli Amp-Hours (mAh).
Cathode: & The positive electrode of a cell.	
Cell:	A single encased electrochemical unit (one positive and one negative electrode) which exhibits a voltage differential across its two terminals. Under the Model Regulations of Tests and Criteria (See UN38.3 Tests), to the extent the encased electromechanical unit meets the definition of a "cell" herein, is a "cell", not a "battery", regardless of whether the unit is termed a "battery" or a "single cell battery" outside of the Model regulations.
CE Mark:	The CE mark (Abbreviation of Conformit Europenne) is a mandatory conformity mark for products placed on the market in the European Community. With the CE mark on the product, the manufacturer ensures that the product conforms to the requirements of the applicable EC directive.
Chemistry:	Refers to the basic material of the negative electrode. Example: Zinc, Lithium, Nickel.
Closed circuit voltage - CCV:	Voltage across the terminals of a battery under load when there is external current flowing.
Coin cells:	A small cell whose diameter is greater than its height. Coin cells are typically lithium chemistry.
Cycle:	One sequence of fully charging and fully discharging a rechargeable cell or battery.
Discharge:	Operation during which a battery delivers current to an external circuit or load.
Discharge characteristics - Discharge curve:	Graphical representation of the change in output voltage over time under various loads and/or ambient temperature.
Electrolyte:	Medium in a battery which causes ions to move to create an electrochemical reaction. Either water or non-aqueous solution is used as solvent. The latter is called non-aqueous electrolyte solution, either organic or inorganic.
End-point voltage:	Specified closed circuit voltage at which a cell is terminated. Also referred to as "cutoff or "final voltage.
Energy Density:	Available energy of a battery per unit volume or unit weight.

^a<http://www.epectec.com/batteries/glossary-of-battery-terms.html#UN-Tests>, visited on Dec 19th, 2014

Table E.2: Battery Terms 2 ^a

IATA:	The International Air Transport Association (IATA) is an international trade group comprised of some 240 airlines and is headquartered in Montreal Quebec, Canada. IATA's stated mission is to represent, lead and serve the airline industry. The main aim of IATA is to provide safe and secure transportation to its passengers. IATA annually publishes the IATA Dangerous Goods Regulations (DGR), which are modeled after the ICAO Technical Instructions. (The 54th Edition became effective on 1-1-2013.) Working closely with governments in the development of the regulations, including ICAO and other national authorities, IATA ensures that the rules and regulations governing dangerous goods transport are both effective and efficient. The U.S. Department of Transportation (DOT) does not officially recognize or enforce the IATA Dangerous Goods Regulations. Instead, the DOT has the authority to enforce the ICAO Technical Instructions.
Internal Impedance:	Internal impedance of a cell that increases as the cell ages or is discharged. This is measured by a 1000Hz Bridge, also called internal resistance. Typical internal impedance of a cell is j100Ohms.
Leakage:	The escape of material from a cell or battery. The most common leakage is electrolyte, which is either very flammable or very corrosive.
Lithium content:	The mass, in grams, of lithium metal contained within the anode of lithium metal or lithium alloy cell. These are, for the most part, primary cells. The lithium content of a lithium battery is the sum of the lithium mass of the anodes of all the cells in the battery.
Load:	External device or method through which a battery is discharged.
Nominal voltage:	Approximate midpoint voltage, during discharge, of a fully charged battery cell. This varies by chemistry with common examples below: Alkaline manganese primary - 1.5V Zinc Carbon Primary - 1.5V Lithium manganese dioxide primary - 3.0V Lithium thionyl chloride primary - 3.6V Nickel cadmium rechargeable battery - 1.2V Nickel metal-hydride rechargeable - 1.2V Nickel Zinc rechargeable - 1.6V Lithium-ion rechargeable - 3.7V Lithium-prismatic rechargeable - 3.7V Lithium-polymer rechargeable - 3.7V Silver Oxide Primary - 1.55V Zinc Air Primary - 1.45V
Open circuit voltage - OCV:	Voltage across the terminals of a battery when no external current is flowing and not under load. The OCV is typically higher than a battery's nominal voltage.
Over discharge:	To discharge a cell to a voltage below its end-point voltage.

^a<http://www.epectec.com/batteries/glossary-of-battery-terms.html#UN-Tests>, visited on Dec 19th, 2014

Table E.3: Battery Terms 3 ^a

Packing Instructions:	Instruc-	The ICAO Technical Instructions and the IATA Dangerous Goods Regulations require compliance to specific Packing Instructions (PIs) in order to offer lithium-metal primary cells and batteries and lithium-ion rechargeable batteries for transport in passenger and cargo aircraft. PI 965: UN3090 Lithium-metal primary cells and batteries. PI 966: UN3091 Lithium-metal primary cells and batteries shipped with equipment. PI 967: UN3091 Lithium-metal primary cells and batteries installed in equipment. PI 968: UN3480 Lithium-ion rechargeable cells and batteries. PI 969: UN3481 Lithium-ion rechargeable batteries shipped with equipment. PI 970: UN3481 Lithium-ion rechargeable batteries installed in equipment.
Protection Module - PCM:	Circuit	The safety circuit installed in all lithium-ion and lithium-polymer rechargeable battery packs to control over-charge, over-discharge and short circuit of the cells within the pack. This circuit is mandated by the UN Manual of Tests and Criteria, paragraph 38.3, Rev. 5.
Protective Devices:		Devices, such as fuses, diodes and current limiters which interrupt the current flow, block the current flow in one direction or limit the current flow in an electrical circuit.
Primary: Rated Capacity:		A cell or battery which is not designed to be charged and discharged. The capacity, in ampere-hours (Ah) of a cell or battery as measured by subjecting it to a load, temperature and cut-off voltage point specified by the manufacturer.
Self-discharge:		Decreasing capacity during storage without load, caused by chemical reaction in a battery. The higher the temperature during battery storage, the greater the rate of self-discharge.
SMBus:		SMBus is the System Management Bus as defines by the Intel Corporation in 1995. It is used in personal computers and servers for system management communications, including battery charge status.
UN3090, UN3480 & UN3481:	UN3091, UN3481:	The IATA Dangerous Goods Regulations and the U.S. Code of Federal Regulations (49CFR Part 172(c)(1)) classify lithium-metal primary and lithium-ion rechargeable cells and batteries as Dangerous Goods; and must be shipped in passenger and cargo aircraft in accordance with specific packing instructions. UN3090: Lithium-metal primary cells and batteries. UN3091: Lithium-metal primary cells and batteries shipped with or in equipment. UN3480: Lithium-ion rechargeable cells and batteries. UN3484: Lithium-ion rechargeable cells and batteries shipped with or in equipment.
UN 38.3 Tests:		In order to offer for transport in passenger and cargo aircraft, lithium-metal primary cells and batteries and lithium-ion rechargeable cells and batteries must comply with Packing Instructions 965 through 970 (as applicable) in The ICAO Technical Instructions "Recommendations on the Transport of Dangerous Goods Manual of Tests and Criteria". This packing instruction includes mandatory provisions for the testing of lithium metal and lithium-ion cells and batteries (Sub-section 38.3).
Vent:		A safety device built into almost all cells designed to release internal pressure in the case of overcharge, over temperature and other abuses. The vent will preclude rupture or disassembly.
Venting:		The release of excessive internal pressure from a cell or battery in a manner intended by design to preclude rupture or disassembly. Venting may also release electrolyte.
Watt-hours:		A cell or battery's nominal voltage multiplied by its rated capacity in amp-hours.

^a<http://www.epectec.com/batteries/glossary-of-battery-terms.html#UN-Tests>, visited on Dec 19th, 2014

F Battery Standards

Table F.1: General battery standards ^a

General battery standards	
Standard Number	Title
IEC 60050	International electro technical vocabulary. Chapter 486: Secondary cells and batteries.
IEC 60086-1, BS 387	Primary Batteries - General
IEC 60086-2, BS	Batteries - General
ANSI C18.1M	Portable Primary Cells and Batteries with Aqueous Electrolyte - General and Specifications
ANSI C18.2M	Portable Rechargeable Cells and Batteries - General and Specifications
ANSI C18.3M	Portable Lithium Primary Cells and Batteries - General and Specifications
UL 2054	Safety of Commercial and Household Battery Packs - Testing
IEEE 1625	Standard for Rechargeable Batteries for Mobile Computers
USNEC Article 480	Storage Batteries

^a<http://www.epectec.com/batteries> Visited on Dec 18th of 2014

Table F.2: Lithium battery standards ^a

Lithium battery standards	
Standard Number	Title
BS 2G 239:1992	Specification for primary active lithium batteries for use in aircraft
BS EN 60086-4:2000, IEC 60086-4:2000	Primary batteries. Safety standard for lithium batteries
BS EN 61960-1:2001, IEC 61960-1:2000	Secondary lithium cells and batteries for portable applications. Secondary lithium cells
BS EN 61960-2:2002, IEC 61960-2:2001	Secondary lithium cells and batteries for portable applications. Secondary lithium batteries
02/208497 DC	IEC 61960. Ed.1. Secondary cells and batteries containing alkaline or other non-acid electrolytes.
02/209100 DC	Secondary lithium cells and batteries for portable applications
BS G 239:1987	IEC 62281. Ed.1. Safety of primary and secondary lithium cells and batteries during transport
BS EN 60086-4:1996, IEC 60086-4:1996	Specification for primary active lithium batteries for use in aircraft
UL 1642	Primary batteries. Safety standard for lithium batteries
GB /T18287-2000	Safety of Lithium-Ion Batteries - Testing
ST/SG/AC.10/27/	Chinese National Standard for Lithium Ion batteries for mobile phones
	United Nations recommendations on the transport of dangerous goods

^a<http://www.epectec.com/batteries> Visited on Dec 19th of 2014

G Power Distribution during Powered Flight

This Appendix provides an overview of the power distribution during the powered flight and indicates how much of the total energy is used in a certain power range.

Total Energy consumed: 5.1978 kWh

- Percentage of total Energy used between 0-0.5kW: 0 % - 0Wh
- Percentage of total Energy used between 0.5-1kW: 0 % - 0Wh
- Percentage of total Energy used between 1-1.1kW: 0 % - 0Wh
- Percentage of total Energy used between 1.1-1.2kW: 0 % - 0Wh
- Percentage of total Energy used between 1.2-1.3kW: 0 % - 0Wh
- Percentage of total Energy used between 1.3-1.4kW: 4.0517 % - 210.5992Wh
- Percentage of total Energy used between 1.4-1.5kW: 6.2682 % - 325.8062Wh
- Percentage of total Energy used between 1.5-1.6kW: 6.3317 % - 329.1091Wh
- Percentage of total Energy used between 1.6-1.7kW: 11.2638 % - 585.4652Wh
- Percentage of total Energy used between 1.7-1.8kW: 11.333 % - 589.0607Wh
- Percentage of total Energy used between 1.8-1.9kW: 14.8469 % - 771.706Wh
- Percentage of total Energy used between 1.9-2kW: 7.9791 % - 414.7341Wh
- Percentage of total Energy used between 2-2.1kW: 0 % - 0Wh
- Percentage of total Energy used between 2.1-2.2kW: 10.3574 % - 538.354Wh
- Percentage of total Energy used between 2.2-2.3kW: 9.1674 % - 476.5025Wh
- Percentage of total Energy used between 2.3-2.4kW: 10.7168 % - 557.032Wh
- Percentage of total Energy used between 2.4-2.5kW: 2.1741 % - 113.0027Wh
- Percentage of total Energy used between 2.5-2.6kW: 4.2277 % - 219.7483Wh
- Percentage of total Energy used between 2.6-2.7kW: 1.2823 % - 66.6492Wh
- Percentage of total Energy used between 2.7-2.8kW: 0 % - 0Wh
- Percentage of total Energy used between 2.8-2.9kW: 0 % - 0Wh
- Percentage of total Energy used between 2.9-3kW: 0 % - 0Wh
- Percentage of total Energy used between 3-3.5kW: 0 % - 0Wh
- Percentage of total Energy used between 3.5-4kW: 0 % - 0Wh

Maximum Power during the mission: 2.6725kW

H Battery Wiring

Table H.1: Wiring Type 1

Wire [Type 2 36V, 1A] -AWG 29 [diameter: 0.286004mm]					
	distance [mm]		distance [mm]		distance [mm]
wire stack 1	498	wire stack 15	498	wire stack 29	498
wire stack 2	463	wire stack 16	463	wire stack 30	463
wire stack 3	428	wire stack 17	428	wire stack 31	428
wire stack 4	393	wire stack 18	393	wire stack 32	393
wire stack 5	358	wire stack 19	358	wire stack 33	358
wire stack 6	323	wire stack 20	323	wire stack 34	323
wire stack 7	288	wire stack 21	288	wire stack 35	288
wire stack 8	245	wire stack 22	245	wire stack 36	245
wire stack 9	210	wire stack 23	210	wire stack 37	210
wire stack 10	175	wire stack 24	175	wire stack 38	175
wire stack 11	140	wire stack 25	140	wire stack 39	140
wire stack 12	105	wire stack 26	105	wire stack 40	105
wire stack 13	70	wire stack 27	70	wire stack 41	70
wire stack 14	35	wire stack 28	35	wire stack 42	35
Wiring to connect cells in parallel [mm]			1680		
total wire length [mm]			24066		

Table H.2: Wiring Type 2

Wire type 2 [36V 84amp] - AWG 7 [diameter: 3.664712 mm]	
Length battery front to motor [mm]	720
Length battery back to motor [mm]	471
Deviation length [mm]	30
Total length [mm]	1191

Table H.3: Wiring Resistances

Wire resistance type 1	
Length conductor [m]	1.191
Cross-sectional area [m^2]	$6.4 \cdot 10^{-8}$
ρ , resistivity [$\Omega \cdot m$]	$1.724 \cdot 10^{-8}$
Total resistance [Ω]	$3.21 \cdot 10^{-4}$
Wire resistance type 2	
Length conductor [m]	24.066
Cross-sectional area [m^2]	$10.55 \cdot 10^{-6}$
ρ , resistivity [$\Omega \cdot m$]	$1.724 \cdot 10^{-8}$
Total resistance [Ω]	$3.93 \cdot 10^{-5}$

I Motor Selection

Table I.1: Different Motors and their characteristics

Geared motors						
Type	Rototmax 1.40	SII-5525-195KV	Rotomax 1.60	A80-8	A80-10	TM685-30 Monster-Antrieb
Manufacturer	Turnigy	Scorpion	Turnigy	Hacker	Hacker	
Range	37.56	37.58	37.1	35.06	35.06	35.23
Cost (incl.gear) [Euro]	281	328	316	759	683	N.A.
Mass (incl.gear) [g]	1715	1708	1849	2450	2450	2400
Continuous power [kW]	2775	2800	2960	3250	3250	3500
Peak power [kW]	4260	4200	4550	5000	5000	5380
Efficiency (incl. Gear)	0.84	0.84	0.84	0.84	0.84	0.84
kV [RPM/V]	288	195	231	218	180	N.A.
Type	Q80-8M	SII-5535-160KV	TG7140	SII-6530-150KV	SII-5535-190KV	SII-6530-180KV
Manufacturer	Hacker	Scorpion	Thin gap	Scorpion	Scorpion	Scorpion
Range	36.33	36.91	36.01	36.44	36.44	36.44
Cost (incl.gear) [Euro]	779	489	N.A.	520	489	521
Mass (incl.gear) [g]	2075	1906	2170	2043	2043	2043
Continuous power [kW]	3560	3750	3850	3900	3900	4550
Peak power [kW]	5500	5600	5920	5800	5800	6800
Efficiency (incl. Gear)	0.84	0.84	0.84	0.84	0.84	0.84
kV [RPM/V]	180	160	N.A.	150	190	180
Type	A100-8	A100-10	Q80-6L	Rotomax 50cc	Rotomax 100cc	Power 360
Manufacturer	Hacker	Hacker	Hacker	Turnigy	Turnigy/Hobbyking	E-flite
Range	33.87	33.53	35.59	36.32	31.73	36.18
Cost (incl.gear) [Euro]	949	949	879	356	467	489
Mass (incl.gear) [g]	2800	2900	2295	2080	3100	2240
Continuous power [kW]	4560	4560	4560	5300	5330	5772
Peak power [kW]	7000	7000	7000	8140	8000	6660
Efficiency (incl. Gear)	0.84	0.84	0.84	0.84	0.82	0.85
kV [RPM/V]	196	150	180	172	167	180
Type	A150-10	Rotomax 150cc	JM1S	HK-7050-340KV	A200-6	
Manufacturer	Hacker	Turnigy/Hobbyking	Joby motors	Scorpion	Hacker	
Range	33.59	30.41	35.79	33.82	31.18	
Cost (incl.gear) [Euro]	1099	534	1162	1001	1250	
Mass (incl.gear) [g]	3100	3500	2800	2700	3590	
Continuous power [kW]	6000	6530	8200	10000	10000	
Peak power [kW]	9000	9800	12600	15000	15000	
Efficiency (incl. Gear)	0.86	0.82	0.89	0.84	0.84	
kV [RPM/V]	133	150	6000	340	151	
Direct drive						
Type	HPD 10	RET 30	12kW type			
Manufacturer	Geiger/Flytec E-drive	Rotex electric	NT-power			
Range	33.72	32.41	32.41			
Cost [Euro]	2000	1300	1300			
Mass [g]	3750	4100	4100			
Continuous power [kW]	1000	1000	1000			
Peak power [kW]	1500	1300	1300			
Efficiency	0.93	0.93	0.93			
Nominal speed [rpm]	2100	2200	N.A.			

J Particle Swarm Optimization for Airfoil Selection

This Appendix describes the inner workings of the particle swarm optimization module for airfoil selection. First the basic workings of particle swarm optimization will be described. Next the application on airfoil optimization will be discussed. Finally some conclusions will be drawn on comparisons between optimized airfoils and existing airfoils.

Particle Swarm Optimization Method

In the propeller design module, a method for optimizing airfoils is searched for. The objective function of this optimization module is the XFOIL module by Mark Drela which calculates 2d aerodynamic coefficients of airfoils from low Reynolds numbers to the higher sub-sonic regime. The use of the XFOIL module already limits the application of gradient based optimization methods since XFOIL is a black box module. No information is available on the gradients since the equations on which the operations of XFOIL are based are very complex and very hard to specify. This means that quasi-Newton methods or gradient descent methods are incompetent of solving the problem. However, an excellent candidate for the optimization would be PSO (Particle Swarm Optimization). PSO is a meta-heuristic optimization approach which is based on a simple mathematical algorithm. One of the difficult problems with airfoil optimization is that the search space may contain many local optima. The advantage of PSO is that with enough initial particles it does not converge to a local optimum but to the global optimum.

The general algorithm on which particle swarm optimization is based is given in figure J.1¹. It is clear that particle swarm optimization is a relative easy optimization method and hence it's usability with regards to the scope of this Design Synthesis Exercise is considered very large.

PSO Application to Airfoil Optimization

In this subsection, the implementation of PSO with regards to airfoil optimization is described. Finally some conclusions on the performance of the tool will be given by comparing some generated airfoils with existing airfoils.

The first step in building an airfoil optimizer is to parametrize the shape of the airfoils. This is done with a b-spline curve. A b-spline is a spline defined by multiple control points and can be seen in J.2a.²

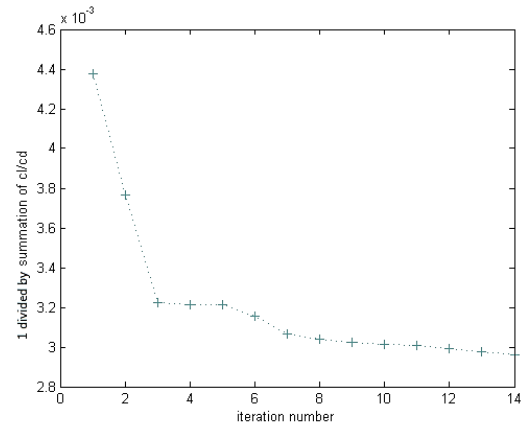
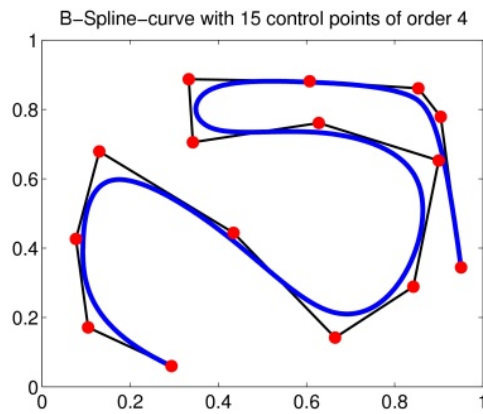
The spline is defined by the control points and the degree. The degree is a measurement of how smooth the curve is, and the control points are points which are approached by the spline. Typically a higher degree leads to a smoother curve but higher divergence from the control points. B-splines are a very useful way of parametrizing a shape. An existing B-spline script for MATLAB was

¹http://en.wikipedia.org/wiki/Particle_swarm_optimization, visited on dec 1th, 2014

²http://m2matlabdb.ma.tum.de/download.jsp?MC_ID=7&SC_ID=7&MP_ID=485, visited on jan 20th, 2015

- For each particle $i = 1, \dots, S$ do:
 - Initialize the particle's position with a **uniformly distributed** random vector: $\mathbf{x}_i \sim U(\mathbf{b}_{lo}, \mathbf{b}_{up})$, where \mathbf{b}_{lo} and \mathbf{b}_{up} are the lower and upper boundaries of the search-space.
 - Initialize the particle's best known position to its initial position: $\mathbf{p}_i \leftarrow \mathbf{x}_i$
 - If $f(\mathbf{p}_i) < f(\mathbf{g})$ update the swarm's best known position: $\mathbf{g} \leftarrow \mathbf{p}_i$
 - Initialize the particle's velocity: $\mathbf{v}_i \sim U(-|\mathbf{b}_{up}-\mathbf{b}_{lo}|, |\mathbf{b}_{up}-\mathbf{b}_{lo}|)$
- Until a termination criterion is met (e.g. number of iterations performed, or a solution with adequate objective function value is found), repeat:
 - For each particle $i = 1, \dots, S$ do:
 - Pick random numbers: $r_p, r_g \sim U(0,1)$
 - For each dimension $d = 1, \dots, n$ do:
 - Update the particle's velocity: $v_{i,d} \leftarrow \omega v_{i,d} + \phi_p r_p (\mathbf{p}_{i,d} - \mathbf{x}_{i,d}) + \phi_g r_g (\mathbf{g}_d - \mathbf{x}_{i,d})$
 - Update the particle's position: $\mathbf{x}_i \leftarrow \mathbf{x}_i + \mathbf{v}_i$
 - If $f(\mathbf{x}_i) < f(\mathbf{p}_i)$ do:
 - Update the particle's best known position: $\mathbf{p}_i \leftarrow \mathbf{x}_i$
 - If $f(\mathbf{p}_i) < f(\mathbf{g})$ update the swarm's best known position: $\mathbf{g} \leftarrow \mathbf{p}_i$
 - Now \mathbf{g} holds the best found solution.

Figure J.1: General algorithm for particle swarm optimization. ω , ϕ_g and ϕ_f are optimization parameters.



(a) Overview of a b-spline. B-splines are used for the airfoil parametrization.

(b) Evolution of the minimum of the objective function after just 14 iterations

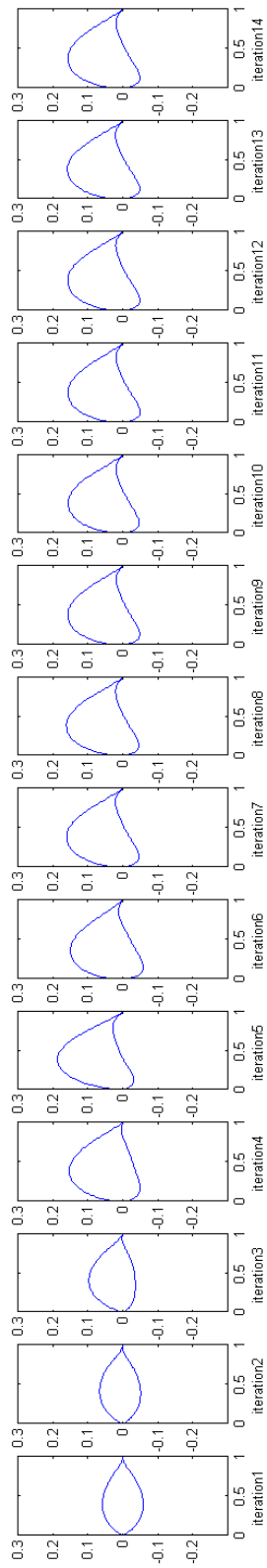
downloaded from the internet. In the particle swarm optimization module, the b-splines are set up by defining control points. Each control point is a set of x and y coordinates which are the dimension vector of one particle. A particle in this case would be a set of control points which defines the shape of an airfoil. During the particle swarm optimization, the control points can take up positions limited in a certain boundary.

The x boundaries of the control points are initialized by discretizing the length of the airfoil by a variable which is used as input of the function. Also the y boundaries of the control points of the airfoil are initialized by taking a certain factor of the maximum thickness of the airfoil. This thickness factor is also used as input for the function. It must be noted that the x and y coordinates of the first and last point are set at 0,0 and 1,0 in order to keep the chord over all airfoils constant. Also the second control point can only vary over the y axis in order to make the leading edge tangent. In addition, two extra dimensions are added to the particle which define the mean camber line. One defines the point of maximum camber, and the other describes the value of the maximum camber. So basically first a symmetric airfoil is created, from which then the x and y components are mapped onto a random generated camberline.

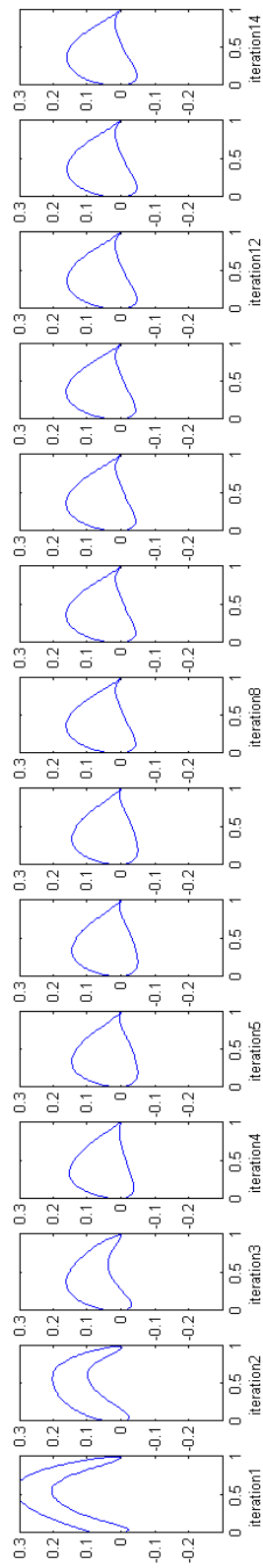
Each time an airfoil is generated by a random set of control points, it calls for the objective function. The objective function is the XFOIL module. An XFOIL interface for MATLAB was downloaded from the internet. This module was modified slightly to be able to cooperate with the particle swarm optimization module. The XFOIL MATLAB module writes batch and corresponding airfoil files which commands XFOIL.exe to analyse the airfoil. The result is then stored and converted to the objective function. An example of an objective function would be to search for an airfoil with the highest average c_l over a certain range of angles of attack. These function values are then passed on to the particle swarm module which couples the function value to the particle that generated that value. The particles each look at their own best value (in their previous versions), and at the global best particle value (the best value of all the particles). Based on those two known particle positions, each particle gets assigned a velocity vector which moves by a certain amount to the particle best position and by a certain amount to the global best position. This makes sure the particles do not converge to a local optimum (provided good optimization parameters are used).

Example results of particle swarm optimization

In figure J.3a and J.3b the evolution of the global best optimum and the particle best optimum are shown. Also in figure J.2b the convergence of the global minimum plotted against iteration number is given. It can be seen that the airfoils converge pretty quickly to an optimum.



(a) Evolution of the global best airfoil, (scale of y-axis blown up)



(b) Evolution of the particle best airfoil, (scale of y-axis blown up)

K Drive Shaft Analysis Method

The method behind the design of the drive shaft is presented in this chapter. Firstly, the max. amount of torque on the drive shaft is set in variable Tm . A range of radii is created ranging from $1mm$ to $5mm$ in steps of $0.1mm$. The enclosed area is then calculated for each radius. Several material types can be analysed in the program. Their specific properties in the form of shear strength, tensile yield strength, density and E-modulus are inserted in the allocated vectors.

Design for Torsion

As a start, the minimal needed thickness of the hollow cylinders wall is calculated using equation K.1. This minimal thickness is determined by the amount of torsion applied on the cross-section. The thickness will be such that the maximal stress on the outermost part of the cylinder is just below the shear strength. The minimal thickness possible was set at $0.5mm$, every results for t below this was thus set to $0.5mm$ to ensure manufacturability.

$$t = \frac{T}{2\pi R^2 \tau_y} \quad (K.1)$$

Knowing the thickness and the mean radius the inner and outer radii are then calculated. This then defines the cross-sections for which the weight per meter is calculated using the density of the materials. Also the maximal shear stress occurring per cross-section is calculated using equation K.2. This is the stress on the outer radius.

$$\tau_{max} = \frac{2TR_{outer}}{\pi(R_{outer}^4 - R_{inner}^4)} \quad (K.2)$$

If this maximal shear stress exceeds the shear strength of the material the value for the outer radius of this cross-section is eliminated from the design options.

Design for Bending

The bending stress is caused by the weight of the propeller suspended from the end of the drive shaft. Equation K.3 is used for this.

$$\sigma_z = \frac{My}{I} \quad (K.3)$$

First the moment distribution over the drive shaft are determined using the free body diagram in figure 3.29. The maximum moment is taken from this and used in the equation. Area moments of inertia are determined per cross-section and the variable y is set equal to the outer radius. If the value for tensile stress exceeds the tensile yield stress this value of the outer radius of the cross-section is eliminated from the design option.

Design for Compression

To design the drive shaft for the compressive load due to the thrust of the propeller the buckling formula was used in equation K.4.

$$F = \frac{\pi^2 EI}{KL^2} \quad (K.4)$$

The dimensionless variable K is the column effective length factor. It's value varies between 0.5 and 2 depending on the way the column, or drive shaft in this case, is supported. It can be either clamped, pinned or free. The drive shaft in the paramotor is taken to be clamped at the motor side

and pinned at the propeller side. This is assumed since a bearing is present close to the propeller. Although the drive shaft is not exactly pinned at the end but a small length away from it the buckling mode is still expected to be similar to a one end clamped, one end pinned column. The factor K was therefore set at 0.699. The buckling load F was determined for each cross-section. If this load was below the maximum expected thrust value the outer radius of this cross section was eliminated from the design options.

The compressive stress due to the thrust force is determined by simply using equation K.5.

$$\sigma_c = \frac{F_{max}}{A} \quad (\text{K.5})$$

Von Mises Stress Criteria

The bending, compressive and torsional stresses can be combined using the Von Mises stress formula in equation K.6. This Von Mises stress should stay below the yield strength of a material in order to make sure this part does not yield and fail in tension.

$$\sigma_y = \frac{1}{\sqrt{2}} \sqrt{[(\sigma_x - \sigma_y)^2 + (\sigma_y - \sigma_z)^2 + (\sigma_z - \sigma_x)^2 + 6\tau_{xy}^2 + 6\tau_{yz}^2 + 6\tau_{zx}^2]} \quad (\text{K.6})$$

In the case of the drive shaft this equation can be simplified to equation K.7 as there is only bending in one direction and torsion in one plane. Here the stress due to bending and compression are combined into one resultant stress in z-direction. Therefore: $\sigma_x, \sigma_y, \tau_{yz}, \tau_{zx} = 0$.

$$\sigma_y = \frac{1}{\sqrt{2}} \sqrt{[2(\sigma_z)^2 + 6\tau_{xy}^2]} \quad (\text{K.7})$$

The cross-sections in which the Von Mises stress exceeds the tensile yield stress are not considered for the design.

Eigenfrequency

In the eigenfrequency analysis of the driveshaft the case of a one side clamped, one side hinged beam is used with uniform loading. Due to time constraints this standard case is taken of which the equations are known. These equations were taken from the paper written by the Modal Analysis and Controls Laboratory of the University of Massachusetts Lowell *UML* (now). It has to be noted however that due to the fact that the beam is not uniformly loaded but point loaded at the end of the shaft the results will not be completely accurate.

The equation for the eigenfrequency is stated as K.8.

$$w_{nf} = A * \sqrt{\frac{EI}{m_{unit} * L^4}} \quad (\text{K.8})$$

Where A is the factor for a certain vibration mode, E is the Young's modulus, I the moment of inertia and m_{unit} the mass per unit length (L). The three modes possible for a fixed-hinged beam deliver the factors for A = 15.4, 50 and 104. The corresponding eigenfrequencies are 72.6Hz, 235.7Hz and 490.3Hz.

L Mail Exchange with Russel Ogden



Stéphanie Folmer <[redacted]>

Stability wing - TU Delft Electric Paramotor

Stéphanie Folmer <[redacted]>
To: Russell Ogden <[redacted]>

Tue, Dec 16, 2014 at 11:33 AM

Dear Russell,

Thanks for your email! Right now we're actually already a bit further into the project, so we decided to abandon the flexible solar panels; due to instability of the wing, but also due to the cost.

However, I do have another question for you. We're in a more detailed design phase of our project now. We have decided to focus on reducing drag and weight as much as possible in order to increase our range. We are designing some sort of cocoon/extended leg container (as light as possible) to fulfill the drag reduction requirement. The results we got from some computational fluid dynamics simulations already look very promising.

We are also focusing on fulfilling our mission (instead of designing a product for a broad audience). Right now we would like to be able to fly from the south to the north of the Netherlands in one day (approx. 314 km), by using an electric paramotor. We are therefore also taking into account that a very experienced pilot would be flying it. In designing our mission we also figured that using the dunes along the coast of the Netherlands in order to soar big parts of the mission would also help in flying the mission more efficient, and therefore less landings in order to recharge the battery will be needed.

As line drag is another pretty big part of the drag, we would like to reduce the total line length by flying a two riser wing, such as the Ozone Mantra R11. Another reason for us to wanting to fly this wing with a paramotor instead of using a dedicated paramotoring wing is because of the higher glide ratio and lower drag than a dedicated paramotor wing would have (especially than one with a reflex profile).

Now here comes my question: Do you think this is possible? To fly a (small - the whole system including cocoon, motor and battery will be less than 22 kg) paramotor with this specific wing? Why or why not? Will it be (sort of) safe? Will it be too unstable? Would it be possible to soar? Is there another wing (low drag, high glide ratio) you would suggest for this configuration?

I hope the story isn't too long. Thank you for your advice in advance!

Kind regards,

Stéphanie Folmer

Russell Ogden <[redacted]>
To: Stéphanie Folmer <[redacted]>

Tue, Dec 16, 2014 at 11:54 AM

Hi Stephanie

Good decision, there is no safe way of adding weight to the top surface of the wing. It would become irrecoverable in the event of a collapse.

Yes it is possible to use an R11 with a motor unit and given the correct conditions it will be able to soar the dunes. If you need the highest performing wing with high levels of stability then the R11 is about as good as it gets, but it needs a good pilot. It is not a 'safe' thing to do, paragliding can never be considered a 'safe' activity. There is always risk. However safety can be mitigated by a good pilot who knows what he is doing.

Good luck.

Cheers

Russ

Russell Ogden

Test Pilot

Ozone Gliders Ltd

Registered in Scotland: sc190898

Registered address: Q Court, 3 Quality Street, Edinburgh

Figure L.1: Extract from the mail conversation with Russel Ogden, a professional paragliding test pilot, where he confirms that the 2-liner wing is safe to fly the paramotor with.

M Prototype Cost Breakdown

Table M.1 depicts the detailed breakdown structure of the prototype cost.

Table M.1: Cost Breakdown for the whole paramotor

Part	Cost [€]
Chassis	1098
Harness	344
Reserve chute	1190
Reserve chute container	79
Fairing	200
Fairing support structure	400
Fairing-to-driveshaft bearing	25
Driveshaft+ brackets	50
Motor	483
Gearing	205
Belt	35
Big Pully incl. bearing	100
Small Pully	20
Connection Plate	20
Second Shaft	30
Motor control	1090
ESC incl wiring	700
Controller Interface	55
Input controller	335
Propulsion	150
Propeller + Hub	150
Power provision	1500
Battery	1100
Battery Management System (BMS)	110
Wiring	40
Casing	250
Bolts	20
Nutrition/Water	(5)
Wing+Lines	(3200)
Total	4546

N SWOT Analysis Detailed Design

The SWOT analysis consists of two main parts, the internal forces and the external forces. The internal forces consist of the strengths and weaknesses. The external forces consist of the opportunities and the threats. SWOT forces are selected using this technique resulting in a confrontation matrix leading to useful SWOT-force combinations.

Scope

To be able to properly analyse the internal and external environment a scope is needed. The scope consists of a goal and the level of analysis. The goal must be SMART (specific, measurable, ambitious, realistic and time-bound). The goal can be used to weigh-off the SWOT forces resulting in a selection for the confrontation matrix. The level of analysis is used to make sure that the SWOT-forces can be properly combined in the confrontation matrix.

The level of analysis that is most suitable for this markets SWOT analysis is clearly the level of the product group. The goal can be deduced from the requirements; the goal is to design and produce an electric paramotor that can fly from the north to the south of the Netherlands in one day and meets all further requirements that have been stated in the DSE Electric Paramotor Project Planning file chapter 1.2.

- This goal is clearly specific since the requirements are all explicitly mentioned.
- This goal is measurable, all features that have to be measured are mentioned in the requirements.
- This goal is ambitious since an electric paramotor with the range described in the requirements, especially not in the price class that is determined for this to be designed electric paramotor.
- This goal is realistic since the battery and electric motor industry have been developing strongly over recent years.

Internal Analysis

For the internal analysis there are two forces that have to be analysed; The strengths and the weaknesses.

N.0.7 Strengths:

- Technologically advanced environment
- Close contact with specialists in the field of flight propulsion, aerodynamics, energy, structures and acoustics.
- Consultant within the team who has a lot of experience in paragliding
- Tutor and coaches with experience in comparable design and development projects
- Diverse skillset/interests within the group (example: law, project planning, etc.)

-
- Hands-on project experience (eco-runner, DUT Racing, VSV, Forze)
 - International group members
 - Located close to the mission location
 - Reputation of TU Delft
 - New design that fosters innovation
 - Good group dynamics
 - Electric paramotor has a competitive low price
 - Team produced a paramotor design program
 - Team has experience in system engineering

N.0.8 Weaknesses:

- No experience with paramotoring within the group
- Limited resources (€5000)
- Limited number of engineers (9)
- Communication in second language within the group
- Longer energising time of the power storage

External Analysis

For the external analysis there are two forces that have to be analysed; The opportunities and the threats.

N.0.9 Opportunities:

- Technological developments in battery technology due to the electric car trend
- New markets such as professional/army and unconventional use cases
- Sustainability awareness
- Finite natural resources
- Material technology developments - from wind turbine engineering/aerospace industry/car industry
- Deregulation

N.0.10 Threats:

- Gasoline powered paramotors
- Other electric paramotor manufacturers
- (Change of) regulations
- Customer scared to deal with electronics due to inexperience/ lack of knowledge
- Current market leaders create aggressive stance towards new entrants

Confrontation Matrix

The internal and external forces that are best suited to fulfill the goal are combined in the confrontation matrix. In the following subsections the different internal and external forces that are found to be most promising in achieving the goal of this project are described.

N.0.11 Selection Internal Analysis

Strengths:

- S1: Close contact with specialists in the field of flight propulsion, aerodynamics, energy, structures and acoustics.
 - This is an important force since the paramotor product group is multidisciplinary and requires expertise from several areas.
- S2: Consultant within the team who has lots of experience in paragliding.
 - This is an important force since hands on experience helps in obtaining sector information since the paragliding community has a lot of contact with the paramotoring community. This also applies when comparing the paragliding product group to the paramotor product group.
- S4: Team produced a paramotor design program
- S3: Team has experience in system engineering

Weaknesses:

- W1: No experience with paramotoring within the group.
 - Even though there is experience with paragliding, there is no experience with paramotoring in the group.
- W2: Limited resources (€5000).
 - The limited amount of resources (€5000) can limit design options for the electric paramotor product group.
- W3: No experience with designing propulsion systems
 - The propulsion system is a big part of the design, learning curves of the development team are not known with respect to propulsion systems, which is an important part of the electric paramotor product group.
- W4: Possible longer energizing time of the power storage
 - This is a weakness of the electric paragliding product group with respect to the current market group. (see the section about current market solutions for examples: section 7.1.1)

N.0.12 Selection External Analysis

Opportunities:

- O1: Technological developments in battery technology due to the current electric car trend
 - Large investments in development are currently made that can be of great use in the development these can directly positively influence the development of the product group of paramotors as a whole.
- O2: New markets such as professional/army and unconventional use cases
 - New markets are useful to be able to increase the development teams bargaining power when buying parts for the electric paramotor, thus can directly positively influence the product group of paramotors for the design team.

- O3: Sustainability awareness.
 - Sustainable awareness and the 'sustainability-hype' can greatly increase interest in paramotoring which can result in a bigger market size for the paramotoring product group as a whole.
- O4: Material technology developments from wind turbine engineering/aerospace industry/car industry.
 - Technological developments in material technology from turbine engineering/aerospace/car industry, can directly positively influence the product group of paramotors as a whole.

Threats:

- T1: Competition from gasoline powered paramotors.
 - Gasoline powered paramotors are the biggest competition in the paramotoring space.
- T2: Competition from other electric paramotor manufacturers.
 - Competing substitute manufacturers can negatively influence the (potential) market size for the to be developed electric paramotor and its product group.
- T3: (change of) Regulations
 - A change in regulations could make it much more difficult or expensive for recreational flyers to continue paramotoring which could (potential) negatively influence the potential market size for the to be developed electric paramotor and its product group.
- T4: If accidents occur, future market for electric paramotors will decrease severely.
 - Accidents and negative press on this could potentially negatively influence the (potential) market size for the to be developed electric paramotor and its product group.

The next step is setting up the confrontation matrix which can be found in figure N.1.

<p><u>Strengths</u></p> <p>S1: Close contact with specialists S2: Consultant within the team S3: System engineering S4: Paramotor design program</p>	<p><u>Weaknesses</u></p> <p>W1: No paramotoring experience W2: limited resources W3: No propulsion system experience W4: Longer energising time</p>
<p><u>Opportunities</u></p> <p>O1: Battery technology developments O2: New markets O3: sustainability awareness O4: material technology developments</p>	<p><u>Threats</u></p> <p>T1: Gasoline powered paramotors T2: Other electric paramotor manufacturers T3: (change of) Regulations T4: Accidents</p>

Figure N.1: Confrontation matrix SWOT analysis

From the confrontation matrix as seen in figure N.1 it is possible to obtain challenges and actions these conclude the SWOT analysis. Challenges can be found by combining internal and external forces which will be followed by actions per challenge to achieve the goal (the goal is mentioned in subsection N: Scope). Actions are stated for all the challenges after the challenges.

N.0.13 Challenges

- Challenge 1: How can the fact that the development team is in close contact with specialists in the field of flight propulsion, aerodynamics, energy, structures and acoustics be used to adjust the design to the opportunity of new battery and material developments. (S1+O1 & S1+O4)

-
- Experts for the different field of engineering will be identified and need to be contacted.

 - Challenge 2: How can the fact that the development team has a paragliding consultant within the group be used to design a product to best suite the opportunity of new markets. (S2+O2)
 - Paragliding consultant can get in contact with paragliding contacts to persuade them to get into paramotoring.
 - Communicate the fact that a paragliding expert is part of the team in order to gain trust of the paramotoring community in the design and the fact that their wishes will be considered.

 - Challenge 3: How can the fact that the team has limited resources be overcome and new markets be attracted for the product group. (W2+O2)
 - The product will be cheaper due to the limited resources, therefore new markets can be found that previously were not interested in the more expensive electric paramotors.

 - Challenge 4: How can the paramotor design programs be used to attract new markets be attracted for the product group. (S4+O2)
 - Design client specific DIY paramotor designs for clients using paramotor design programs.
 - Use paramotor design programs to connect clients to paramotor suppliers for a premium. -
 - Use paramotor design programs to connect clients of different product groups to paramotor suppliers for a premium.

 - Challenge 5: How can the teams experience in system engineering be used to overcome the threat of the competition in the gasoline powered paramotors industry which are cheaper. (S4+T1)
 - By optimizing system engineering program to characteristics of interest for specific client.

Conclusion Market Analysis

This Appendix presented the SWOT analysis (internal and external analysis) for the detailed design. It resulted in five challenges that can be categorised in two main focus areas. One of which was to use the strength of the hands-on project experience of the group within a technological favourable environment to achieve a good design and thereby attract more customers. The second focus area is to use the paramotor design programs and system engineering experience to overcome the threat of the competition and the high prices of the paramotor.